HYDRO-MECHANICAL ANALYSIS OF SHRINKAGE AND SHRINKAGE CRACKING DUE TO ENVIRONMENTAL LOADS ON SATURATED TO UNSATURATED EXPANSIVE SOILS

By

HUSSEIN AL-DAKHEELI

Bachelor of Science in Civil Engineering

University of Baghdad

Baghdad, Iraq

2011

Submitted to the Faculty of the
Graduate College of the
Oklahoma State University
in partial fulfillment of
the requirements for
the Degree of
MASTER OF SCIENCE
December, 2016

HYDRO-MECHANICAL ANALYSIS OF SHRINKAGE AND SHRINKAGE CRACKING DUE TO ENVIRONMENTAL LOADS ON SATURATED TO UNSATURATED EXPANSIVE SOILS

Thesis Approved:

Dr. Rifat Bulut

Thesis Adviser

Dr. Xiaoming Yang

Dr. Mohamed Soliman

Name: HUSSEIN AL-DAKHEELI

Date of Degree: DECEMBER, 2016

Title of Study: HYDRO-MECHANICAL ANALYSIS OF SHRINKAGE AND SHRINKAGE CRACKING DUE TO ENVIRONMENTAL LOADS ON SATURATED TO UNSATURATED EXPANSIVE SOILS

Major Field: CIVIL ENGINEERING

Abstract: The volumetric strain of expansive soils due to the change of water content has a significant importance in geotechnical and geoenvironmental engineering. The volumetric strain occurs due to the development of the effective stress in the soil. Expansive soils swell in wet seasons and shrink in dry seasons. In the field, soil shrinkage causes vertical settlement and cracking. It is widely accepted that cracks occur when the lateral tensile stress exceeds the soil tensile strength. The tensile stress is induced from the restraint conditions of the soil shrinkage. When the soil is subjected to desiccation, its hydraulic properties (e.g. water content, hydraulic conductivity) change. The variations of the soil hydraulic properties can also vary its mechanical behavior (e.g. effective stress, strength, fracture tendency). The variation of the soil hydro-mechanical behavior makes studying the shrinkage and cracking a difficult task. In addition, due to the complexity of the physicochemical interactions taking place in the soil particles-water system, predicting the effective stress that causes the volumetric strain in the soil is very challenging. Soil suction has been widely used to characterize the hydro-mechanical behavior. In this thesis, soil suction is vitally employed to study the soil shrinkage and shrinkage cracking. That is achieved by studying: i) the factors that influence the volume change due to the change of suction, and ii) the soil cracking behavior from the stress and strain developed in the soil during the desiccation. To fulfill that, comprehensive literature review and experimental tests have been undertaken. The experimental tests involve subjecting soils with different plasticity indices and preparation conditions to air drying to induce shrinkage and cracking in the soils. That is conducted using the restrained ring testing method. In this test, the stress is measured using strain gauges while the shrinkage (strain) is predicted using the digital image processing. The results emphasize that the crack initiates at a stage very close to the air entry value or the end of the normal shrinkage zone. Further, the results also indicate that a soil can develop similar internal stresses prior to cracking for various initial water contents.

TABLE OF CONTENTS

LIST OF TABLES

Table Page

LIST OF FIGURES

Figure Page

CHAPTER I

INTRODUCTION

1.1. Background

The volumetric strain of expansive soils due to the change of the water content has a significant importance in geotechnical and geoenvironmental engineering. Expansive soils swell in wet season and shrink in dry season. That causes distresses to the overlying structures (e.g. pavements and residential houses), buried structures (e.g. pipelines), and lateral structures (e.g. retaining walls). The light-weight structures such as the foundation of the residential houses and pavements are highly affected by the movement of expansive soils. The level of the volume change mainly depends on the soil volume change potential, moisture permeability properties, the moisture boundary conditions, and the environmental conditions.

Jones and Holtz (1973) reported that the cost of damage caused by expansive soils exceeds the double of the cost caused by all natural disasters including tornados and earthquakes. Due to its importance, many research studies and specialty conferences have been held exclusively for this subject.

The drying shrinkage can lead to cracking in the soil layers. Cracks can substantially decrease the strength and increase the compressibility and permeability (Morris et al. 1992). The existence of cracks in the soil layers utilized for the environmental purposes can result in losing their functions (Peron et al. 2009). The presence of cracks in pavement shoulders can extend the seasonal moisture variation and hence subject the subgrades to more movements. In extreme conditions, cracks can initiate in the subgrade and may propagate to cause longitudinal cracks in the pavement layers. Such cases have widely been reported (Luo and Prozzi, 2009; Bulut et. al. 2014; Wanyan et. al. 2015).

Soil movement is caused by the high ability of the clay particles to interacting with the water. This interaction is owing to the high specific surface area of the clay particles (e.g. montmorillonite) in addition to their large cation exchange capacity and substantial isomorphous substitution (Mitchell and Soga 2005). The physicochemical interactions of the soil particles-water system are still not well understood due to their high complexity.

1.2 Aim and objectives

This research investigates the mechanism of the soil shrinkage and cracking. That is achieved in two directions: i) to study the factors that influence the volume change due to the change of water content or suction and ii) to study the soil cracking behavior from the stress and strain developed in the soil during desiccation. The objectives of this thesis is to study the following points:

1- The relation between the soil water characteristic curve and the volume change, particularly, the soil shrinkage characteristic curve.
2- The ability of the models proposed based on the soil water characteristic curve in predicting the hydraulic conductivity and the diffusivity function of unsaturated expansive soils.
3- The relationship between the crack initiation and propagation and the suction of soils under desiccation.

4- The stress-strain regime the soil experiences during drying that leads to cracking.

To meet these objectives, comprehensive literature review and laboratory tests are conducted. The laboratory tests involve free and restrained shrinkage tests in addition to the suction measurements. The restrained shrinkage is undertaken using the restrained ring testing method. In this test, soils with different properties and preparation conditions are subjected to air drying to shrink and induce cracks. During desiccation, the developed stresses are measured using micro strain gauges. The shrinkage of the sample is also measured using the digital image analysis technique before and after cracking.

1.3 Organization of Thesis

Chapter 2 reviews the concept of the unsaturated soil mechanics, the volume change of expansive soils, and the soil cracking phenomenon.

Chapter 3 investigates the ability of the models proposed based on the soil water characteristic curve in predicting the hydraulic conductivity and moisture diffusivity functions of fine-grained soils.

Chapter 4 presents new understanding to the soil volume change, particularly the soil shrinkage and its relationship with the soil water characteristic curve.

Chapter 5 proposes a simple model to predict the crack initiation and growth based on the soil suction and shrinkage characteristics.

Chapter 6 explains the laboratory testing program of the free and restrained shrinkage tests in addition to the suction and tensile strength measurements.

Chapter 7 presents and discusses the experimental results for: i) the relation between the soil water characteristic curve and the soil shrinkage, ii) the stress and strain developed during the soil shrinkage and cracking, and iii) the soil tensile strength characteristics during desiccation.

Chapter 8 concludes the results and gives recommendations for the future studies.

CHAPTER II

LITERATURE REVIEW

2.1. Unsaturated Soil Mechanics

Unsaturated soil is a soil that has three phases, namely, air, water, and soil particles. Most of the theories and principles in soil mechanics were initiated based on the saturated soils having two phases, water, and soil particles, starting from the pioneer works of Terzaghi (1925) and (1943) for the effective stress theory and the soil consolidation theory, respectively. Thereafter, extensive research has been undertaken to reformulate the classical theories of saturated soils to involve the unsaturated soils or propose new constitutive models for unsaturated soils.

Soil suction is always invoked to model and predict unsaturated soil behavior and property functions such as hydraulic conductivity, moisture diffusivity, shear strength, and volume change. Soil suction is the affinity of soil for water. It consists of two major components namely matric suction and osmotic suction. Matric suction arises from the capillary action and surface energy of the soil particles, while osmotic suction results from the ionic concentration of the pore water (Bulut and Leong 2008).

2.2 Soil Water Characteristic Curve

The soil water characteristic curve (SWCC) is the relationship between the suction and water content. Various unsaturated soil property functions, e.g. hydraulic conductivity, can be derived from the SWCC. The typical shape of a SWCC is shown in Figure 2.1.

For drying from fully saturated conditions, the SWCC has a breaking point referred to as air entry point (Figure 2.1), at which the soil starts to desaturate and becomes unsaturated. The other breaking point shown in Figure 2.1 is the residual point, at which the increase of suction is accompanied by less water reduction. The two breaking points divide the SWCC into three zones: boundary effect zone, transition zone, and residual zone (Figure 2.1). SWCC reveals a hysteresis for wetting and drying process (Figure 2.2). Figure 2.2 also shows the scanning path from drying curve to wetting curve and vice versa.

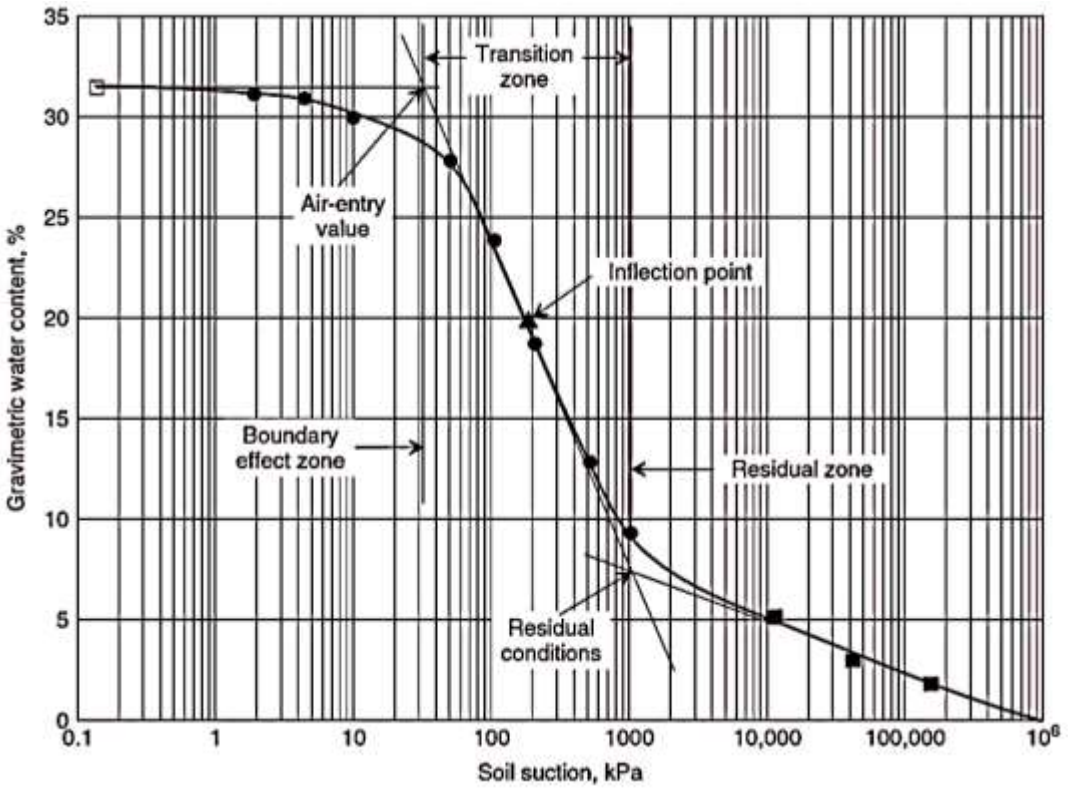

Figure 2.1 Typical SWCC for Drying Process (Fredlund et al. 2012)

It is widely accepted that the maximum suction for all soils corresponding to zero water content is being 1000 MPa (e.g. Fredlund and Xing 1994). That means all soils can show suction ranging from 0 to 1000 MPa. However, the shape of SWCC differs from soil to soil depending on the type of soil mineralogy, particle size, and particle size distribution. A typical SWCC for sandy, silty, and clayey soils is depicted in Figure 2.3.

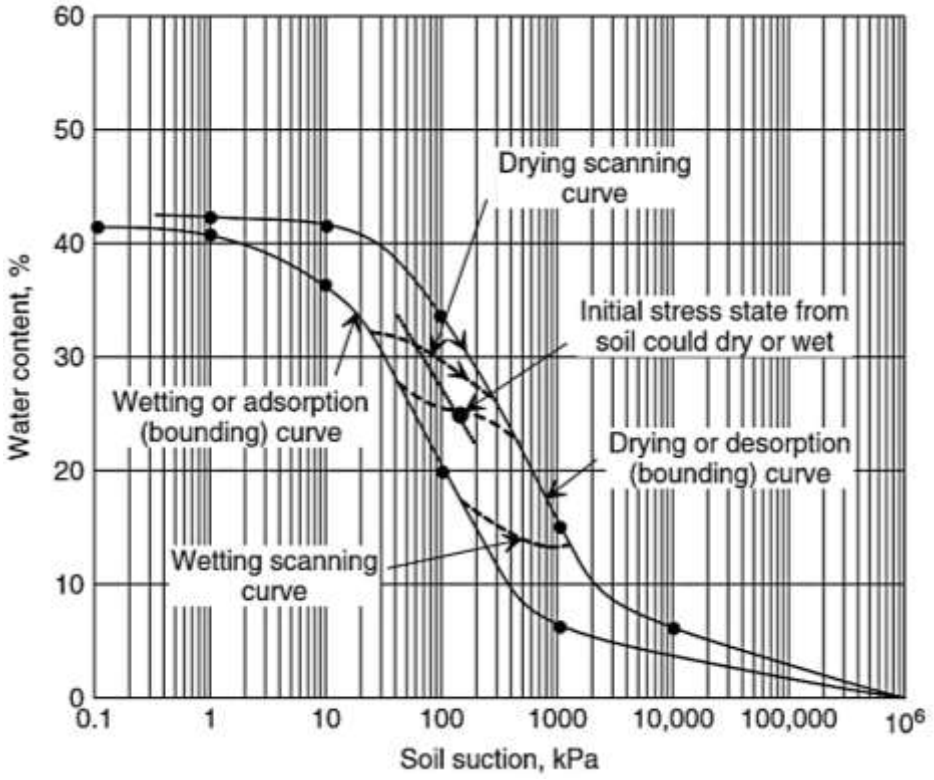

Figure 2.2 Hysteresis in the SWCC (Fredlund 2003, Cited in Fredlund et al. 2012)

Several closed form empirical expressions have been proposed to model the whole soil water characteristic curve from discrete data (e.g. Gardner 1958; Brooks and Corey 1964; Mualem 1976; van Genuchten 1980; Fredlund et al. 1994). The van Genuchten (1980) model is the most frequently

used model in soil science community (Equation 2.1), while it is the Fredlund and Xing (1994) model in geotechnical engineering community (Equation 2.2).

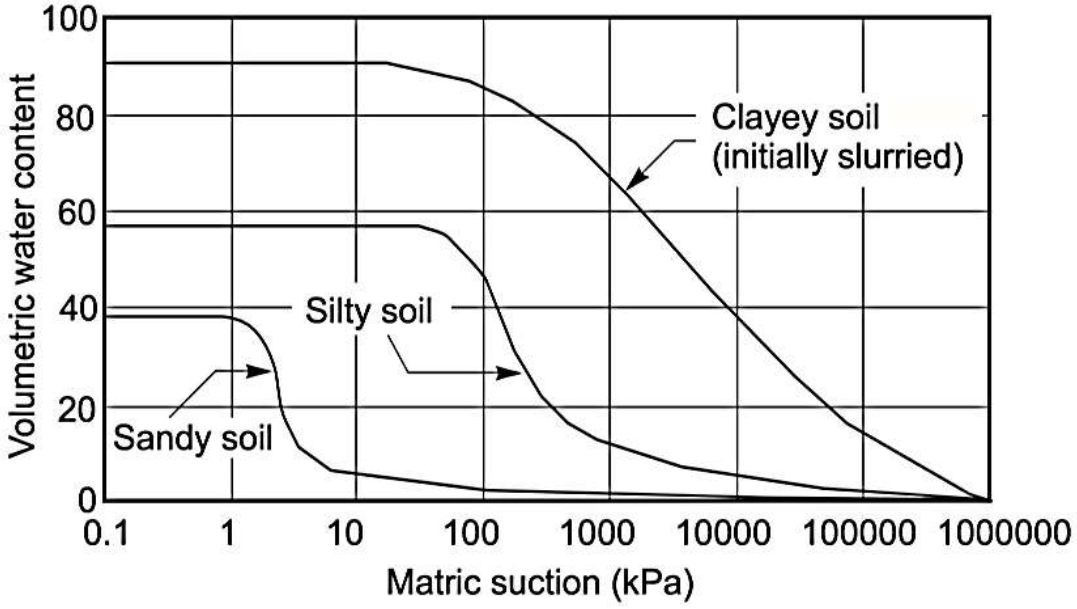

Figure 2. 3 Soil Water Characteristic Curve for Sandy, Silty, and Clayey Soils (Fredlund and Xing 1994)

$$w(\psi) = w_r + \frac{w_s - w_r}{[1 + (a\psi)^n]^m} \tag{2.1}$$

$$w(\psi) = \left[1 - \frac{\ln(1 + \psi/\psi_r)}{\ln(1 + 10^6/\psi_{r)}}\right] \frac{w_s}{\{\ln[\mathrm{e} + (\psi/a)^n]\}^m} \tag{2.2}$$

Where $w(\psi)$ is the gravimetric water content for a given suction ψ, w_s is the saturated water content, w_r is the residual water content, ψ_r is the residual suction, and a, n, m are the curve fitting parameters.

2.3 Suction Measurement

Various techniques have been used to measure the soil suction. These methods can be divided into direct and indirect methods. Direct methods involve axis translation technique and tensiometer sensor. Indirect methods include thermocouple psychrometer, chilled-mirror psychrometer, filter paper, thermal conductivity, and electrical conductivity (Bulut and Leong 2008). Every method has its own limitations and shortcomings such as range of application, cost, reliability, and practicality (Bulut and Leong 2008). Table 2.1 summarizes the commons used techniques for suction measurements.

Table 2.1 Suction Measurement Techniques and their Equilibrium Time and Measured Suction Range, (After Fredlund et al. 1993, Bulut et al. 2001, Bulut and Leong 2008), Cited in Chen (2015)

Suction	Techniques / Devices	Suction (kPa)	Equilibrium Time
Matric Suction	Jet-fill tensiometer	0-90	Several minutes
	UMS T5-10 tensiometer	0-160	Several minutes
	Null-typeaxis translation apparatus	0-1500	Several hours to days
	Electrical conductivity sensor	0-1500	6-50 hours
	Thermal conductivity sensor	10-1500	Hours to days
	In-contact filter paper	50-30000 (or higher)	5-14 days
Total Suction	Thermocouple psychrometer	300-7000	1hour
	Chilled-mirror hygrometer	500-30000	10 minutes
	Non-contact filter paper	50-30000 (or higher)	5-14 days
Osmotic suction	Pore-fluid squeezer	Entire range	days

2.3.1 Tensiometer

Tensiometer is a device for direct measurement of the matric suction of soil. It has a porous ceramic cup, (e.g., air entry porous material). When the equilibrium is attained between the water pressure in the ceramic cup and that in the soil, the pore water pressure or matric suction can directly be read on the pressure gauge. While this technique can be used to accurately measure the matric suction, it cannot measure high suction values, greater than 100 kPa (up to 150 kPa for UMS T5-10 tensiometer). In addition, it cannot measure the osmotic suction since there is no a semi-permeable membrane for ionic salts soluble in pore water of soil. However, it directly measures the soil suction within few minutes without a need to any calibration curve, and it can be used to measure suction in the laboratory and the field. Before using the tensiometer sensor, it should be filled with water and the air bubbles should be removed from the system. If UMS T5-10 tensiometer is used, the tube (glass shaft) and the sensor body (Figure 2.4) should not contain any trapped air bubbles, because otherwise the suction reading will not be accurate.

2.3.2 Chilled-Mirror Psychrometer

The chilled mirror psychrometer (known also as WP4) utilizes a technique to measure the total suction using the chilled mirror dew point under isothermal conditions (Figure 2.5). The principle of the measurement technique is by predicting the total suction from the relative humidity using Kelvin equation. That is achieved in a sealed chamber inside which the liquid phase of the water of the soil sample is equilibrated with the vapor phase in the chamber space. An infrared thermometer and a thermocouple are attached to the inside of the chamber to measure the sample temperature and the dew point temperature respectively, from which it is possible to predict the soil suction using Kelvin equation (Bulut and Leong 2008).

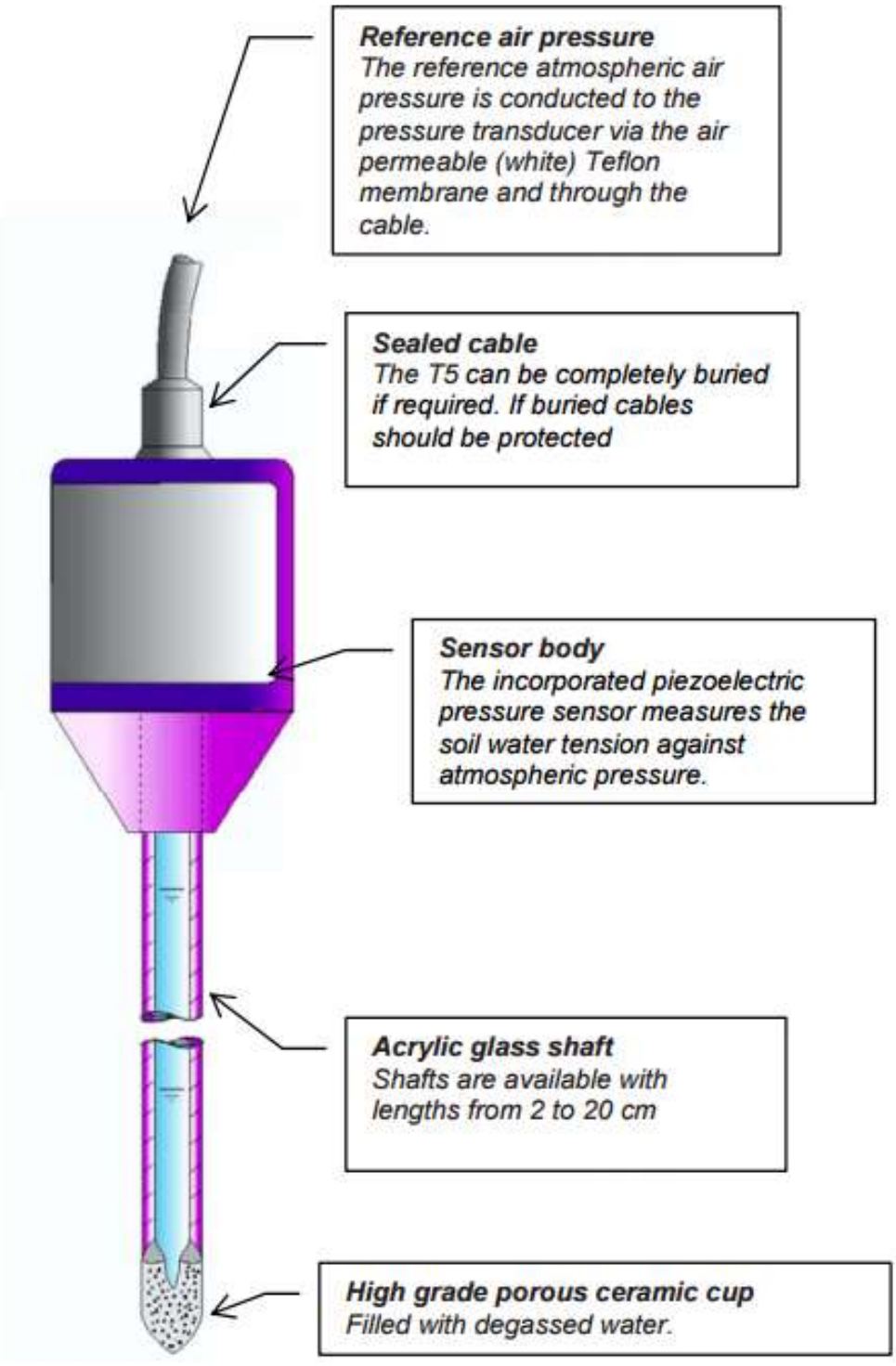

Figure 2.4 UMS T5 Tensiometer Sensor (UMS T5/T5x User Manual)

Bulut et al. (2002) investigated the accuracy of this device using salt solutions at different concentrations with known osmotic suctions. The authors also compared the results from WP4 with those from filter paper method. They highlighted that WP4 gives non accurate suction at low values but very good results for high suction (e.g. greater than 1000 kPa).

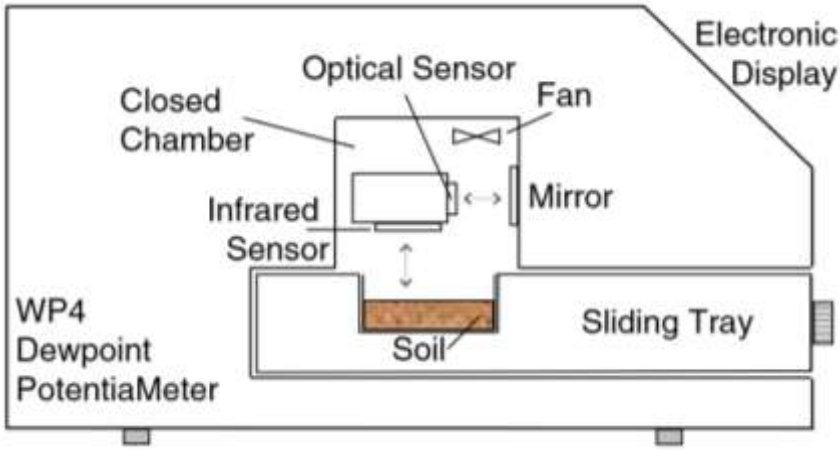

Figure 2.5 Schematic Drawing of the Chilled Mirror Psychrometer Device (WP4), (Bulut and Leong 2008)

2.4 Volume Change

The volume change potential of expansive clayey soils can cause damages and distresses to the overlying structures (e.g. pavements), buried structures (e.g. pipelines), and lateral structures (e.g. retaining walls). Expansive soils shrink when losing water and swell when gaining water. Therefore, the rate of the volume change mainly depends on the hydraulic conductivity function of soils.

The volume change tendency is owing to the physicochemical interactions between soil particles and water. Such interactions are dominant in clay particles, which develop high potential for swelling and shrinking. Due to their complexity, the physicochemical phenomena accompanied with the clay-water interaction are still not fully understood. Among different groups of clay minerals, e.g. mica-like, smectite, and chlorite, smectite minerals have the most potential for changing in volume, owing to their extensive isomorphous substitution and cation exchange capacities (Mitchell and Soga 2005). The more expansive minerals are available in the soil, the more plastic the soil becomes.

Numerous symposia and conferences have been held exclusively for studies on expansive soils, mostly to find reliable prediction methods and solutions. Prediction methods of expansive soil movements can be categorized into three groups: empirical or semi-empirical methods, oedometer or consolidation based methods, and suction based methods (Lytton et al. 2004). Most empirical or semi empirical methods are developed based on Atterberg limits and clay content for local soils. Therefore, their accuracy and applicability are most likely suitable for those soils (Lytton et al. 2004). Consolidation based methods are used to estimate either the free swelling with no applied load or the swelling pressure by keeping the volume constant. Some researchers such as Dhowian et al. (1987) have found that this method overestimates the swelling potential.

On the other hand, suction based methods are preferable since the suction is directly relevant to the physicochemical interactions in the soil pores. Moreover, suction is one of the stress state variables governing the soil behavior (Fredlund and Morgenstern 1977). Soil suction can be used to provide the soil volume change characteristics from low water content to very high water content.

For the sake of simplicity, most suction based methods approximate a linear relationship with a single coefficient between the suction (in logarithm scale) and the soil volume strain. While that is true for a wide range of water contents or suctions, the whole characteristics of the volume change and its boundaries in terms of suction, water content, and degree of saturation for different expansivity levels of clayey soils are needed for better understanding of this subject. Soil volume change characteristic and its relation to the soil water characteristic curve (SWCC) will be discussed in the next chapter. Table 2.2 presents a summery for the existing suction based methods according to a recent review by Vanapalli and Lu (2012).

Table 2.2 Summary for the Existing Suction Based Methods (from Vanapalli and Lu (2012))

Author	Equation/Description
Aitchison (1973)	$\Delta H = \frac{1}{100}\int_0^{H_s} I_{Pt}\,\Delta u\,\Delta h$ ΔH = surface movement; I_{Pt} = instability index of the soil; Δu = change in suction, in pF units, at depth z z below the ground surface; Δh = thickness of the soil layer under consideration; H_s = depth of the design suction change
Lytton (1977)	$\Delta H = \gamma_k H \log_{10}(h_f/h_i) - \gamma_\sigma H \log_{10}(\sigma_f/\sigma_i)$ h_f, h_i = final and initial water potentials; σ_f = applied octahedral normal stress; σ_i = is the octahedral normal stress above which overburden pressure restricts volumetric expansion; γ_k, γ_σ = two constants characteristic of the soil.
Johnson & Snethen (1978)	$\Delta H = H\frac{C_\tau}{1+e_0}\log\frac{h_0}{h_f + \alpha\sigma_f}$ $C_\tau = \alpha\, G_s/(100\, B)$ $\log h_0 = A - B\, w_0$ H = the stratum thickness; C_τ = suction index; α = compressibility index; e_0 = initial void ratio; h_f = final matric suction , kPa; σ_f = final applied pressure, (overburden + external load), kPa; h_0 = matric suction without surcharge pressure, kPa
Snethen (1980)	$\Delta H = H\frac{C_\tau}{1+e_0}(A - B\, w_0) - \log(\tau_{mf} + \alpha\,\sigma_f)$ $C_\tau = \alpha\, G_s/100\, B$ $\log \tau_m = A - B\, w_0$ C_τ = suction index; τ_{mf} = final matric suction; σ_f = final applied pressure (overburden + external load); α = compressibility factor A, B = constants (y-intercept and slope of soil suction versus water content curve, respectively).

Table 2.2 (continued) Summary for the Existing Suction Based Methods (from Vanapalli and Lu (2012))

Author	Equation/Description
McKeen (1992)	$\Delta H = -\gamma_h H \log \frac{h_f}{h_i}$ $\gamma_h = -\frac{\Delta v/v_i}{\log_{10}\frac{h_f}{h_i}}$ $\Delta H = H C_h \log \Delta\tau f s$ $C_h = (-0.02673)(d_h/d_w) - 0.38704$ $f = (1 + K_0)/3$ $s = (1 - 0.01(\%SP)$ γ_h = suction compression index; h_f, h_i = final and initial weighted suction, respectively. $\Delta v/v_i$ = volume change with respect to initial volume. C_h = suction compression index, is the slope of volume change-soil suction curve; $\Delta\tau$ = the suction change in pF; f = the lateral restraint factor; K_0 = the coefficient of earth pressure at rest, equal to 1; s = the coefficient for load effect on heave; SP = the percent of swell pressure applied.
Mitchell & Avalle (1984)	$\Delta H = I_{Pt} \Delta u H$ $I_{Pt} = \frac{\Delta L/L}{\Delta w} \cdot \frac{\Delta w}{\Delta u}$ I_{Pt} = instability index; Δu = soil suction change.
Hamberg & Nelson (1984)	$\Delta H = H \frac{C_w}{1 + e_0} \Delta w$ $C_w = \frac{\Delta e}{\Delta w}$ $\Delta H = H \frac{C_w}{1 + e_0} \log (h)_i$ $C_h = C_w D_h$ C_w = suction modulus ratio; Δw = change in water content; C_h = suction index with respect to void ratio; D_h = suction index with respect to moisture content.

Table 2.2 (continued) Summary for the Existing Suction Based Methods (from Vanapalli and Lu (2012))

Author	Equation/Description
Dhowian (1990)	$\Delta H = H \frac{C_\psi}{1+e_0} \log \frac{\psi_i}{\psi_f}$ $C_\psi = \frac{\alpha G_s}{100B}$ $\Delta H = H \frac{\alpha G_s}{1+e_0} (w_f - w_i)$ $\Delta H = H C_w (w_f - w_i)$ $C_w = \alpha G_s / (1+e_0)$ C_ψ = suction index; ψ_i = initial suction; ψ_f = final suction; α = volume compressibility factor B = slope of suction versus water content relationship; G_s = specific gravity of solid particles; C_w = moisture index
Fityus & Smith (1998)	$\Delta H = H I_v \alpha (w_{0i} - w_{0f})$ $\Delta H = H C_w (w_f - w_i)$ I_v = volume index; α = empirical factor accounting for confining stress differences in lab and field; w_{0i}, w_{0f} = average initial water content and the average final water content, respectively; σ_v = vertical stress at the midpoint of layer.
Briaud et al. (2003)	$\Delta H = H_f (\Delta w - E_w)$ $E_w = \Delta w (\Delta V / V_0)$ $f = (\Delta H / H_0)(\Delta V / V_0)$ E_w = shrink–swell modulus, slope of the water content versus the volumetric strain line; f = shrinkage ratio, ratio of the vertical strain to the volumetric strain

2.5 Soil Drying Cracking Phenomenon

As soil shrinks during drying process, at some stage, it may develop cracks. Typically, soil in the field undergoes one dimensional vertical shrinkage before cracking (Abu-Hedjleh and Znidarcic 1995). It cracks when the horizontal tensile stress exceeds the soil tensile strength (Morris et al. 1992). The horizontal tensile stress is induced due to the restraint condition of shrinkage in the horizontal direction owing to the cohesion between soil particles. The soil relieves the internal stresses caused by the increase of suction by changing in volume (i.e. reduction of void ratio). Since soil has some tensile strength that may arise from the apparent cohesion between the soil particles, it will restrict the displacement in the horizontal direction which, in turn, will develop the horizontal tensile stress. As the crack initiates at the soil surface, it can propagate downward depending on the changes in the soil suction profile. It has been widely accepted that the desiccation cracking takes place in Mode I fracture (Harison et al. 1994).

Soil cracking increases the hydraulic connectivity and compressibility and decreases the strength (Morris et al. 1992). That has led to various problems in engineering applications. Some application problems caused by soil cracking have been summarized by Kodikara and Costa (2013), listed in Table 2.3.

Table 2.3 Summary of the Studies Showing Soil Cracking Effect on Different Applications (Kodikara and Costa 2013)

Discipline	Application
Geotechnical Engineering	• Slopes – There is significant evidence that cracking at the crest area of the slopes trigger the initiation of slope failure (Take 2003) • Flood dykes – Progressive failures that take place in UK's extensive dyke system (extending up to 35,000 km with an annual maintenance budget of £450 million) are triggered commonly by desiccation cracking that takes place in the downstream slope, subsequently providing seepage paths and block uplifting during flooding (Dyer 2009). Canal systems also suffer from desiccation cracking induced distress. • Dams – Embankment dams experience internal erosion leading to piping failures, which accounts for about 50% dam failures and accidents. Potential erosion pathways are assisted by cracks formed by desiccation above phreatic surface, differential settlement, hydraulic fracturing and earthquakes (Foster et al. 2000)
Geo-environmental Engineering	• Compacted clay landfill liners and covers and Geosynthetic clay liners – Thermally induced or evaporation induced desiccation and differential settlement induced cracking of these components in modern waste landfills is a major issue providing unwanted pathways for escape of leachate and gas (Daniel and Wu 1993; Zhou and Rowe 2003) • Deep nuclear waste isolation – Bentonite buffer zones can undergo thermal drying, shrinkage and cracking near the waste package (Park et al. 2001)
Transport Engineering	• Cracking in road pavements – Reactive soil induced cracking in road bases is a major problem and inure substantial annual maintenance costs worldwide (Chakrabarti et al. 2002; Lytton et al. 1976)
Mining and Resources Engineering	• Mine tailings managements – Cracking in mine tailings influences its drying rates and stability (Morris et al. 1992) and induce changes in the permeability creating environmental consequences because of the potential pollutant generation on infiltration (Rodriguez et al. 2007)
Agricultural Engineering / Soil Science/Geology	• Fracture of soils is important consideration in tillage and water and chemical usage in agricultural engineering (Chertkov 2002; Ahmad 1996) • In irrigated lands cracks allows the water and solutes to flow rapidly through the soil bypassing the dry root zone, thus leading to water and nutrient shortage for crops (Bronswijk 1991) • Formation of fissures and gilgai formation in soil has been a subject of research in soil and geo-science (Kodikara et al. 2002)
Materials Engineering	• Cracking and warping (or curling) cause problems in many coating and material elaboration processes that are based on the drying of colloidal suspensions (Pauchard et al. 1999)
Planetary Sciences	• Formation of giant polygons on Earth and Mars, and evidence of presence of water (El Marry et al. 2012)

The last two-three decades have witnessed considerable attention to the studies of the soil cracking. Some studies analyze the crack formations and crack intensity factors for soils subject to desiccation (Yesiller et al. 2000; Atique and Sanchez 2011; Tang et al. 2011; Peron et al. 2013; Safari et al. 2014). Other studies investigate the fracture parameters governing the soil cracking such as the tensile strength, fracture toughness, critical J integral (Harison et al. 1994; Wang et al. 2007; Prat et al. 2008; Amarasiri et al. 2011; Costa and Kodikara 2012; Lakshmikantha et al. 2012). Other studies track the stress that leads to crack initiation (Thusyanthan et al. 2007; Abou Najm et al. 2009).

Analytical studies have also been undertaken to characterize the desiccation cracking in a fracture mechanics framework (Morris et al. 1992; Konrad and Ayad 1997; Amarasiri and Kodikara 2011).

Morris et al. (1992) presented three solutions of the cracking problem based on the elasticity theory, transition between tensile and shear failure, and linear elastic fracture mechanics (LEFM). For the first two solutions, the authors solved the problem by formulating the horizontal tensile stress or horizontal principle stress for zero lateral strain. This stress will be equal to the tensile strength at the time of crack initiation. The authors, therefore, assumed that the crack depth is where the tensile stress equalizes the soil tensile strength. However, their solutions do not predict the crack space. The authors predicted the crack depth based on the three solutions. They pointed out that the LEFM based solution predicts higher crack depth than that predicted by the other two solutions.

Abu-Hedjleh and Znidarcic (1995) proposed that the shrinkage of soft fine-grained soils can be modeled by four stages: consolidation under one-dimensional compression, desiccation under one-dimensional shrinkage, propagation of vertical cracks; and desiccation under three dimensional shrinkage. A crack is initiated in the second stage when the total lateral stress at the crack tip is equal to the tensile strength. The crack can propagate to the depth at which the void ratio reaches the critical void ratio. The authors considered that soil shrinkage takes place in only two stages, the

first in which the soil remains saturated and decreases in volume until it reaches the shrinkage limit which is also the air entry value beyond which the shrinkage ceases and the soil starts desaturating. They claimed that this is the case of the soft fine-grained soils in slurry conditions.

Konrad and Ayad (1997) presented a framework to predict the crack depth and crack space based on the linear elastic fracture mechanics (LEFM). The crack initiates at the surface when the lateral total stress reaches the soil tensile strength at the critical suction which can be estimated from the soil friction angle and tensile strength. Then, the crack propagation is predicted by the LEFM when the stress intensity factor is equal to the fracture toughness while the space between the primary cracks is determined from the horizontal stress relief distribution around the crack.

CHAPTER III

HYDRAULIC CONDUCTIVITY AND MOISTURE DIFFUSIVITY FUNCTIONS OF UNSATURATED FINE-GRAINED SOIL

3.1 Introduction

Hydraulic conductivity and moisture diffusivity functions command the level of the soil-environment interaction. They govern the water and vapor flow horizontally and vertically in soils. Therefore, they control the suction profile regime as a response to seasonal environmental variations. In fact, they control the variations of the soil hydro-mechanical behavior such as effective stress, volumetric strain, shear strength, and resilient modulus.

The moisture flow is usually modeled by Richard's equation or diffusivity equation. The one dimensional partial differential form in one direction of both Richard's equation (Equation 3.1) and diffusivity equation (Equation 3.2) is given as follows:

$$\frac{\partial}{\partial x}\left[k(h)\frac{\partial h}{\partial x}\right] = c(h)\frac{\partial h}{\partial t} \tag{3.1}$$

$$\frac{\partial \psi}{\partial t} = D\frac{\partial^2 \psi}{\partial x} \tag{3.2}$$

Where h is the total pressure head, $k(h)$ is the hydraulic conductivity, x is the elevation, $c(h)$ is the water storage capacity or the slope of the water retention curve, D is the coefficient of moisture diffusivity, ψ is the soil suction, t is the time. The total head is $h = \psi + x$ and the diffusivity is $D(h) = k(h)\frac{\partial h}{\partial \theta}$, where θ is the volumetric water content. Since $h = \psi$ for relatively small elevations as compared with suction values (Mitchell 1979; Aubeny and Lytton 2003), for linearization and the sake of simplicity, Equation 3.1 can probably be reduced to Equation 3.2. Equation 3.2 provides a simple expression for transient water flow. Once the boundary conditions are identified for soils in the laboratory or the field, the diffusion coefficient can be derived if suction measurements are taken at a certain depth in the soil profile for different time snapshots. Mitchell (1979) presented solutions for Equation 3.2 for several boundary conditions of common soil problems. One of these solutions is adopted in this chapter for soil sample column subject to evaporation in the laboratory condition.

Numerous empirical, macroscopic, and statistical models have been developed to predict the permeability function from soil water characteristic curve (SWCC) (Childs and Collis-George 1950; Brooks and Corey 1964; Mualem 1976; van Genuchten 1980; Fredlund et al. 1994; Leong and Rahardjo 1997). The most frequently used models are van Genuchten (1980) in soil science and Fredlund et al. (1994) in geotechnical engineering.

The validity of the SWCC models against experimental data for both hydraulic conductivity and moisture diffusivity functions of expansive soils has rarely been investigated. That is due to the low permeability properties of expansive clay soils which make it a challenging and time consuming task to measure the permeability and diffusivity function in the laboratory. This chapter will first explain the level of shortcomings of these models and second present an alternative method for deriving both parameters from SWCC models.

3.2 Prediction of Permeability and Diffusivity Functions

3.2.1 SWCC Models

For predicting the permeability function from SWCC, this study adopts the model of Fredlund, Xing, and Huang (1994) (referred as FXH in this chapter), and van Genuchten and Mualem (1980) (referred as VM in this chapter). FXH's model is given as follows:

$$k(\psi) = k_{sat} \frac{\int_{\psi}^{\psi_r} \frac{w(y) - w(\psi)}{y^2} w'(y) dy}{\int_{\psi_{aev}}^{\psi_r} \frac{w(y) - w_s}{y^2} w'(y) dy} \tag{3.3}$$

Where, $k(\psi)$ is the unsaturated coefficient of permeability, k_{sat} is the saturated coefficient of permeability, ψ is the total suction, ψ_{aev} is the air entry suction, ψ_r is the residual suction, w is the gravimetric water content, and y is a dummy variable of integration. Equation 3.1 couples with Fredlund and Xing (1994)'s SWCC model (referred as FX in this chapter):

$$w(\psi) = \left[1 - \frac{\ln(1 + \psi/\psi_r)}{\ln(1 + 10^6/\psi_{r)}}\right] \frac{w_s}{\{\ln[\mathrm{e} + (\psi/a)^n]\}^m} \tag{3.4}$$

Where w_s is the saturated water content, and a, n, m are the curve fitting parameters. Also, VM's model is given as follows:

$$k(\psi) = k_{sat} \frac{\{1 - (a\psi)^{n-1}[1 + (a\psi)^n]^{-m}\}^2}{[1 + (a\psi)^n]^{0.5m}}, \qquad m = 1 - 1/n \tag{3.5}$$

Where $k(u)$, k_{sat}, ψ, a, n, and m are the same as defined in FX and FXH models. Equation 3.5 can be coupled with van Genuchten and Mualem's SWCC model (van Genuchten 1980):

$$w(\psi) = w_r + \frac{w_s - w_r}{[1 + (a\psi)^n]^m} \tag{3.6}$$

Where, w_r is the residual water content, w, ψ, a, n, m, and w_s are the same as defined above.

Diffusion coefficient of unsaturated soils is the result of the coefficient of permeability and the slope of soil water characteristic curve (e.g. Childs and Collis-George 1950), as follows:

$$D(\psi) = K(\psi)\left|\frac{d\psi}{d\theta}\right| \tag{3.7}$$

Where, $D(\psi)$ is the diffusion coefficient, and θ is the volumetric water content. After predicting the permeability function, the diffusivity function can be found from Equation 3.7. The slope of SWCC ($d\psi/d\theta$) in Equation 3.5 can be estimated from the first derivative of SWCC equation.

3.2.2 Diffusivity Test

Diffusivity test is simply one dimensional evaporation of a cylindrical soil sample sealed from all sides but one surface subject to the atmosphere. The solution of the one dimensional partial differential equation of diffusivity (Equation 3.2) for the boundary conditions (Equations 3.8, 3.9, 3.10) of this test is presented by Mitchell (1979) as in Equation 3.11:

$$\psi(\mathrm{x}, 0) = \psi_o \tag{3.8}$$

$$\frac{\partial\psi(0,t)}{\partial x} = 0 \tag{3.9}$$

$$\frac{\partial\psi(L,t)}{\partial x} = -he[\psi(L,t) - \psi_a] \tag{3.10}$$

$$\psi(x,t) = \psi_a + \sum_{n=1}^{\infty} \frac{2(\psi_o - \psi_a)\sin z_n}{z_n + \sin z_n \cos z_n} \exp\left[-\frac{z_n^2\, Dt}{L^2}\right] \cos\left[\frac{z_n x}{L}\right] \tag{3.11}$$

Where, ψ_o is the initial suction in the soil sample, D is the diffusion coefficient, L is the sample length, x is coordinate, z_n is a coefficient derived from the solution of $cot\, z_n = z_n/Lhe$, where he is the evaporation coefficient. ψ_a is the atmospheric suction in the laboratory, which can be calculated from Kelvin's law:

$$\psi_a = \frac{RT}{V} \ln(RH) \quad (3.12)$$

Where, R is the universal gas constant, T is the absolute temperature, V is the molecular volume of water, and RH is the relative humidity.

The test starts when the soil sample with constant suction commences to evaporate from one surface. While evaporating, suction is measured using two calibrated thermocouple psychrometers inserted near the exposed surface (Fig. 3.1). Suction values with time and psychrometer position *x* (measured from the bottom of the sample) can be substituted in Equation 3.11 to inversely estimate the diffusion coefficient after calculating the evaporation coefficient, *he*, from Equation 3.10. The surface suction in Equation 3.10, $\psi(L,t)$, is determined by assuming a linear extrapolation of suction values from psychrometer 1 and 2.

3.2.3 Instantaneous Profile Method

The instantaneous profile method (IPM) is a testing technique that employs suction-time or water content-time measurements in a soil profile to assess the permeability using Darcy's law (Equation 3.13) (Lu and Likos 2004). Laboratory measurement involves a cylindrical sample, remolded or undisturbed, subjected to moisture gradient in its profile by wetting or (and) drying for one or both boundaries.

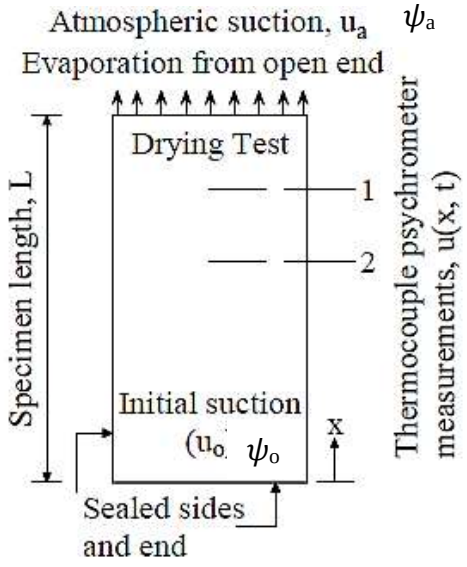

Figure 3.1 Schematic Drawing of Diffusivity Test (Adapted from Mabirizi and Bulut 2010).

This method is first postulated by Richards and Weeks (1953), and later developed and used by other researchers (e.g. Watson 1966; Hamilton et al. 1981; McCartney et al. 2007). In this study, IPM is adopted to determine the permeability coefficient for the samples in the diffusivity test. As the evaporation begins from one side of the sample, which has initially constant suction, moisture gradient will be launched in the soil sample profile. While the thermocouple psychrometer only measures suction, water content can be derived from the SWCC and substituted in Equation 3.13. If a is any point in the sample profile, A is the cross sectional area of the sample, ΔV_w is the volume of water that pass through A at this point, i is the hydraulic gradient at this point, and Δt is the change in time, then, Darcy's permeability coefficient is given as follows:

$$k = \frac{-1}{i}\frac{\Delta V_w}{A\,\Delta t} \qquad (3.13)$$

The details of how to obtain ΔV_w and i in the IPM model is explained in Lu and Likos (2004).

3.3 The Permeability and Diffusivity Function Derived from SWCC Models versus Experimental Data

In this section, a comparison between the permeability and diffusivity function predicted from the SWCC models and experimental results from diffusivity test and instantaneous profile method (IPM) are conducted. The experimental results are extracted from Thakur (2005). The results show that the SWCC models underestimate both parameters by several orders (Figure 3.2 and 3.3). However, the results from IPM come in a relatively good agreement with those from diffusivity testing method (Figure 3.4). This can be attributed to the theoretical backgrounds that have led to development of these models since they neglect the physicochemical phenomena which play an important role in the water flow in clay soils. Besides, in most cases these models are validated for sandy or silty sandy soils since clay soils have low permeability properties which make it a challenging and time consuming task to measure the permeability and diffusivity function in the laboratory.

Even though the experimental results in Figure 3.2 and 3.3 come higher than SWCC models, their slope is similar. The latter may mean if the SWCC model is corrected by some factor, the results may attain good agreement. That will be discussed in the next section.

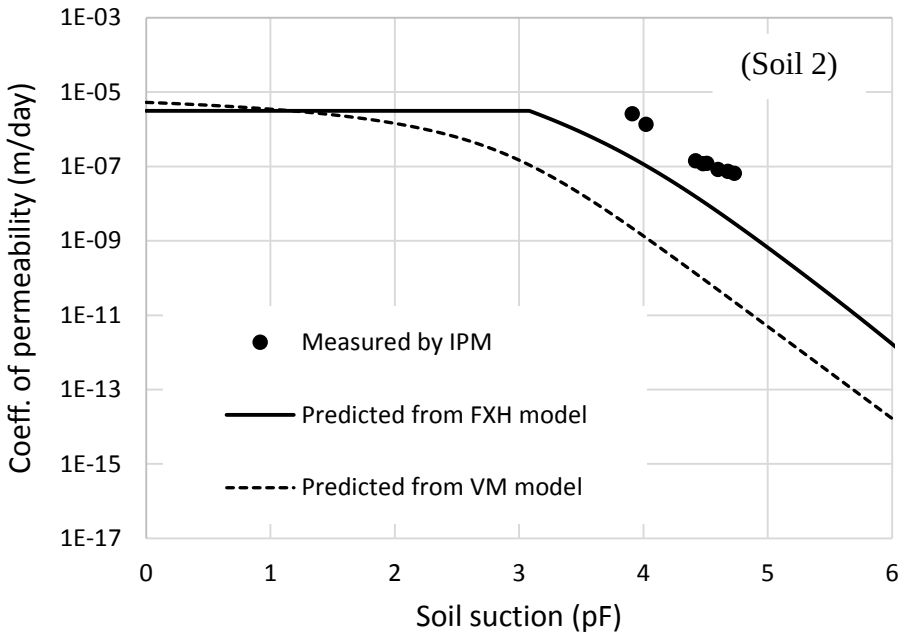

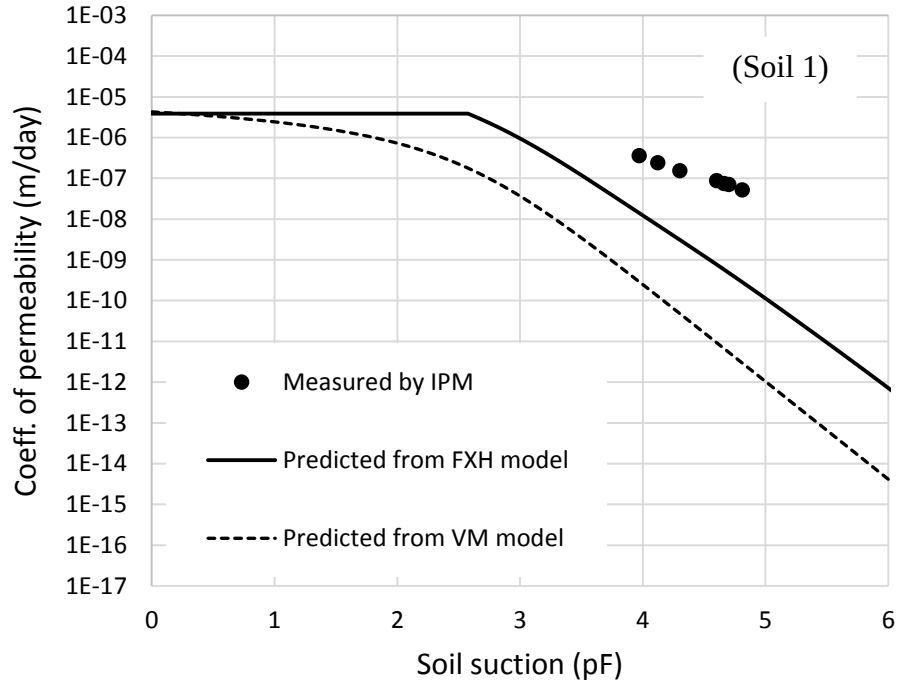

Figure 3.2 Comparison between the Permeability Function Derived from IPM and That from SWCC Models (Texas soil)

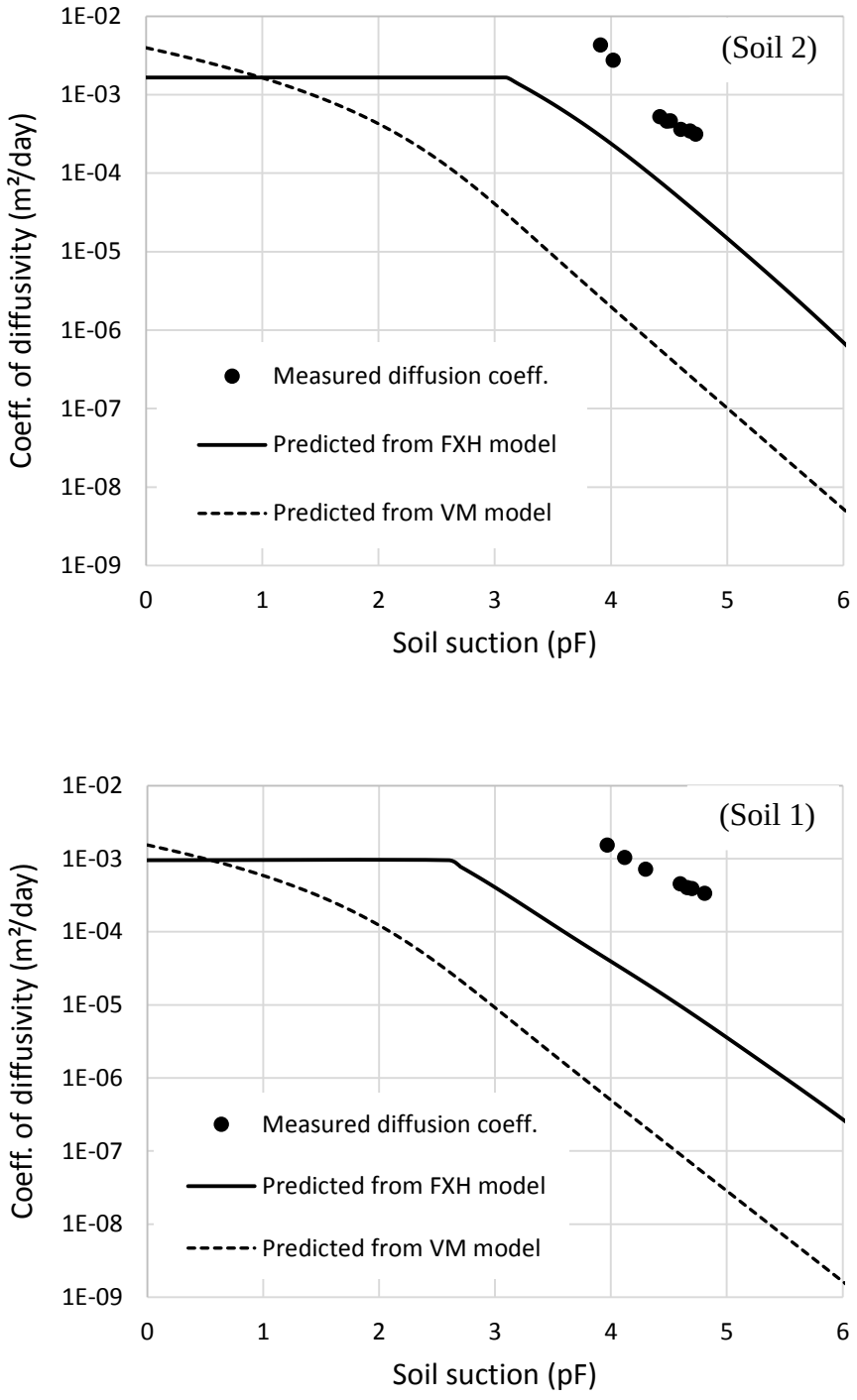

Figure 3.4 Comparison between the Diffusivity Function Measured from Diffusivity Test and That from SWCC Models (Texas soil)

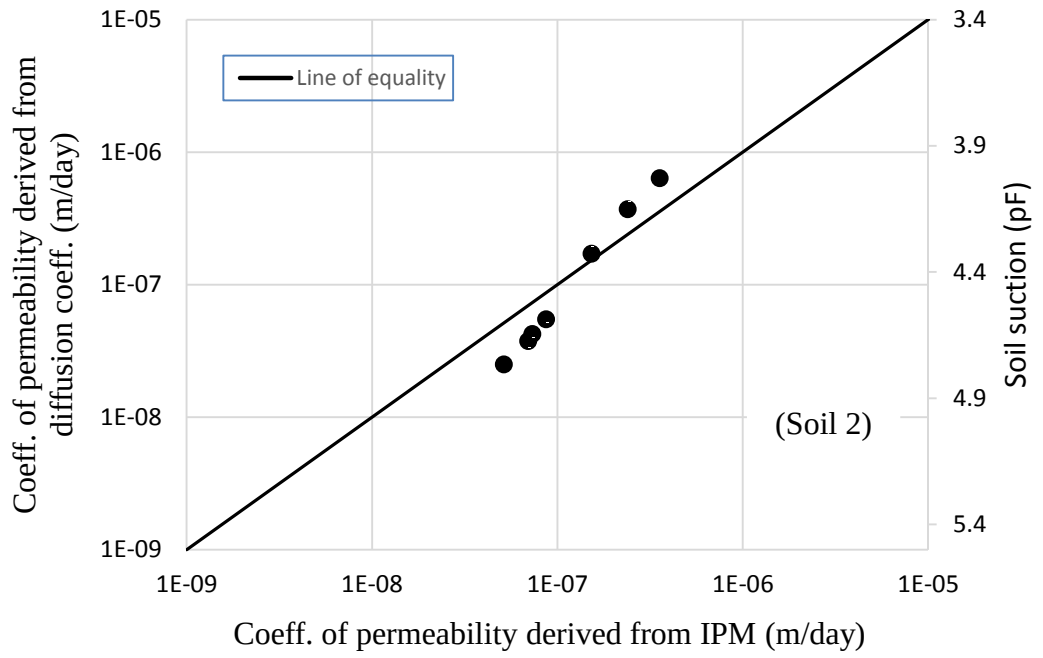

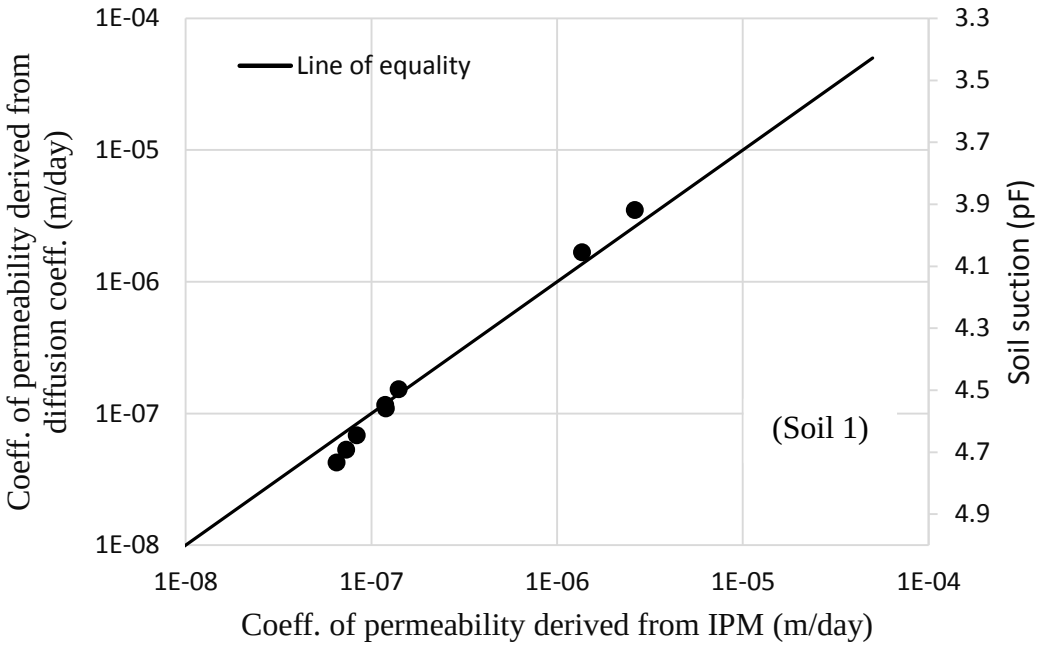

Figure 3.5 Comparison between the Permeability Function Derived from IPM and That from Diffusivity Test (Texas soil)

3.4 A Correction Factor for the Prediction of Permeability and Diffusivity Function of Fine-Grained Soils from SWCC Models

Referring to the previous section that the SWCC models underestimate the permeability and diffusivity functions but with similar slopes from the experimental results, a correction factor is proposed hither. The idea to correct for the prediction of the permeability function has also been suggested by Mualem (1986) and Fredlund et al. (1994). However, the correction factor proposed by the latter authors takes into account the tortuosity in the soil which decreases the predicted permeability. Fredlund et al. (1994) equation with the correction factor, *F*, can then be written as follows:

$$k(\psi) = F\, k_{sat} \frac{\int_{\psi}^{\psi_r} \frac{w(y) - w(\psi)}{y^2} w'(y) dy}{\int_{\psi_{aev}}^{\psi_r} \frac{w(y) - w_s}{y^2} w'(y) dy} \tag{3.14}$$

The parameters of the above equation are identified in Section 3.2.1. The correction factor can also be applied to the empirical models. Leong and Rahardjo (1997) stressed that most of empirical equations for the prediction of the permeability function from the SWCC can be represented by the following equation:

$$k(\psi) = k_s \Theta^p \tag{3.15}$$

In terms of the correction factor, it can be rewritten as follows:

$$k(\psi) = F\, k_s \Theta^p \tag{3.16}$$

Where k_s is the saturated coefficient of permeability, Θ is the effective saturation, p is an exponent fitting parameter. The effective saturation is given as follows:

$$\Theta = \frac{\theta - \theta_r}{\theta_s - \theta_r} \tag{3.17}$$

Where θ_r is the volumetric water content at the residual stage and θ_s is the volumetric water content at the fully saturation condition. The effective saturation can also be expressed by any SWCC model. For Fredlund and Xing (1994) model, it can be written as follows:

$$\Theta = \frac{1}{\{\ln[e + (\psi/a)^n]\}^m} \qquad (3.18)$$

Substituting Equation 3.18 in 3.16, Equation 3.16 can be rewritten as follows:

$$k(\psi) = F\, k_s \left[\frac{1}{\{\ln[e + (\psi/a)^n]\}^m}\right]^p \qquad (3.19)$$

To check the concept of the correction factor proposed in Equations 3.14 and 3.19, experimental results from Thakur (2005) are employed. The results are derived from diffusivity tests, explained in Section 3.2.2, for undisturbed samples of two clayey soils from Texas. The basic geotechnical properties of the two soils are listed in Table 3.1. The SWCC of both soils is depicted in Figure 3.6. The results of the permeability function based on Equations 3.14 and 3.19 against the experimental results are illustrated in Figure 3.7. The diffusivity function is also determined from Equation 3.7 using the predicted permeability function and the slope of the SWCC and plotted against the experimental results in Figure 3.8.

Table 3.1 Properties of Studied Soils

	Soil (1)	Soil (2)
Passing sieve No. 200 (%)	100	100
Clay content (%)	25	25
Liquid Limit (%)	50	49
Plasticity Index (%)	32	30
Initial suction (pF)	3.47	3.81
Dry unit weight (gm/cm^3)	1.5	1.51
Sat. coeff. of perm. (m/day)	1.04E-05	9.50E-06

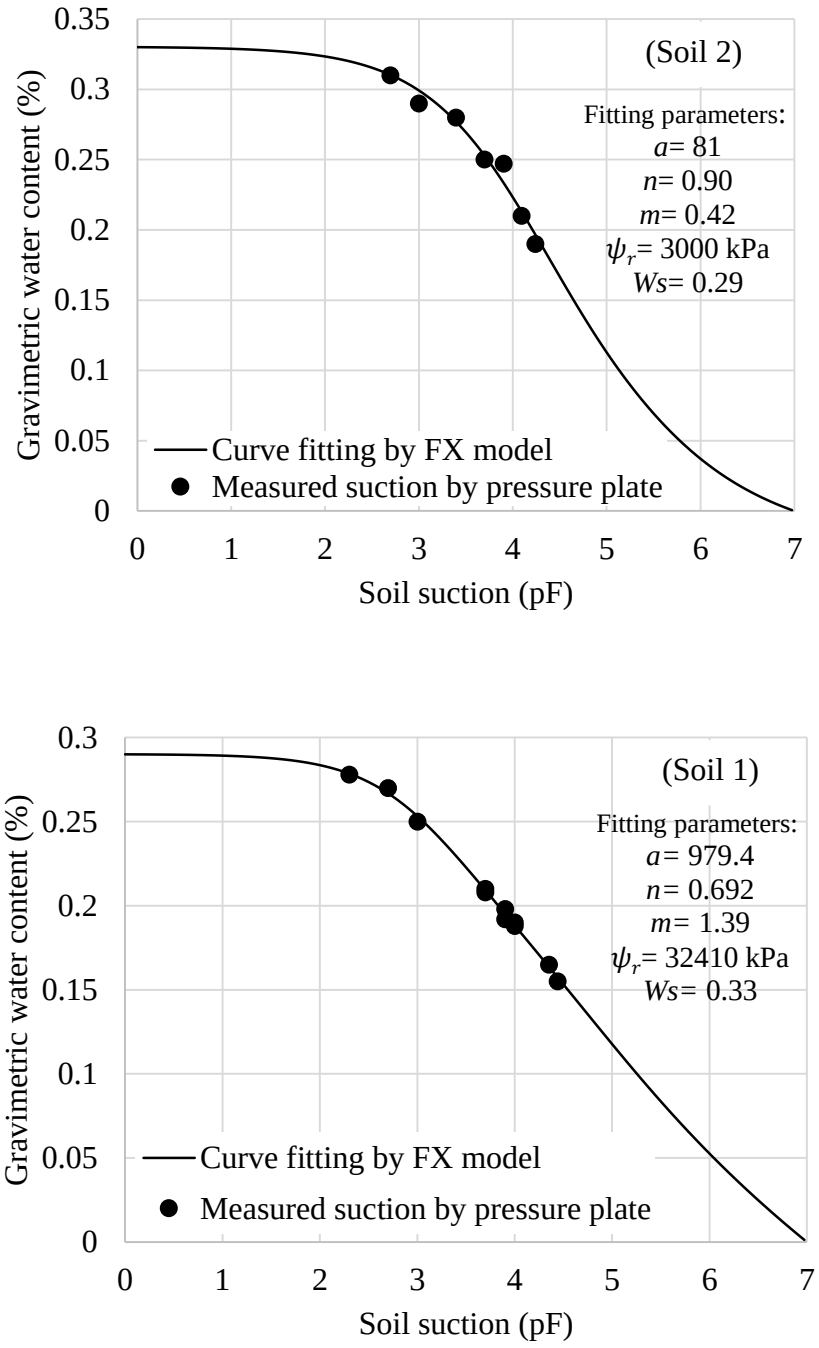

Figure 3.6. The SWCC of the Two Soils Studied (Experimental Data from Thakur (2005), Texas soil)

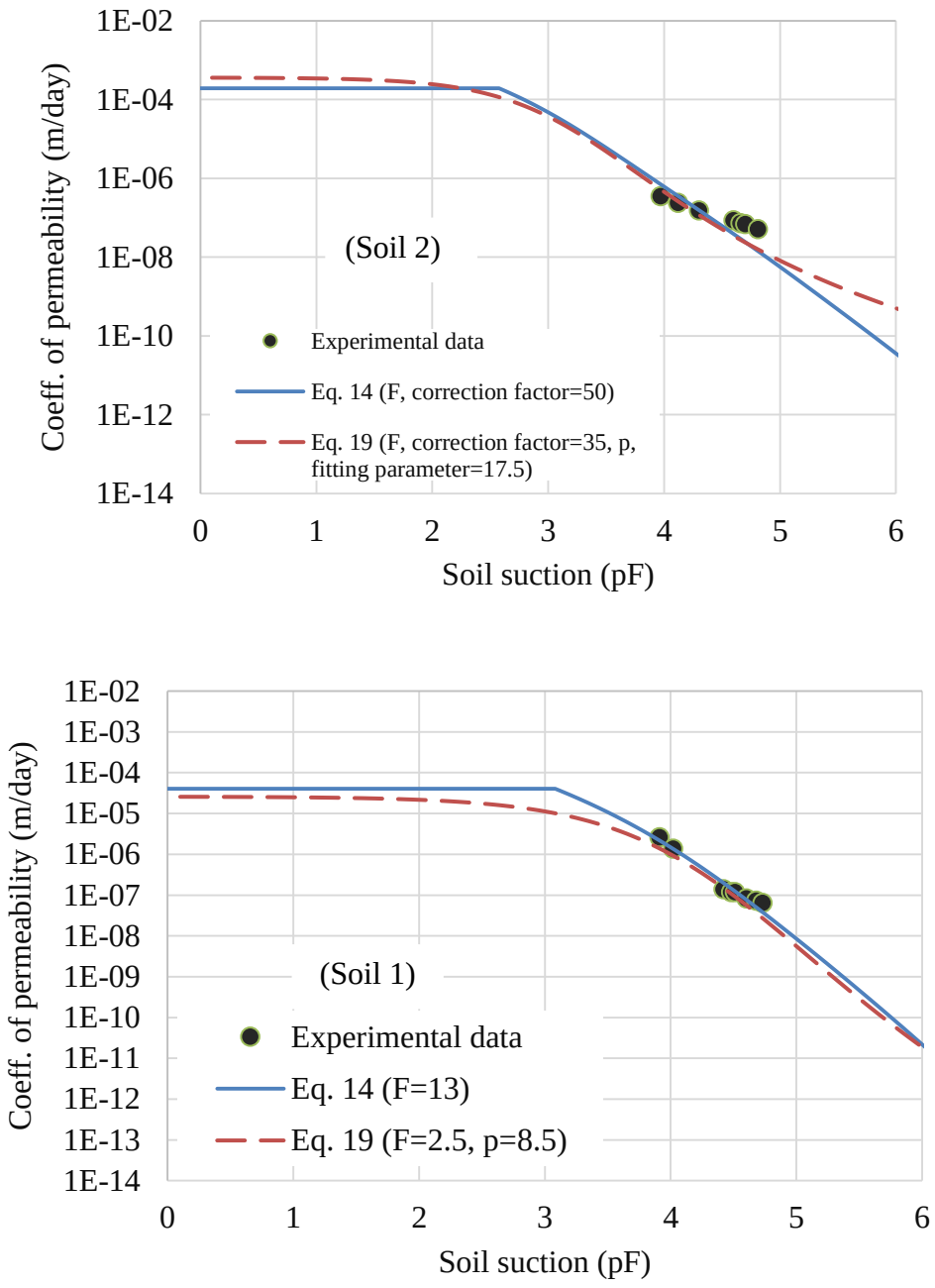

Figure 3.7 Adjusted Permeability Function against the Experimental Results

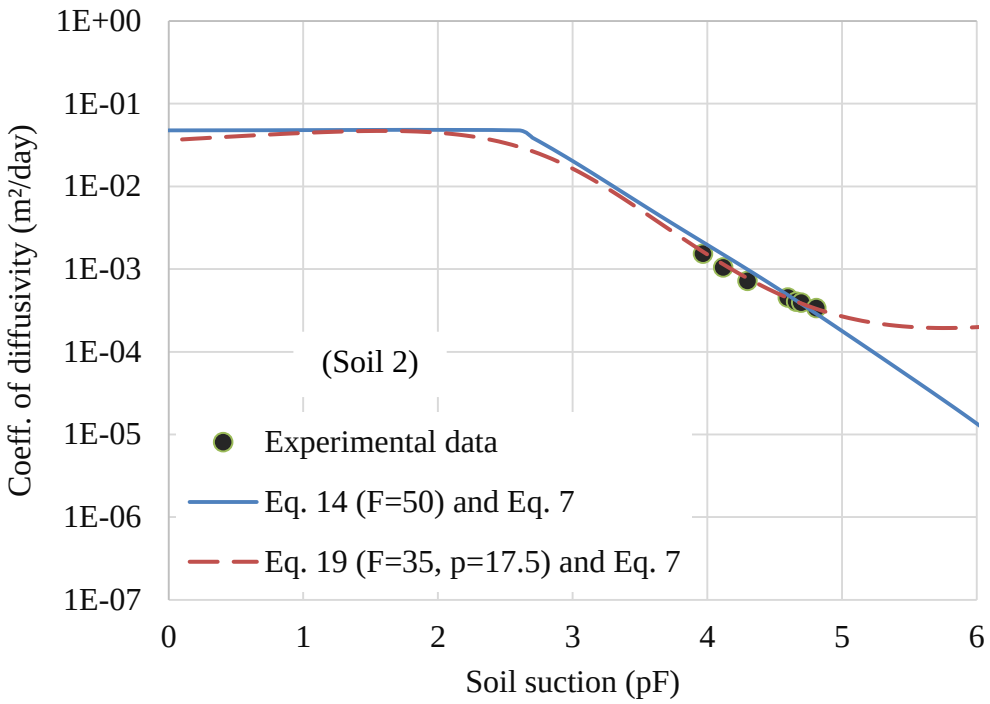

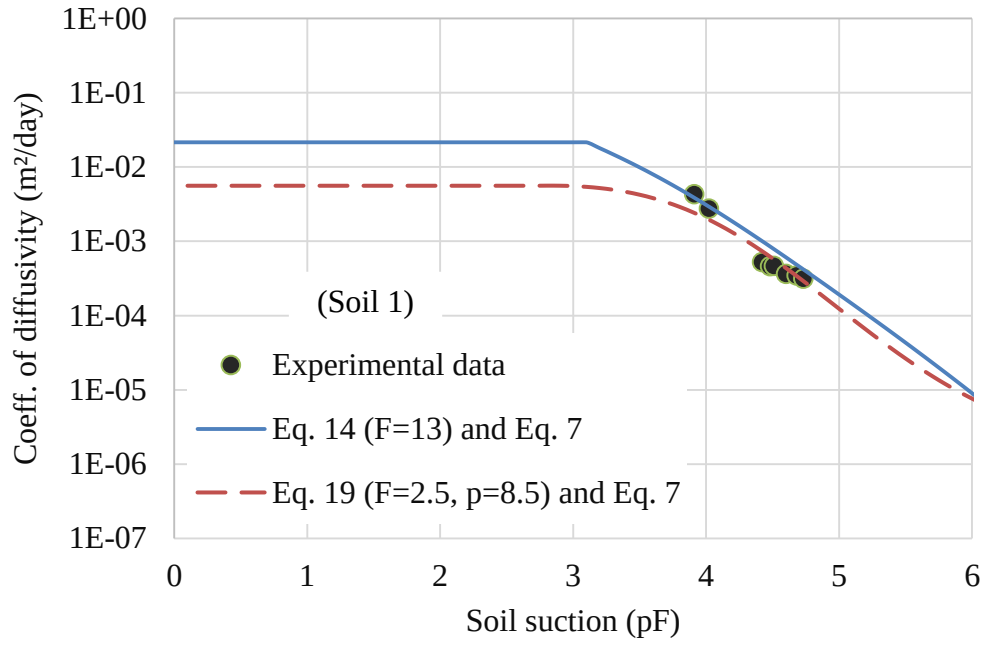

Figure 3.8. Diffusivity Function Derived from the Adjusted Permeability Function and the Slope of the SWCC Using Equation (3.7) versus Experimental Results (Texas soil)

Figure 3.7 and 3.8 show that the correction factor gives better prediction that is in a good agreement with the experimental data for both the permeability and diffusivity functions using the corrected Fredlund et al. (1994) model (Eq. 3.14) or the corrected general empirical model (Eq. 3.19). Due to the limited test results analyzed herein, no relationship is built for the correction factor. Nevertheless, the results indicate that the correction factor, F, may correlate to the fitting parameter *a* of the SWCC, which is related to the air entry value. Large *a* value reveals small F. The empirical equation provides a residual zone of the predicted permeability and diffusivity functions at high suction levels which indicates a realistically predicted tendency of both functions. In the empirical model the fitting parameter, p, controls the slope of the curve while the F parameter can shift the slope for the desire range, which gives high flexibility of prediction. The estimated p parameter for both soils is higher than the reported values in Fredlund et al. (2012). It is recommended for future research studies that the correction factor idea is improved for better prediction of permeability properties of clay soils. More experimental data for a wide suction range can possibly lead to relations between the correction factor and other soil parameters such as the SWCC fitting parameters.

3.5 Summary

This chapter presents the prediction of the permeability and diffusivity functions from the SWCC using two frequently used models (i.e. FXH and VM). It demonstrates the level of shortcomings of these models by comparing their results against those predicted experimentally for clayey soils by the diffusivity test and instantaneous profile method. These models significantly underestimate both functions for clayey soils because they do not take into account the physicochemical interactions between the clay particles and water which has an important role in water transformation and also they are rarely validated with the experimental data of clayey soils for wide suction range. To address that, a correction factor is proposed. The corrected FXH model and general empirical equation render high agreement with the experimental results. More experimental

results on clay soils are needed for more validation studies of the SWCC models and to find relationships between the correction factors and some other soil parameters, particularly curve fitting parameters of the SWCC.

CHAPTER IV

VOLUMETRIC STRAIN IN SATURATED AND UNSATURATED SOILS DUE TO SUCTION CHANGE

4.1 Abstract

The soil volumetric strain due to the suction change has a significant importance in the geotechnical and geoenvironmental engineering. It causes distresses to the overlying structures (e.g. pavements), buried structures (e.g. pipelines), and lateral structures (e.g. retaining walls). The volume change can lead to cracking in the soil layers utilized for the environmental purposes and thus losing their functions. Further, the strain from the suction change is the hydraulic part of the soil elastic-plastic behavior. In spite of the common believe that the soil water characteristic curve (SWCC) and the soil suction-volumetric strain curve share the same basic soil features, the interpretation of the suction-strain relation in a single framework with the soil water characteristic curve (SWCC) has not been well explained. This research provides new understanding to the volumetric strain corresponding to the suction change. Based on the explanation of the soil shrinkage characteristic curve (SHCC), this study, first, demonstrates that both the SWCC and SSSC have a unique slope referred to as the virgin line. Second, both slopes can be related in a simple equation which covers wide range of volume change. Finally, a unified framework is presented for the relation among the water content, suction, degree of saturation, and volume change for clay soils.

4.2 Introduction

Since the swelling and shrinkage of expansive soils cause significant problems to many geotechnical and geoenvironmental engineering applications, the prediction of volume change has been paid extensive attention. Research studies and specialty conferences have been undertaken exclusively for this subject. Basically, the expansive soils show swelling when wetting and shrinkage when drying. The level of volume change mainly depends on the soil volume change potential, moisture permeability properties, and the boundary conditions, mainly the environmental conditions. Different methods have been proposed to evaluate the soil volume change potential. In general, these methods can be categorized in three groups: consolidation based methods, empirical based methods, and suction based methods (Lytton et al. 2004). Among them, the suction based methods are preferable because the soil suction is the driving parameter to the volume change in the soil and also it is a stress state variable governing the soil behavior (Fredlund et al. 2012). Most approaches of predicting the soil volume change potential or modelling the soil behavior adopt a linear response of the soil deformation to the change of suction in the logarithm scale. While this is true for a narrow range of suction experienced in the field, building the soil volume change characteristics can lead to accurate prediction of the swelling and shrinkage behavior and better modelling to the saturated and unsaturated soil behavior.

This chapter presents new interpretation to the soil volumetric strain due to the suction change. First, it will be shown that the slopes of the soil water characteristic curve (SWCC) and the void ratio-suction curve (e-log s curve) are unique and the virgin lines for both curves. Both slopes can also be related in a simple equation. This chapter demonstrates a better interpretation of both curves in a unified framework. Finally, it is emphasized that both curves can be modelled with the same closed form equation but with different fitting parameters.

4.3 Soil Shrinkage Characteristic Curve

The soil shrinkage characteristic curve (SHCC) is the relationship between the water content and the void ratio. Typically, the SHCC is divided into three zones: the normal shrinkage, the residual shrinkage, and the zero shrinkage. The three zones of shrinkage are depicted in Figure 4.1. SHCC shows that the soil experiences linear shrinkage within the normal shrinkage zone wherein the loss of water is compensated by a reduction in the void volume to keep the degree of saturation close to 100% until it reaches the air entry point where the shrinkage becomes non-linear (i.e. the loss of water is greater than the reduction of the volume of voids). Then, the shrinkage almost ceases at the point of shrinkage limit (S.L.), wherein the soil reaches its minimum void ratio. Therefore, the shrinkage behavior in the soil with regard to the SHCC can be divided into two stages, linear shrinkage in the saturated (or near saturated) regime and non-linear shrinkage in the unsaturated regime. The slope of linear shrinkage is equal to the specific gravity per the degree of saturation (Gs/S).

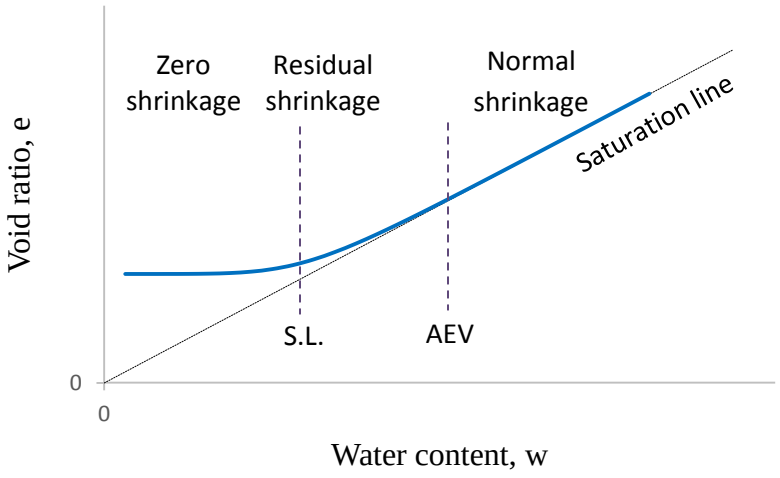

Figure 4.1 Typical Shape of the Soil Shrinkage Characteristic Curve (SHCC)

The approach is probably valid for pure clay soils in slurry form desiccating from full saturation. For soils with high sand content, structural shrinkage prior to the normal shrinkage stage can exist

particularly for compacted soils (Peng et al. 2009; Li et al. 2014). The structural shrinkage occurs due to the drying from the macropores that exist between coarse particles in the soil mass (Chertkov 2007). Table 4.1 lists data from Rao (2012) showing shrinkage magnitude for each stage of two compacted soils. One is referred to as black cotton soil (BCS) with high montmorillonite content, and the other is referred to as red soil (RS) with high kaolinite content. Figure 4.2 depicts shrinkage curves for BCS with different compaction conditions. This chapter only focuses on the SHCC of pure clay soils, and no more discussion about structural shrinkage will be given. How to derive the SHCC for only clay portion from the SHCC of the soil is explained by Chertkov (2007).

Table 4.1 Shrinkage Magnitude for Two Compacted Soils to the Maximum Dry Density and Optimum Moisture Content (After Rao 2012)

Soil name	Sand	Silt	Clay	Liquid limit %	Plastic limit %	OMC %	MDD, g/cm3	Shrinkage magnitude		
								SS %	PS %	RSH %
BCS	16	29	55	84	23	28	1.42	3.88	24.43	5.96
RS	59	16	24	39	19	17	1.73	2.34	4.56	0.61

OMC: optimum moisture content of standard Proctor, MDD: maximum dry density of standard Proctor, SS: structural shrinkage, PS: primary shrinkage, RSH: residual shrinkage

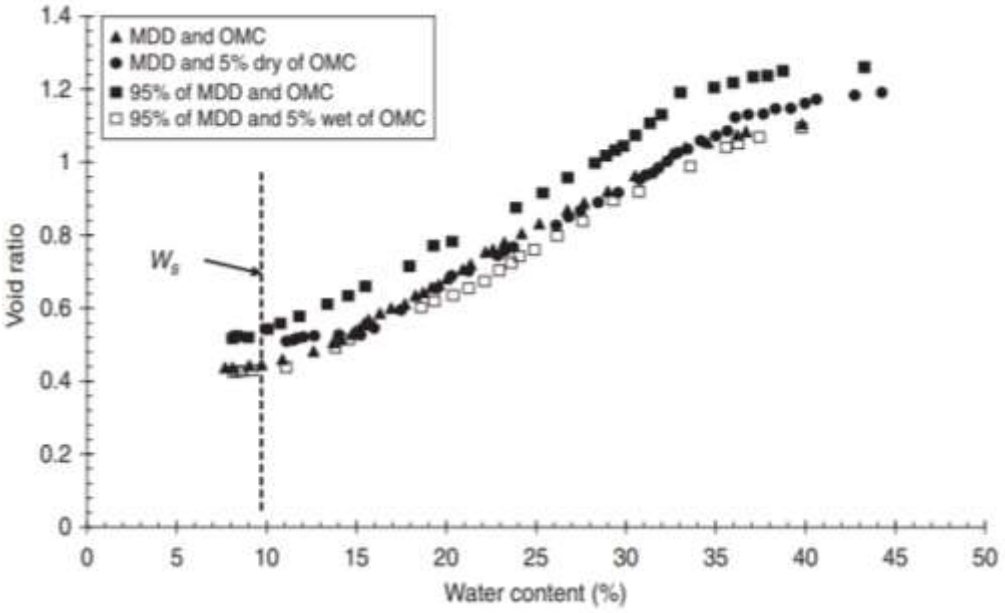

Figure 4.2 Shrinkage Curve for High Expansive Soil (BCS1) for Different Compaction Conditions (Rao 2012).

The interpretation of the two stages of shrinkage zones (i.e. normal and residual) from the microscale level of soil pores can be understood from the swelling process (Braudeau et al. 2004) since the swelling is reverse to the shrinkage. In swelling, pores of expansive soils can accommodate several layers of water (Likos 2004), owing to the large cation exchange capacity and substantial isomorphous substitution of the clay particles (e.g. montmorillonite) in addition to their high specific surface area (Mitchell and Soga 2005). Such water layers constitute the diffuse double layer. In shrinkage, as the soil is drying and decreasing the water content, the layers of water will be reduced. However, when the air bubbles enter the water-soil particles system (Fig. 4.3b), the shrinkage tendency will start to decrease with the decrease of water content and the increase of air until it ceases at the shrinkage limit, the loss of water is substituted by air (Fig. 4.3c)

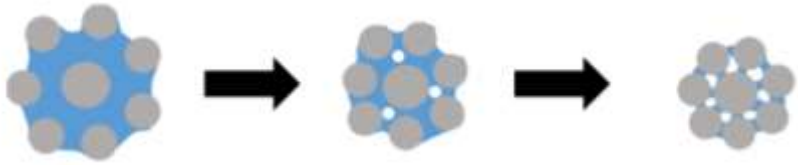

(a) **(b)** **(c)**

Figure 4.3 Micro-Pore System for Shrinkage Stages: (a) Fully Saturated State (b) State of the Air Entry (c) State of Shrinkage Limit.

Since the soil volume change generally depends on the plasticity level, the plasticity index (PI) controls the shape of the SHCC. The higher is the PI, the greater is the void ratio at the air entry stage, and thus the residual shrinkage (Fig. 4.4).

Moreover, the shrinkage limit (SL) depends on the liquid limit (LL). Soils with high LL usually have lower SL (Rao 2012).

Several closed form equations have been proposed in the literature to model the SHCC (Fredlund et al. 2002; Cornelis et al. 2006; Leong and Wijaya 2015). In this study, the Fredlund et al. (2002) model will be employed. It is given as follows:

$$e(w) = a\left[\frac{w^c}{b^c} + 1\right]^{\left(\frac{1}{c}\right)} \qquad (4.1)$$

Where $e(w)$ is the void ratio for a given water content (w), a, b, and c are curve fitting parameters.

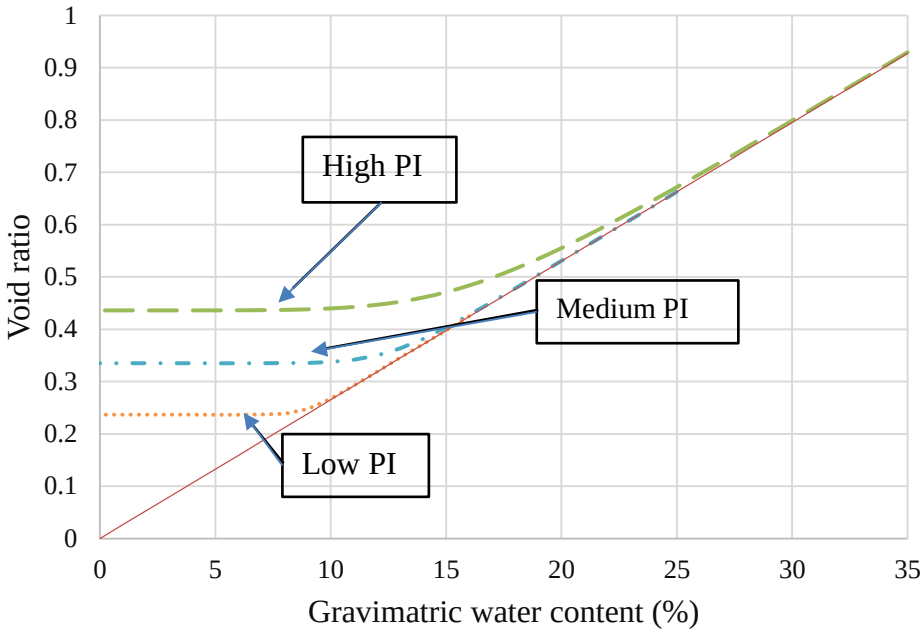

Figure 4.4 SHCC for Different PI Levels

The SHCC has a considerable effect on the determination of the air entry value (AEV) from the soil water characteristic curve (SWCC), and hence the final shape of the SWCC. Representing the SWCC by the degree of saturation instead of the gravimetric or volumetric water content to take the volume change into account is essential to correct for the actual AEV (Fig. 4.5) (Houston and Fredlund 2013; Wijaya et al. 2015; Bani Hashem and Houston 2015).

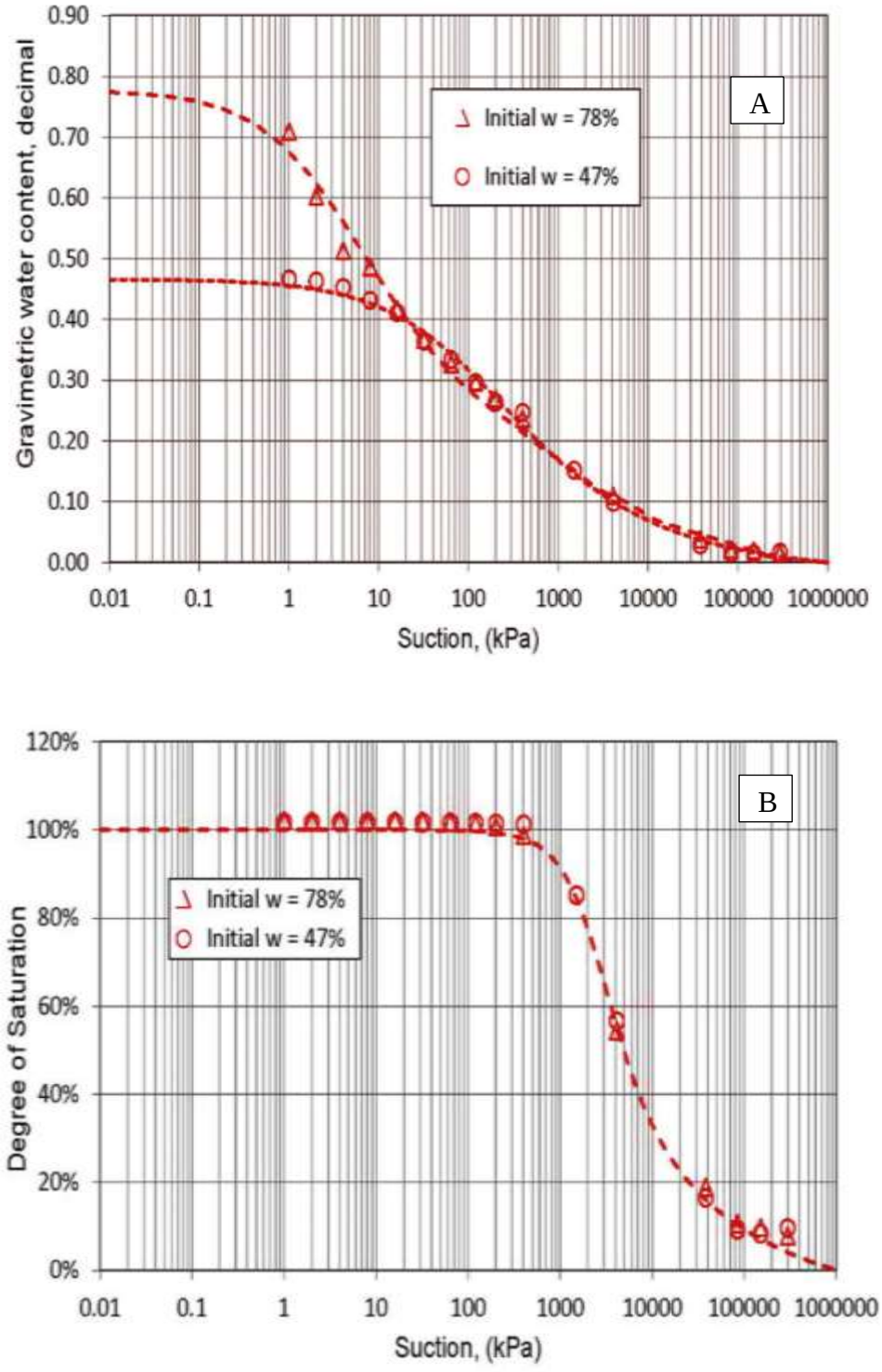

Figure 4.5 The Effect of the Volume Change on the SWCC (Fredlund and Houston 2013).

A) Suction vs. Water Content, B) Suction vs. Degree of Saturation (Oil Sands Tailings Soil)

4.4 Suction-Strain Relationship

The SHCC can be represented by suction instead of water content. Suction-void ratio curve (e-log s) provides an important tool to model the volume change as a consequence of the change in suction profile. The e-log s curve can be constructed if both SWCC and SHCC are known. Figure 4.6 depicts a SWCC in terms of the gravimetric water content and the degree of saturation for a soil, and Figure 4.7 shows the SHCC for the same soil. The e-log s curve for this soil is then generated and illustrated in Figure 4.8. The three relations (i.e SWCC, SHCC, e-log s curve) can be interpreted in a unified framework. The point p in the suction vs. water content curve in Fig. 4.6 corresponds to the pre-shrinkage suction in Fig. 4.8. However, the AEV in the suction vs. degree of saturation in Fig. 4.6 corresponds to the point of AEV in Fig. 4.7 as well as in Fig. 4.8.

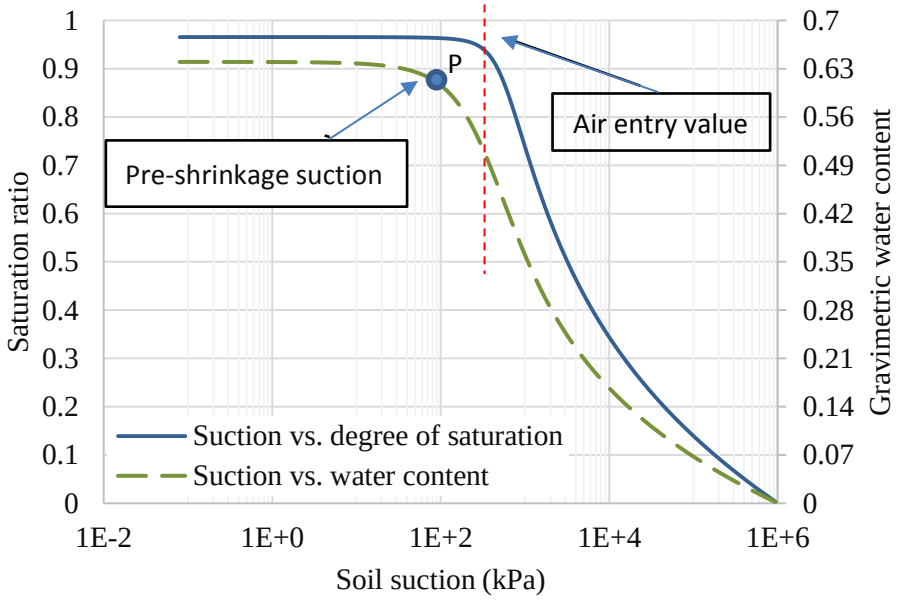

Figure 4.6 SWCC of Expansive Clay from Karnataka State (Generated from the Curve Fitting Parameters for Data from Thyagaraj and Rao (2010), Cited in Wijaya et al. (2015))

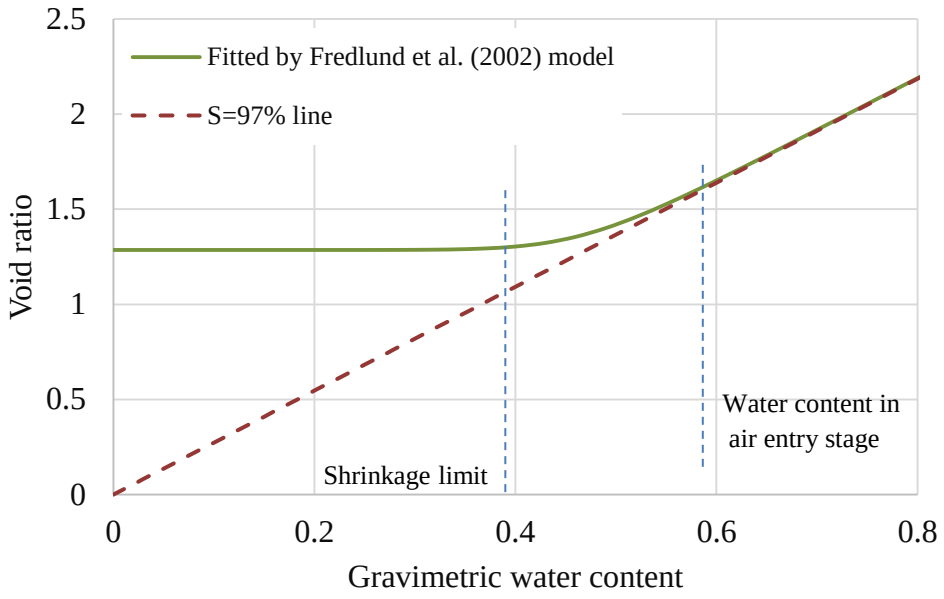

Figure 4.7 SHCC of Expansive Clay from Karnataka State (Generated from the Curve Fitting Parameters for Data from Thyagaraj and Rao (2010), Cited in Wijaya et al. (2015))

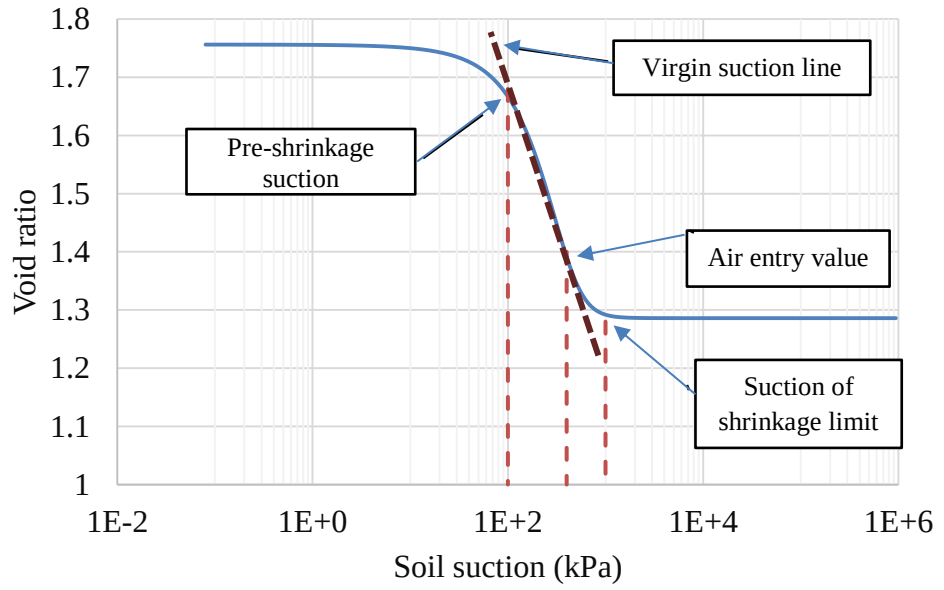

Figure 4.8 The e-log s Curve of Expansive Clay from Karnataka State (Generated from the Curve Fitting Parameters for Data from Thyagaraj and Rao (2010), Cited in Wijaya et al. (2015))

Moreover, the shrinkage limit in the SHCC and e-log s curves does not correspond to the residual suction or water content in SWCC. Clear evidence for it is that, as can be seen from SHCC, the water content at the air entry value and the shrinkage limit for the low PI soils are very close (or even the same point), which essentially leads to considering the AEV being the residual suction as well.

Referring to the analogy between the e-log s curve and the classical e-log p curve, where p is the effective applied pressure, the linear line from the pre-shrinkage suction point to the shrinkage limit of suction in Fig. 4.8 is the virgin shrinkage line which is similar to the virgin compression line in the e-log p curve. Data from Fredlund et al. (2011) for e-log s curve shown in Figure 4.11 can indicate that the soil shows similar virgin line or slope even though it starts drying from different void ratios. The latter explanation for e-log s curve can be extended to the SWCC. The SWCC also has such a unique virgin line for suction as shown in Fig. 4.9 (Li et al. 2014) and Fig. 4.10 (Fredlund et al. 2011) so that in spite of starting drying from different water contents and densities, all curves unify in the virgin suction line to render the same slope for SWCC. That is because different initial densities from various compaction efforts slightly or do not change much the pore size distribution of the soil particles (Li et al. 2014). However, it is conservative to extend the latter concept to the difference between the drying SWCC of slurried and compacted soils (see Bani Hashem 2013).

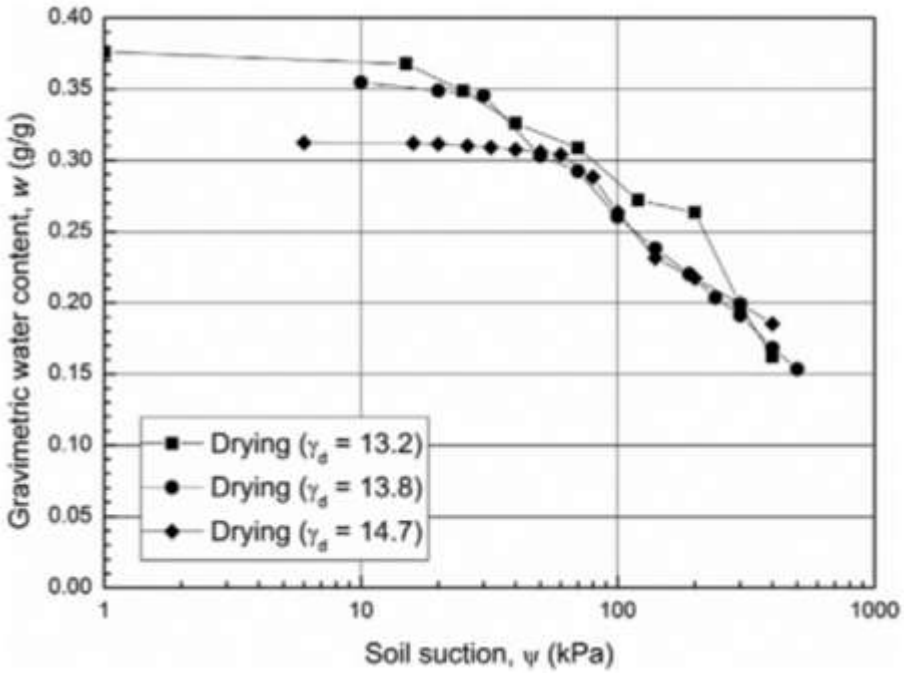

Figure 4.9 SWCC for Silty Clay Soil with Sand for Different Densities (Adapted from Li et al. (2014)).

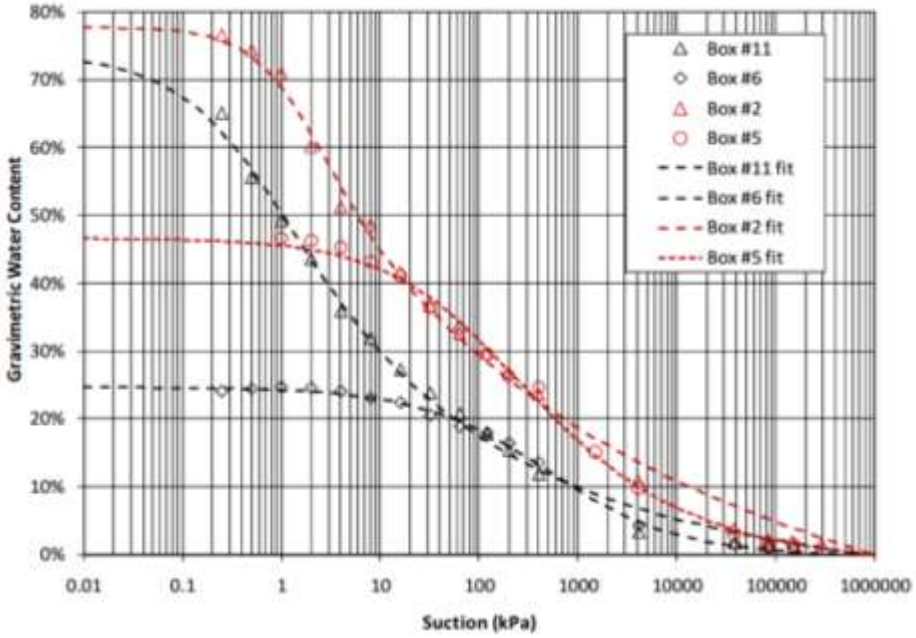

Figure 4.10 SWCC for Oil Sands Tailings, Slurry Samples with Two Initial Water Contents (adapted from Fredlund et al. (2011))

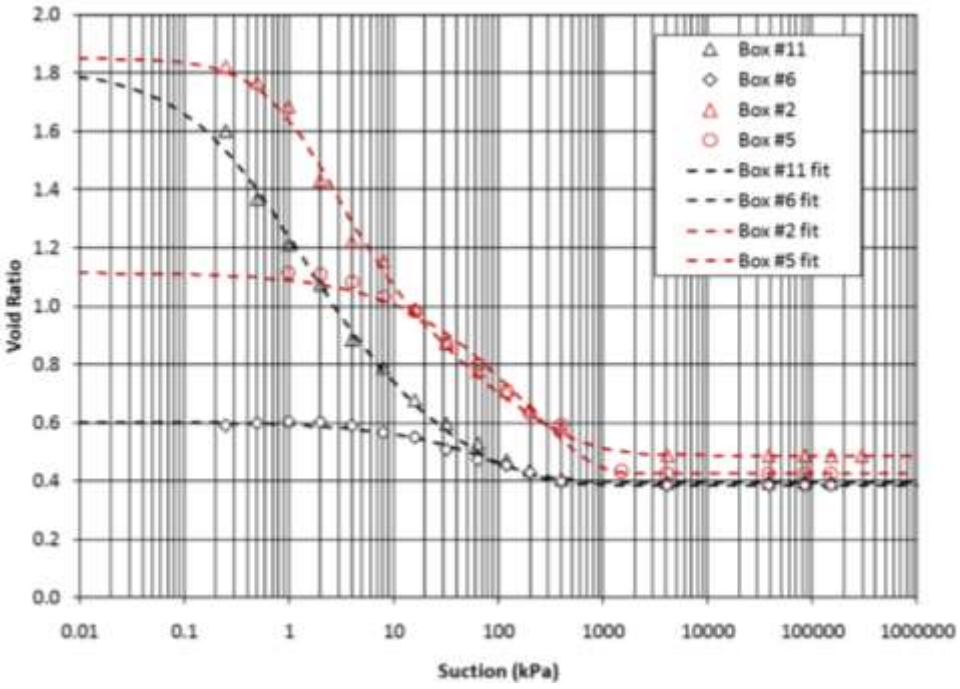

Figure 4.11. The e-log s Curve for Oil Sands Tailings, their SWCC Shown in Fig. 4.10 (Adapted from Fredlund et al. (2011))

4.5 The Link between SHCC and SWCC

It has always been of interest to directly connect the soil volume change to the soil water characteristic curve (SWCC) since both mainly depend on the soil mineralogy such that they share the same soil features. For example, the shape of the SWCC can be derived from the soil grain size distribution and Atterberg limits (Lytton 1994; Zapata et al. 2000; Lytton et al. 2004). McKeen (1992) classified the soil volume change potential based on the slope of the SWCC ($\Delta h/\Delta w$) for suction (h) being in pF, or *log* kPa (Table 4.2).

Table 4.2 Volume Change Classification Based on the SWCC Slope (McKeen 1992)

Cat.	Δh/Δw	Remarks
I	> -6	Special Case
II	-6 to -10	High
III	-10 to -13	Moderate
IV	-13 to -20	Low
V	< -20	Nonexp.

In this section the slope of the SWCC is linked to the slope of the e-log s curve using a simple method. From the SHCC (Fig. 4.12), the normal shrinkage strain (ε_v) is given as follows:

$$\varepsilon_v = \frac{Gs/S}{1+e_o}\Delta w\,, \qquad \varepsilon_v = \Delta e/(1+e_o) \tag{4.2}$$

Where Gs/S is the slope of SHCC, Gs is the specific gravity, S is the degree of saturation, and e_o is the initial void ratio.

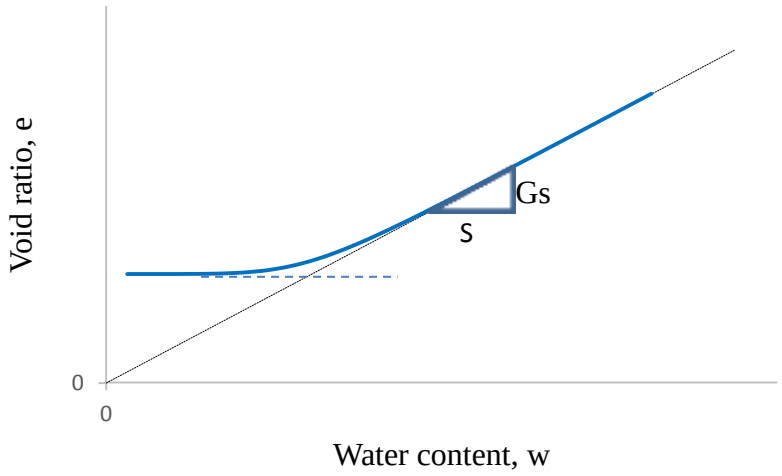

Figure 4.12. The Slope of Normal Shrinkage in SHCC

The normal shrinkage takes place at a single degree of saturation, being unity for fully saturated soils. As explained previously, the slope of SWCC and SHCC is referred to as suction virgin line (SVL). Therefore, the suction range from the pre-shrinkage suction point to the AEV (or to the end of the normal shrinkage stage in case of compacted soils) falls on the suction virgin line of both SWCC and e-log s curve, and the normal shrinkage zone of SHCC. This approach is illustrated using Figures 4.13, 4.14a, 4.14b for the SHCC, SWCC, and e-log s curves, respectively, for the Lake Hefner soil from Oklahoma. This soil can be considered low to moderate in expansivity. Therefore, considering the SVL of SWCC and the slope of the suction vs. water content, (e.g., $S_w = \frac{\Delta w}{\Delta \log s}$), Equation 4.2 can be rewritten as follows:

$$\varepsilon_v = \frac{\frac{Gs}{S}}{1 + e_o}\left(S_w \, log \frac{s_{aev}}{s_p}\right) \tag{4.3}$$

Where s_{aev} is the air entry value, and s_p is the pre-shrinkage suction. Since the slope of SVL of e-log s curve is the suction compression index, $SCI = \frac{\varepsilon_v}{\Delta \log s}$, for saturated soils the slope of drying SWCC can be related to the slope of the drying e-log s curve by the following equation:

$$SCI = \frac{Gs}{1 + e_o} S_w \tag{4.4}$$

This equation is similar in form to the one proposed by the US Department of the Army (1983). This equation represents the normal shrinkage starting from the pre-shrinkage suction. Since some soils (e.g. highly expansive soils) can show considerable residual shrinkage, however, for complete description of suction-void ratio relationship from very low suction to very high suction (e.g. beyond the shrinkage limit), e-log s curve can be modelled by the same closed form equation for SWCC. Thus, using Fredlund and Xing (1994) model, the e-log s curve is expressed as follows:

$$e(s) = e_{min} + \frac{e_o - e_{min}}{\left\{\ln\left[2.72 + \left(\frac{s}{a}\right)^n\right]\right\}^m} \tag{4.5}$$

Where e_{min} is the minimum void ratio reached at the shrinkage limit stage, e_o is the initial void ratio, *a*, *n*, and *m* are fitting parameters. Note that the values of the fitting parameters in Equation (4.5) are different from those in the SWCC model. Therefore, for predicting the strain for any suction increase, the $\varepsilon_v = \Delta e/(1 + e_o)$ equation is employed. If suction increases from s_1 to s_2, then the volumetric strain is given as follows:

$$\varepsilon_v = \frac{e_o - e_{min}}{1 + e_o}\left[\frac{1}{\left\{\ln\left[2.72 + \left(\frac{s_2}{a}\right)^n\right]\right\}^m} - \frac{1}{\left\{\ln\left[2.72 + \left(\frac{s_1}{a}\right)^n\right]\right\}^m}\right] \tag{4.6}$$

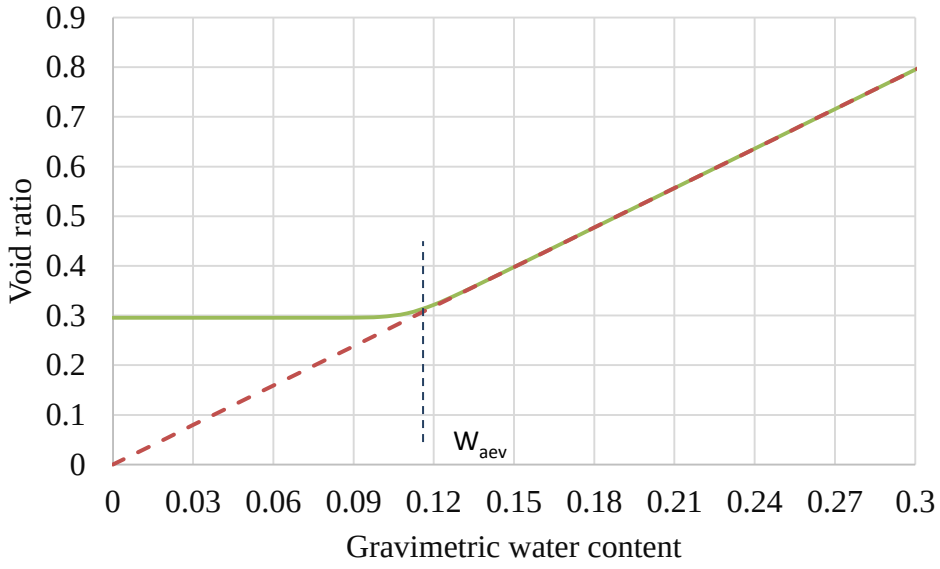

Figure 4.13. The SHCC of Lake Hefner Soil

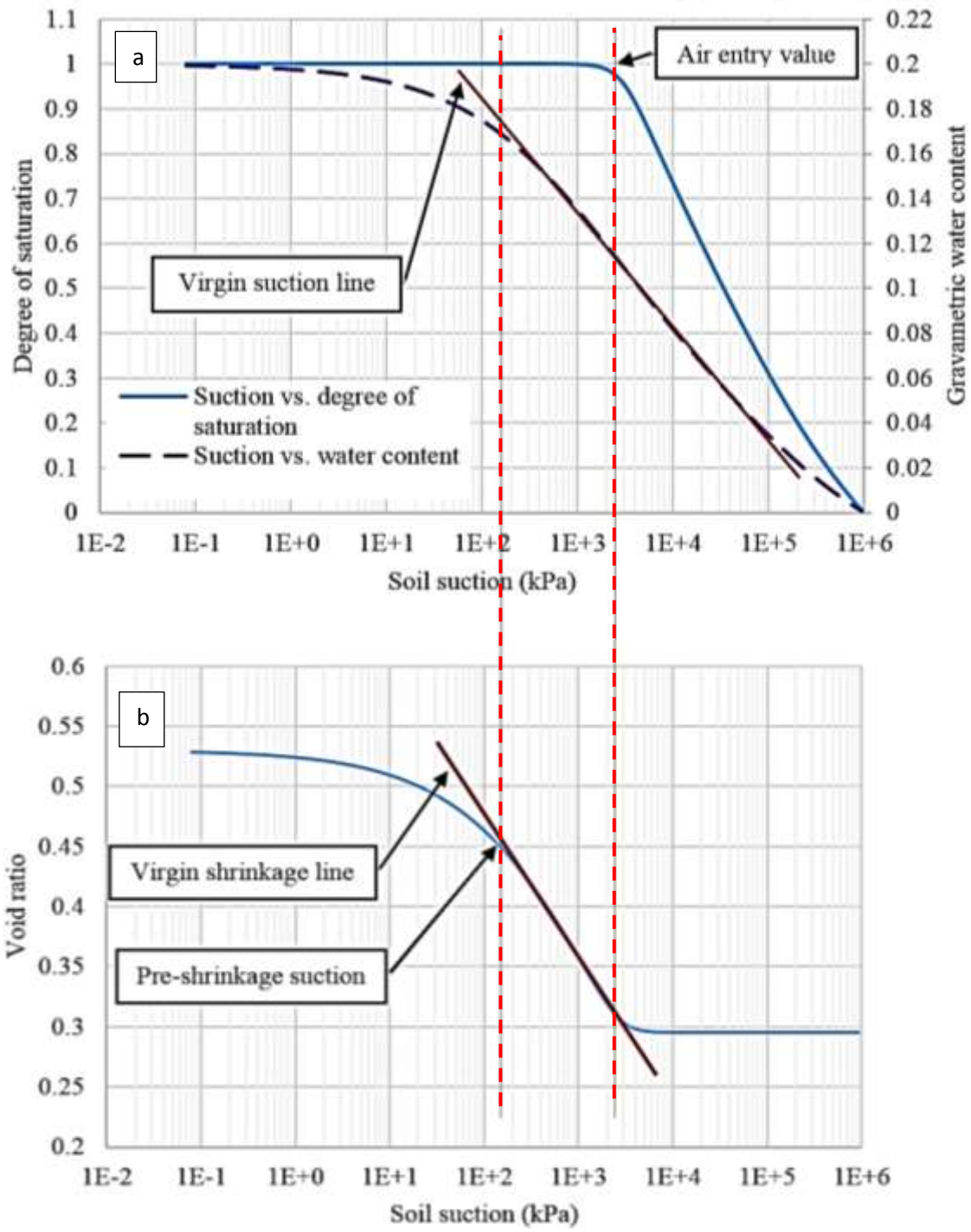

Figure 4.14 a) The SWCC of Lake Hefner soil, b) The e-log s Curve of Lake Hefner Soil

The above curves illustrate that the initial degree of saturation which is 100% for fully saturated clay soils accommodates wide range of water content until it reaches the air entry point. This concept is illustrated for Lake Hefner soil in Figure 4.15.

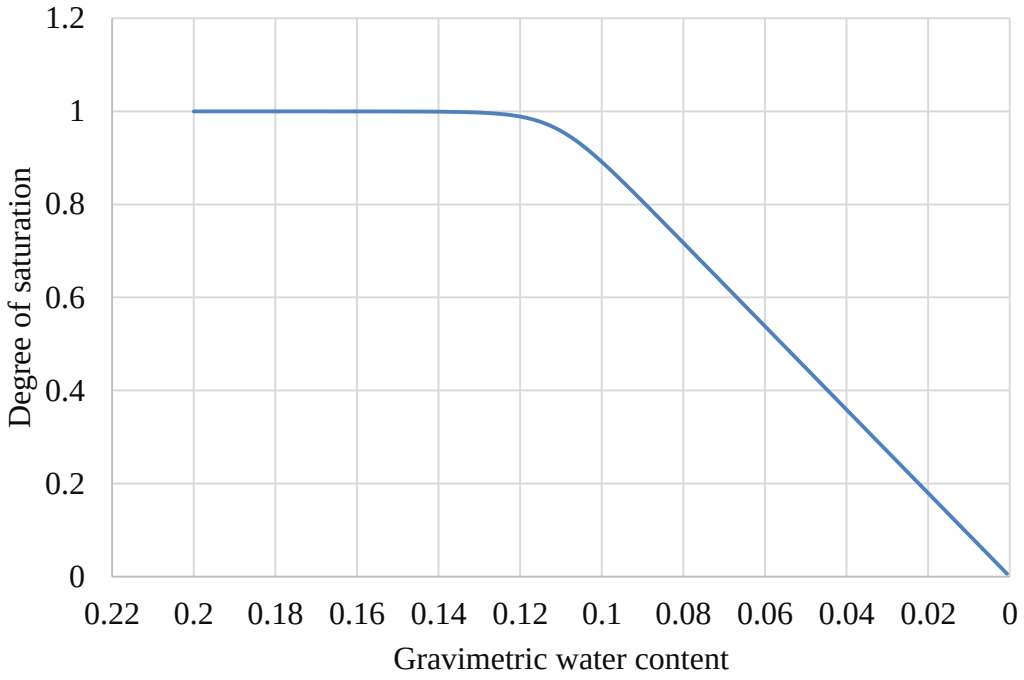

Figure 4.15 Degree of Saturation versus Gravimetric Water Content Curve of Lake Hefner Soil

4.6 Summary and Conclusions

In this chapter, new interpretation for the volume change of clay soils is presented. It is pointed out that:

1- The void ratio versus suction curve (e-log s curve) and the soil water characteristic curve (SWCC) have a unique slope referred to as shrinkage virgin line (SVL) similar to the compression virgin line in the classical consolidation theory

2- The slope of SVL of the soil water characteristic curve (i.e. suction vs. gravimetric water content) is related to the slope of SVL of e-log s curve, which is the suction compression index, by a simple equation.

3- A unified framework for the relation among the gravimetric water content, void ratio, degree of saturation, and suction, is presented. It indicates that the air entry point should be identified from the SHCC or from the degree of saturation versus suction curve. The analysis of the results shows that the residual point in the SWCC is not the shrinkage limit. Similarly, the breaking point in the gravimetric water content versus suction curve and e-log s curve is the pre shrinkage suction and not the air entry value. The normal shrinkage takes place for a single degree of saturation, being 100% for fully saturated soils. The normal shrinkage describes a linear curve in the e-log s curve from the pre-shrinkage suction to the air entry value.

4- Both the SWCC and e-log s curves can be modeled with the same closed form expressions but with different curve fitting parameters.

It is recommended for future research to pursue the swelling path for wetting SWCC in similar way followed in this chapter for complete representation of the volume change.

CHAPTER V

A PRACTICAL MODEL FOR SHRINKAGE SETTLEMENT AND CRACKING DUE TO CHANGE OF SUCTION

5.1 Introduction

The desiccation from dry climate induces effective stress in the soil due to the increase of negative pore water pressure, soil suction. The effective stress causes shrinkage in clay soils. The vertical shrinkage develops settlement in the soil while the lateral shrinkage can happen and initiate cracks when the lateral tensile stress exceeds the soil tensile strength. Therefore, the shrinkage settlement and cracking take place simultaneously. In spite of the notable research efforts directed at studying both phenomena, shrinkage settlement and cracking mechanisms are still not well understood. This chapter, first, critically examines the crack initiation mechanism and the possibility to extend it to explain the crack growth and propagation. Second, the study investigates the tensile strength characteristic curve in clay soils. Third, a simple and rational approach is proposed to modelling both the shrinkage settlement in addition to the crack depth and width as a response to the change in soil suction profile.

5.2. Air Entry Value and Crack Initiation

Despite the high complexity involved in the soil cracking phenomenon, numerous researches have indicated that crack first initiates when the suction of saturated soils subject to desiccation attains the air entry value (AEV), whereat soils commerce to desaturate (e.g. Lloret et al. 1998; Nahlawi and Kodikara 2006; Rodríguez et al. 2007; Peron et al. 2009; Shin and Santamarina 2011; Shannon et al. 2015; Saleh-Mbemba et al. 2016). Similar findings are also observed in this study as explained in Chapter 7. Similar observations have also been reported for other materials (Brinker and Scherer (1990) for gels; Slowik et al. (2009) and (2010) for concrete). Peron et al. (2009) gave more possibility that that can be justified by the cavitation formed in the soil due to the heterogeneous nucleation when a new thermodynamic phase (i.e. gas bubbles) exists. Further, the water content of the AEV is very close (or equal) to the plastic limit (e.g. see Fredlund and Houston 2013) so that the soil often does not show a fracture behavior before that water content. That is also proven by the ductility level description demonstrated by Harison et al. (1994). The authors classified the soil based on the water content into three categories: region 1-the water content greater than the plastic limit and the soil showing no fracture behavior; region 2-the water content between the plastic limit and shrinkage limit and the soil transiting from the plastic to brittle behavior; and region 3-the water content less than the shrinkage limit and the soil showing brittle fracture. While the compaction conditions and the stress path history have been reported to affect the crack initiation, results from this study (Chapter 7) confirm that such factors influence on the crack initiation also affect the AEV. Nevertheless, for compacted clays the critical suction of crack initiation falls at the end of the normal shrinkage stage (see Figure 5.1). More discussions about the crack initiation and growth and also its interpretation based on the tensile stress and strength will be given in the coming sections.

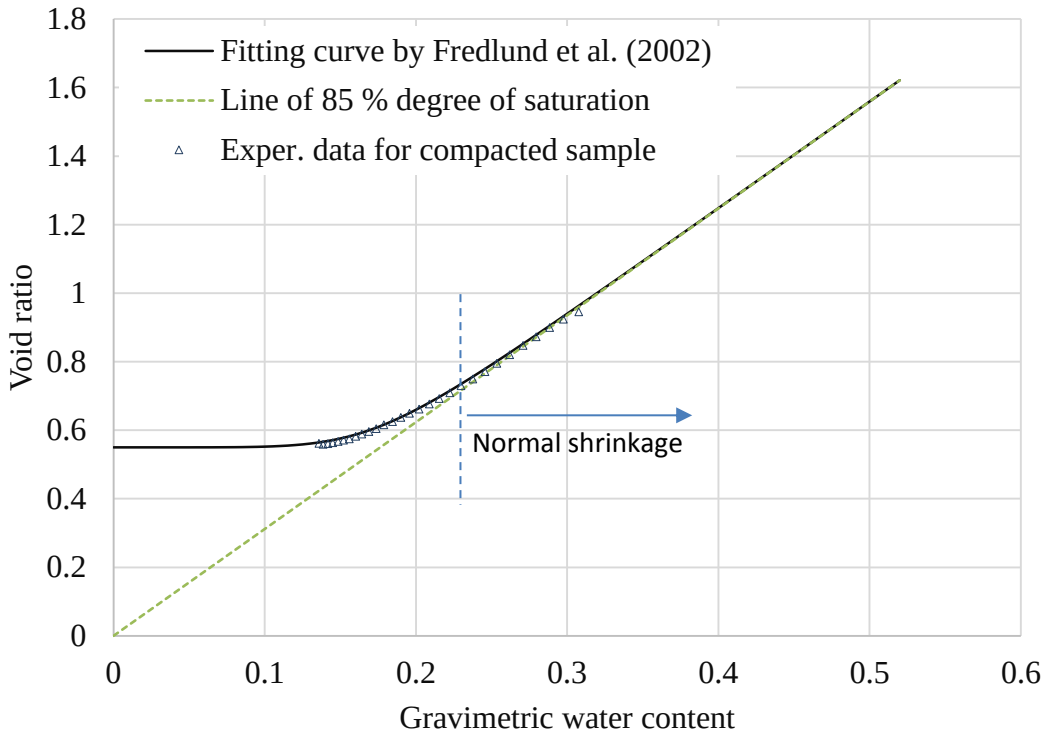

Figure 5.1. Typical Soil Shrinkage Characteristic Curve of Compacted Clayey Soil (Data from Free Shrinkage Test for Compacted Ardmore Soil)

5.3 Crack Propagation

This research adopts that the crack propagates downward to a depth where the tensile stress exceeds the tensile strength (Morris et al. 1992). Further, For the sake of simplicity and since extensive experimental evidences have emphasized that the tensile stress exceeds the soil tensile strength at the air entry value (AEV) of suction, this research assumes that the AEV is the critical suction in the suction profile where the crack propagates to. Two important points arise here. First the crack propagation is explained by the crack initiation mechanism. In other words, new crack surface does not form until the suction gains the AEV. To investigate that experimentally, samples with artificial

cracks are subjected to desiccation. The results are shown in the next chapter. Second this assumption neglects the overburden pressure. That is because its contribution as compared with the soil suction is inconsiderable. On contrary, it might hinder the crack propagation. That can be perceived from the expression of elasticity for the tensile stress in soil profile by assuming zero lateral strain prior to the crack initiation, as follows (Morris et al. 1992):

$$(\sigma_x - \psi_a) = \frac{-v}{1-v}(\sigma_z - \psi_a) + \frac{E}{H(1-v)}(\psi_a - \psi_w) \qquad (5.1)$$

Where $(\sigma_x - \psi_a)$ is the net horizontal stress, $(\sigma_z - \psi_a)$ is the net vertical stress, $(\psi_a - \psi_w)$ is the pore air pressure minus the pore water pressure which is equal to the matric suction, E is the compression modulus with respect to the mechanical stress, H is the compression modulus with respect to the matric suction, and v is the Poisson's ratio. Note that the sign is substituted negative for the first term and positive for the second since the tensile stress results in negative values. Therefore, the first term contributes against the crack propagation. Further, if the vertical stress is substituted by (γh), γ is the soil unit weight and h is the soil depth, obviously, the first term gives much less magnitude then the second one. That is because the crack takes place in shallow depths, and expansive soils can develop high suction values.

Hence, the crack depth is pertinent to the active seasonal zone, the soil depth beyond which slight or no seasonal suction change occurs. Table 1 shows field observations to the active and cracking depth. AS 2870 (1996) generally suggests to consider the crack depth a half of the soil active depth.

Table 5.1. Soil active and crack depth due to seasonal suction variation in some Australian and Canadian regions (AS 2870.1-1988, cited in Morris et al. 1992)

Location	Depth of seasonal suction change (m)	Depth of cracks (m)
Australia		
Adelaide	4.0	1.8–2.0
Melbourne	2.0	2.0–3.0
Sydney	1.5	
Hunter Valley	2.0	0.5
Brisbane	1.5	0.5
Wodonga	3.0	
Canada		
Winnipeg	3.0	6.0

5.4 Tensile Strength Characteristic Curve

During drying, the soil gains tensile strength resulting from the increase of suction and the decrease of void ratio (soil densification). Such variation of the soil tensile strength can add more complexity to the cracking problem. Therefore, identifying the characteristic curve of the tensile strength for desiccated soils is helpful to determine the stage of crack initiation. Various studies have conducted different methods to experimentally predict the soil tensile strength (Narain and Rawat 1970; Harison et al. 1994; Favaretti 1995; Nahlawi et al. 2004; Vesga and Vallejo 2006; Rodriguez et al. 2007; Wang et al. 2007; Zeh and Witt 2007; Vesga 2009; Villar et al. 2009; Trabelsi et al. 2010; Tang et al. 2014; Uday et al. 2014; Narvaez et al. 2015). Maybe the most used method for the estimation of tensile strength is the splitting tensile strength test (known also as Brazilian test). However, the results from the literature do not show obvious tendency for the relationship between the tensile strength and water content, soil suction, or degree of saturation. Harison et al. (1994) and Wang et al. (2007) found that the tensile strength increases with the reduction of water content. Some others detected a peak value to the tensile strength (Lakshmikantha et al. 2012; Tang et al. 2014) (Figure 5.2).

However, some researchers emphasized that the development of the tensile strength during desiccation follows the shrinkage path of the soil (Vesga 2009; Villar et al. 2009; Uday et al. 2014) (Figure 5.3). This is a rational description to the tensile strength of drying soils since the increase of the tensile strength is directly related to the shrinkage densification of the soil, but more research is still needed in this matter. Similar kind of shape for the tensile strength characteristics curve has been demonstrated for sandy soils by Lu et al. (2009) (see Figure 5.4).

Vesga (2008) displayed that the tensile strength of the soil increases linearly as the water content decreases in the saturated state. His results are derived from direct tensile tests conducted by axially tensioning bowtie-shaped specimens of kaolinite clay. However, this tendency hinders in the funicular state (Figure 5.3). That happens when the air bubbles exist and the soil commences to desaturate. Then, the tensile strength decreases in the pendular state, which is the unsaturation zone (Figure 5.3). Results from Villar et al. (2009) showed that the tensile strength gains a peak value with a water content close to the saturation for clay soils measured by the splitting tensile strength test.

The discrepancies of the tensile strength curve derived by different studies can probably be attributed to the testing methods the authors employ in their researches such as the testing devices, compaction conditions, and also the desiccation process conditions.

Nevertheless, a general description to the common results of the tensile strength characteristic curve is discussed herein. First, most studies have found a peak value to the tensile strength. This peak value occurs close to the end of the normal shrinkage or the air entry value for initially saturated soils. That means the peak value occurs while the soil is still close to the initial degree of saturation. That is the case of clay soils which do not show structural shrinkage.

The latter can be attributed to the variation of the soil mechanical behavior with the change of its water content. After the soil loses its moisture and becomes unsaturated, the brittleness increase.

That increase is most likely due to the formation of the cavitation and thus causes a reduction in its tensile strength. Furthermore, for very high water contents, the soil has low tensile strength because the soil at this stage is very soft. In other words, as the soil transits from the fully saturated state to the unsaturated state, the soil ductility or pliability decreases significantly, and a fracture failure is most likely induced

This observation can probably justify the cracking event at the stage of the air entry value.

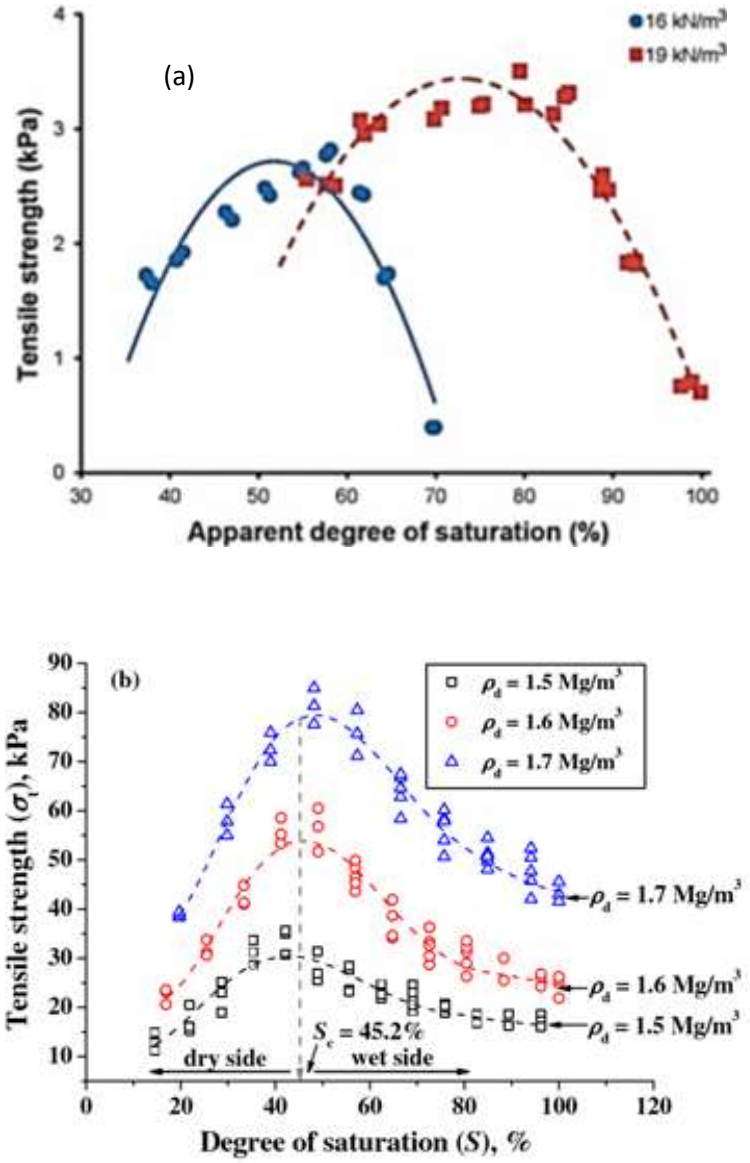

Figure 5.2. Tensile Strength versus Degree of Saturation for a Compacted Clay Soil (a) Lakshmikantha et al. (2012), (b) Tang et al. (2014)

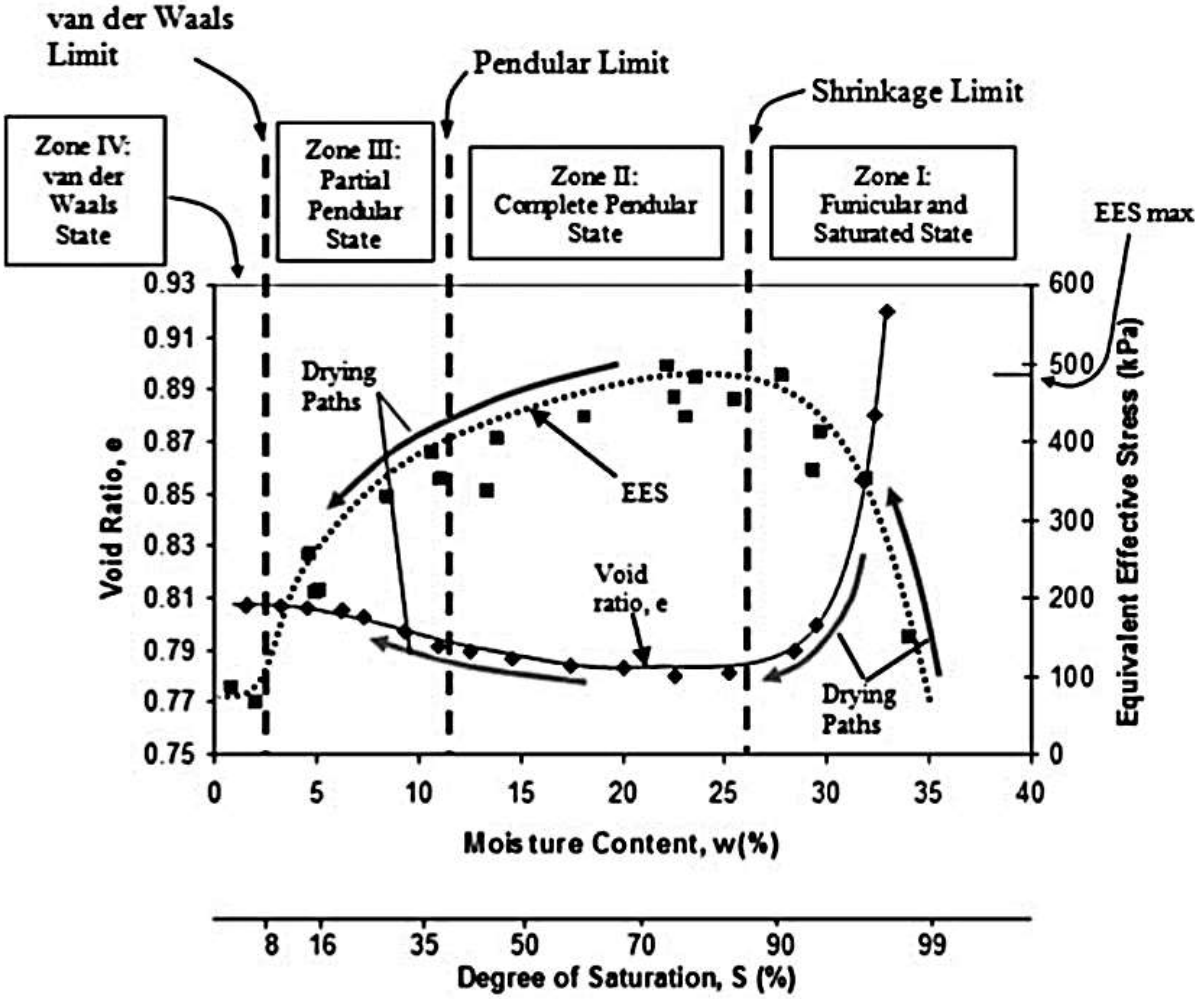

Figure 5.3. Tensile strength and Shrinkage Characteristic Curve (Vesga 2009). Note: the equivalent effective stress is also the soil tensile strength.

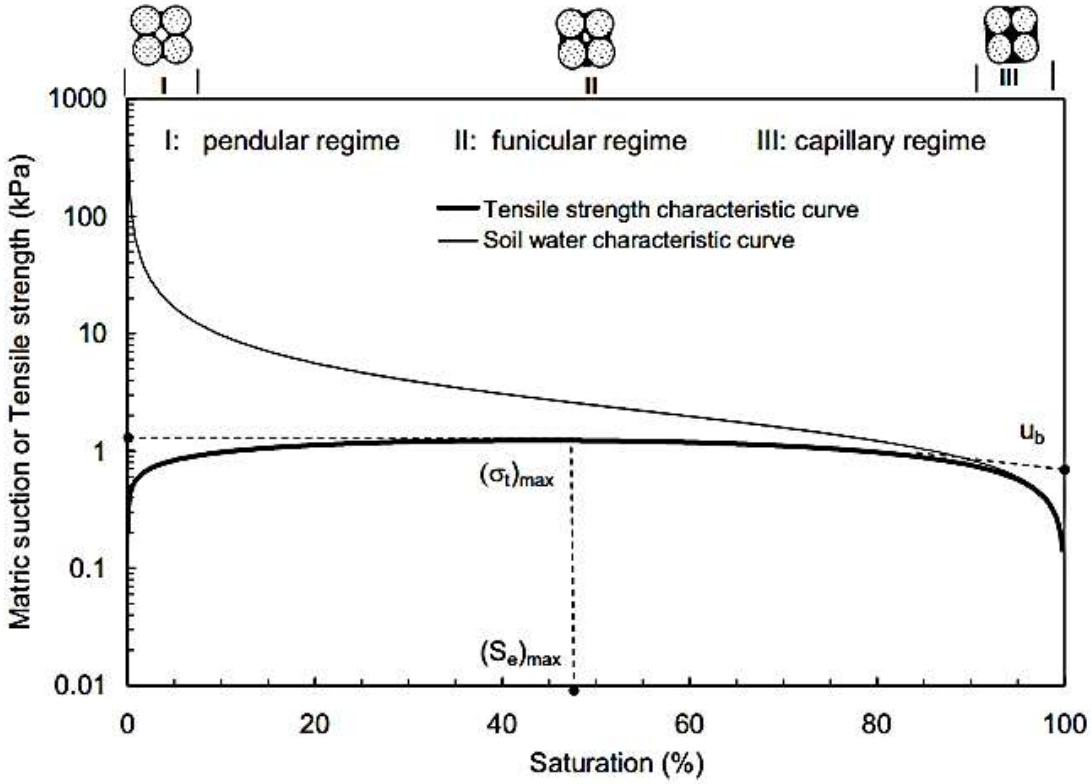

Figure 5.4. Tensile strength characteristic curve of sandy soil (Lu et al. 2009).

5.5 Shrinkage and Cracking Modelling

Referring to the discussions presented in the previous sections, a simple model for soil cracking in the field can be proposed. That is achieved by setting the crack as an event in the soil shrinkage process. Therefore, the soil shrinkage characteristic curve is the key parameter in this model. A typical curve of the soil shrinkage characteristic is shown in Figure 5.5.

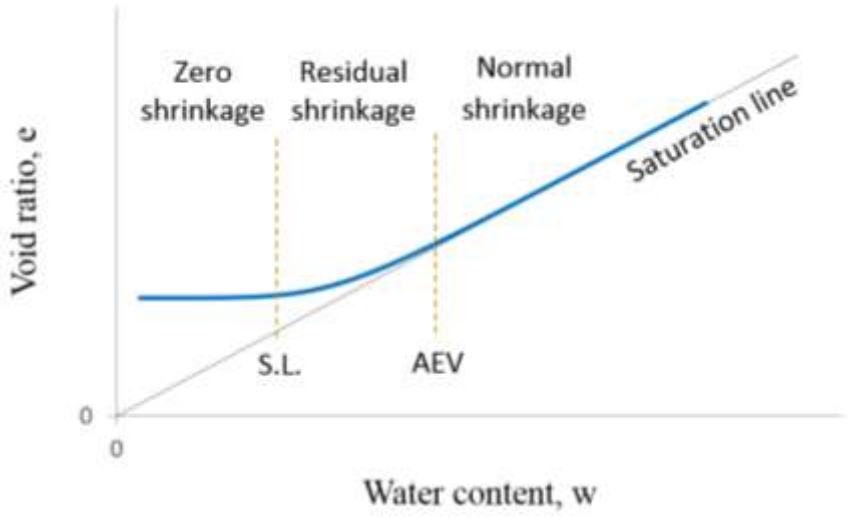

Figure 5.5. A Typical Curve of the Soil Shrinkage Characteristic

The model assumes the following points:

1- Cracks initiate in the soil when the soil shrinkage reaches the end of the normal shrinkage zone.

2- The soil experiences one dimensional vertical settlement shrinkage before it reaches the cracking event.

3- After the crack initiation, the soil experiences three dimensional shrinkage, vertical settlement and horizontal cracking.

4- Cracks propagate to the depth where the soil shrinkage is no longer normal (Figure 5.5).

The first and last assumptions are discussed in the previous sections. The second and third assumptions that the soil undergoes one dimensional shrinkage before cracking and three dimensional shrinkage after cracking have been widely observed in the field (e.g. Abu-Hejleh and Znidarcic 1995).

After obtaining the horizontal shrinkage from the three dimensional shrinkage stage, full characteristics to the soil cracking can be predicted. That is possible if the crack patterns and the space between cracks are identified. Then, the crack intensity factor concept can be used to convert the horizontal shrinkage to real crack geometry. The crack intensity factor is the ratio between the area of the surface cracks and the total soil surface area (Yesiller et al. 2000).

Thus, for generalization the critical suction of crack initiation will be referred to as ψ_{NS}, being the AEV for initially fully saturated soils. ψ_{NS} is the suction that occurs at the end of the normal shrinkage stage. Therefore, this thesis describes two subsequent stages for the soil shrinkage given as follows:

First (normal shrinkage stage)

Suction $\leq \psi_{NS}$

Tensile stress $\leq$ tensile strength

1D shrinkage settlement

Second (residual shrinkage stage)

Suction $> \psi_{NS}$

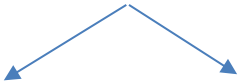

Vertical settlement

Horizontal shrinkage converted to crack characteristics

Thus, for any change of the soil suction profile due to the desiccation process, the shrinkage settlement, crack space, and crack depth are given as follows:

- Shrinkage Settlement (SHS):

$$SHS = \gamma_h(log\psi_{NS} - log\psi_i) + (1 - f)\gamma_h\left(log\psi_f - log\psi_{NS}\right) \quad (5.2)$$

- Lateral Shrinkage translated as crack characteristics (CS):

$$CS = f\left(log\psi_{NS} - log\psi_f\right) \quad (5.3)$$

- Crack depth (D_{crack}):

$$D_{crack} = 2\sqrt{\alpha t}\, erfc^{-1}\frac{log\psi_{NS} - log\psi_i}{log\psi_a - log\psi_i} \quad (5.4)$$

Where: γ_h is the suction compression index, ψ_{NS} is the suction of the end of the normal shrinkage, ψ_f is the initial suction, ψ_f is the final suction, f is a cracking factor, α is the diffusion coefficient, *t* is the time, ψ_a is the air suction from the climate at the soil surface can be calculated from Kelvin's law:

$$\psi_a = \frac{RT}{V}\ln(RH) \quad (5.5)$$

Where, R is the universal gas constant, T is the absolute temperature, V is the molecular volume of water, and RH is the relative humidity.

Equation (5.4) is derived from Mitchell (1979) model for the change in suction at any depth for constant surface suction (ψ_o):

$$\Delta\psi = \psi - \psi_i = (\psi_f - \psi_o)(1 - erf\frac{z}{2\sqrt{at}}) \quad (5.6)$$

For clay soils Lytton et al. (2004) suggested to take the cracking factor, f, between 1/3 and 1. Experimental results from Shin and Santamarina (2011) and Tang et al. (2011) of soil cracking suggested that the soil experiences negligible vertical shrinkage during the horizontal shrinkage. Therefore, f can be taken larger than 0.8. Note that Equation 5.2 gives SHS for suction between the pre-shrinkage value and the shrinkage limit stage. This range is the most likely experienced in the field, particularly to the high expansive soils which can undergo shrinkage till very high suction. However, for low plasticity soils, the shrinkage can cease at relatively lower suction values (e.g.

less than 1 MPa). As a result, the final suction, ψ_f, should become the suction value of shrinkage limit if it exceeds the latter. This is common for the soil surface conditions where the suction reaches high value (e.g. 1 MPa) after less than a month. Results from diffusivity test for one dimensional evaporation due to air drying (temperature 24 c^o and relative humidity 50%) of a saturated sample from Lake Hefner soil (PI=14) show that suction at 3 cm from the sample surface reaches 1 MPa after around 18 days (Figure 5.6).

Consequently, the shrinkage settlement can be estimated from the fitting model of the void ratio vs. suction curve (e-log s curve). In this case the vertical shrinkage and the crack characteristics can be predicted for any suction increase at any depth. Then the shrinkage settlement and the crack characteristics can be formulated as follows:

$$SHS = \frac{e_o - e_{min}}{1 + e_o}\left[\frac{f}{\left\{\ln\left[2.72 + \left(\frac{\psi_{NS}}{a}\right)^n\right]\right\}^m} - \frac{1}{\left\{\ln\left[2.72 + \left(\frac{\psi_i}{a}\right)^n\right]\right\}^m} + \frac{1-f}{\left\{\ln\left[2.72 + \left(\frac{\psi_f}{a}\right)^n\right]\right\}^m}\right] \quad (5.7)$$

$$CS = \frac{(e_o - e_{min})(f)}{1 + e_o}\left[\frac{1}{\left\{\ln\left[2.72 + \left(\frac{\psi_f}{a}\right)^n\right]\right\}^m} - \frac{1}{\left\{\ln\left[2.72 + \left(\frac{\psi_{NS}}{a}\right)^n\right]\right\}^m}\right] \quad (5.8)$$

Where e_{min} is the minimum void ratio occurring at the shrinkage limit stage, e_o is the initial void ratio the shrinkage starts from, a, n, m are curve fitting parameters for e log s curve.

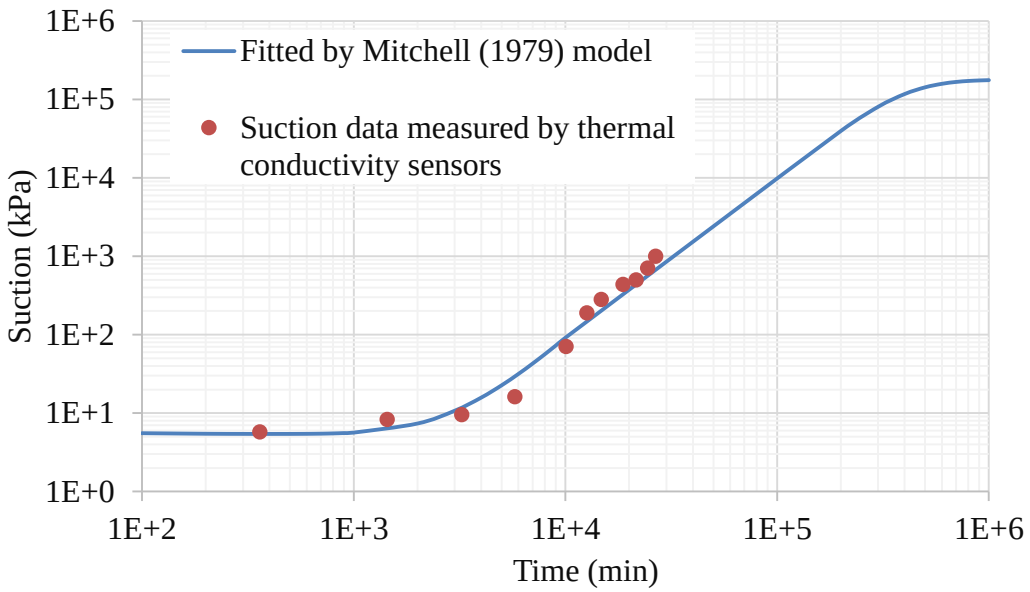

Figure 5.6. Suction versus Time in Diffusivity Test (Data from Mantri 2014)

CHAPTER VI

LABORATORY TESTING PROGRAM AND MATERIAL PROPERTIES

Soil samples with different plasticity indices were collected from various sites (i.e., Ardmore, Osage, and Lake Hefner) in Oklahoma. These soils were processed by air drying and crushing into fine particles using a grinder before conducting any tests and specimen preparation. The basic geotechnical engineering properties were obtained for all the soils (i.e. Grain size distribution, Atterberg limits, standard Procter compaction). All the tests were conducted following ASTM standards. The properties of all the soils are summarized in Table 6.1.

Table 6.1. The Properties of the Tested Soil

Soil name	Clay content (%)	Silt content (%)	Fine sand content (%)	Plastic limit (%)	Liquid limit (%)	Optimum moisture content (%)	Max. dry density (gm/cm^3)
Ardmore	40	47	13	24	55	27	1.45
Osage	42	49	9	23	56	27	1.46
Lake Hefner	30	54	16	15	29	17	1.82
Lake Hefner 1	39	43	18	19	37	20	1.77
Lake Hefner 2	23	59	18	13	21	14	1.92

The major experimental program of this thesis includes four parts: 1- Restrained ring test 2- Suction measurement 3- Free shrinkage test 4- Splitting tensile test for tensile strength determination.

6.1 Restrained Ring Test

The restrained ring test (RRT) is a testing technique in which the soil sample is constrained from free shrinkage in order to induce shrinkage cracking in the soil. During shrinkage, the soil internal stress can be evaluated using micro strain gauges.

6.1.1 Sample Preparation

Small size and large size samples were prepared for the RRT test. Small size samples were 10.16 cm in diameter and 1.55 cm in height, while the large size samples were 15.24 cm in diameter and 1.65 cm in height. For both sample sizes, standard-mold compacted and PVC-mold compacted specimens were prepared. The standard-mold compacted specimens were prepared using the standard Procter compaction method with the standard mold (10.16 in diameter and 11.65 cm in height) following ASTM D698. However, the PVC-mold compacted specimens were obtained by compacting the soil inside the PVC ring un two layers with each layer receiving 36 blows using a wooden rod with rubber cab (diameter = 2.54 cm).

The standard-mold specimens were compacted at optimum moisture content. The specimens were subsequently extracted from the mold, covered in plastic wrap and aluminum foil, and stored in ice-chests for moisture (suction) equilibrium for three days. From the standard-mold samples, the small size, test specimens were made using the PVC ring (10.16 cm in diameter and 1.55 cm in height).

The PVC-mold compacted specimens were prepared at optimum water content (OWC) and approximately 4% above the OWC following the compaction procedure described above. Furthermore, both small and large size PVC-mold specimens were prepared at high water contents, but still below the liquid limit of the soil. These high water samples were molded inside the PVC rings easily without any compaction effort, but only leveled the soil surface with a flat plate just

flush with the height of the ring. These samples are referred to as high-water content specimens thereafter. Since the diameter of the standard-mold compacted samples were the same as that of the small size PVC ring, it was easily pushed around the circumference of the soil sample (Figure 6.1). The specimen was cut carefully and trimmed from both surfaces inside the PVC ring (Figure 6.1).

Figure 6.1. The Compacted Sample inside the PVC Ring

For all the soil samples, a hole with 5.5 cm in diameter was made carefully in the center of the sample using a sharp-edge steel ring without disturbing the soil. Then, the sample was carefully extracted from the PVC ring (Figure 6.2). All the specimens were covered with plastic wrap and aluminum foil and left in ice-chests for one week for curing and moisture equilibrium.

Figure 6.2 The Sample with a Hole Made by a Sharp-Edge Steel Ring

6.1.2 Starting the Test

Before starting the test, the soil specimen was sealed by plastic wrap from the bottom and a rubber band from the circumference to maintain the sealing for uniform shrinkage as the soil sample shrinks radially (Figure 6.3). Attention was given to prevent the rubber band from applying any pressure on the soil by keeping it loose for sealing purpose only.

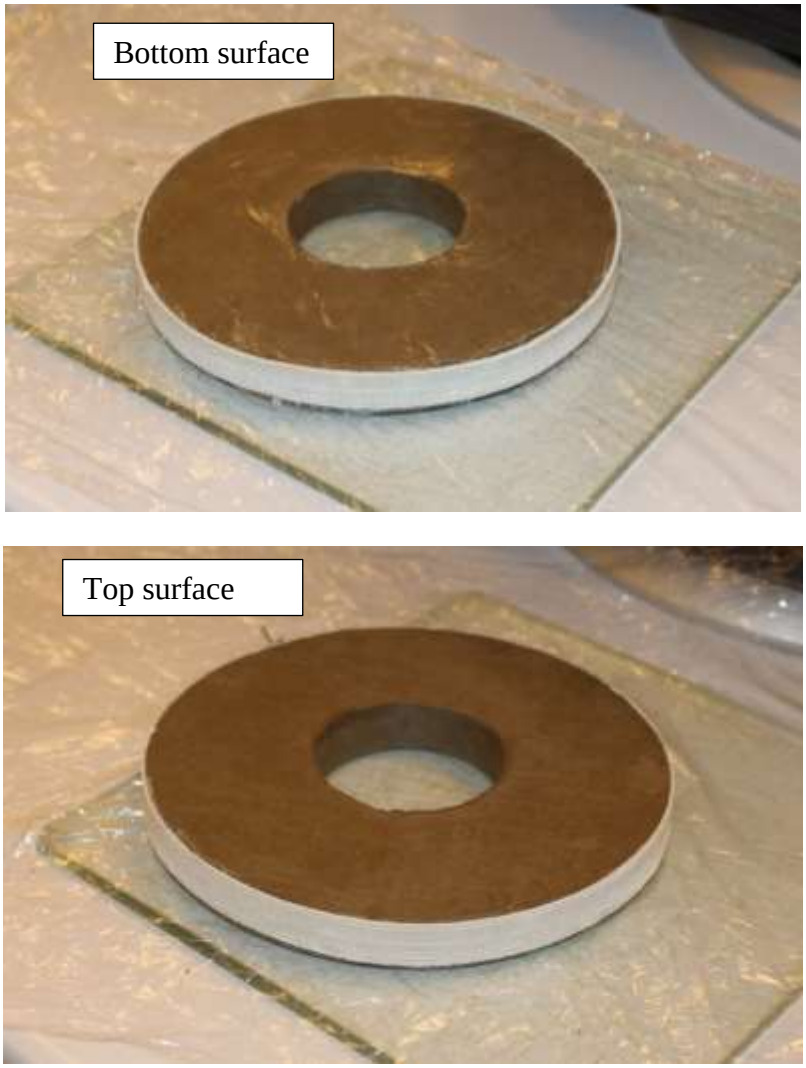

Figure 6.3. The Sample with the Rubber Band and the Plastic Wrap from the Bottom

Before starting the test, the weight of the sample was recorded on a balance (Figure 6.4). Finally, white sand particles or black rubber particles depending on the soil color were randomly spread out on the sample surface (Figure 6.5). That is to help run the analysis using the digital image technique.

Figure 6.4 Weighing the Specimen before Starting the Test

Figure 6.5 Spreading out White Sand Particles on the Sample Surface

As the test starts by air drying the soil specimen, a high resolution camera is installed to take one picture every 15 minutes. When the soil shrinks, it applies a pressure on the ring wall. This pressure is sensed by the strain gauges in the inner face of PVC ring. The strain gauges are accessed to a

data acquisition system connected to a computer to save the recordings along with the time. After the crack initiates in the soil, the test is ended. The dimensions of the sample are measured by a caliber. Then, the sample is oven dried for the final water content determination.

6.2 Suction Measurements

To predict the soil water characteristic curve (SWCC), two devices are utilized: a WP4 device for high suction measurements (suction > 0.3 MPa) and a tensiometer sensor for low suction measurements (suction < 0.07 MPa). Both devices are checked for their accuracy before using them. The WP4 device is calibrated by chemical solutions at known osmotic suctions, while the tensiometer is filled with water and checked by measuring the suction of the de-ionized water. Since two conditions of the soil samples are carried out in the restrained ring test (RRT), standard-mold compacted and PVC-mold compacted specimens, two kinds of drying SWCCs are predicted. That is achieved by preparing identical samples to those tested in RRT, same initial water content and density. Two cylindrical samples, 6.4 cm in diameter and 1.9 cm in height, are prepared for a single SWCC. For every suction measurement, soil sample is left to air drying for until it reaches the desired water content and then stored for equilibrium for 24 hours. If suction is measured by tensiometer, then it is directly inserted in the soil sample. The sensor and the soil sample are sealed by plastic wrape and left for one hour (see Figure 6.6) before taking the reading. The initial suction for some high-water content specimens is also measured using the tensiometer by the same way (Figure 6.7). However, if suction is measured by WP4, small pieces are cut from the cylindrical sample to fill almost the half space of WP4 measurement cap (see Figure 6.8). The suction results obtained from WP4 and tensiometer are considered equal to total and matric suction, respectively. However, in these reconstituted soil samples, it is assumed that the osmotic suction component is negligible, and therefore, total suction is approximately equal to matric suction.

Figure 6.6 Measuring the Soil Suction Using Tensiometer

Figure 6.7 Measuring the Initial Suction of Some High-Water Content Specimens of the Restrained Ring Test Using Tensiometer

Figure 6.8 Measuring the Soil Suction Using WP4 Device

6.3 Free Shrinkage Test

Free shrinkage tests (FST) are conducted on identical soil samples (6.4 cm in diameter and 1.9 cm in height), which represent the same initial conditions of the specimens tested in the RRT. FST is carried out by air drying the soil sample on a balance. As the sample shrinks and loses water, two fixed cameras are installed to capture image series, one image per 30 minutes. One camera captures images from the top view and the other from the side view. These digital images are used to analyze the soil volume change with time, water content, and suction. White silica flour particles are randomly spread out on the sample surfaces to help capturing the displacement by the digital imaging. After few days, less than one week, when the water loss is ceased or becomes negligible, the test is stopped and the sample is oven dried for the final water content determination.

FST are conducted for two kinds of specimens: i) compacted specimens at optimum water content and ii) non compacted specimens at high water content (slightly below the liquid limit). The specimens were prepared by mixing the air dried soil particles thoroughly with water. The high-

water contents specimens were easy to mold inside the steel ring (6.4 cm in diameter and 1.9 cm in height) without compaction. The compacted samples were prepared by mixing the soil particles with water content close to the optimum moisture content. The soil is compacted in three layers using standard mold and standard compaction following ASTM D698. After extracting the compacted cylindrical soil, the same steel ring with 6.4 cm in height and 1.9 cm in diameter was carefully inserted in the compacted cylindrical specimen. Then, the soil from both steel ring surfaces were gently cut and trimmed. All the specimens were covered with plastic wrap and aluminum foil and left in ice-chests for one week for curing and moisture equilibrium.

6.4 Measurement of Tensile Strength

The splitting tensile test (also known as the Brazilian test) is conducted to predict the tensile strength characteristic curve of Ardmore soil.

6.4.1 Sample Preparation

Identical high-water content specimens of Ardmore soil were prepared. The mixing water content was 49%. After it was mixed thoroughly with the water, the soil is molded inside a steel ring with 7.15 cm in diameter and 3.15 cm in height. No compaction effort was carried out to mold the soil inside the ring since the water content was slightly less than the liquid limit (i.e. 55%). Therefore, it was easy to mold the soil inside the ring. Then, the specimen was trimmed carefully using a flat plate just flush with the height of the ring. Finally, the specimen was carefully extracted from the ring (Figure 6.9). Following this procedure, identical specimens with a high water content and degree of saturation were obtained (Figure 6.9). These specimens were covered with plastic wrap and aluminum foil and left in ice-chests for one week for curing and moisture equilibrium

To obtain different water contents, suctions, and degree of saturations, these specimens were air dried (Figure 6.10). After meeting the desired water content, each specimen was covered with plastic wrap and aluminum foil and left in ice-chests for one day for moisture equilibrium. Some

specimens developed some visual cracks on the specimen surface. These specimens were discarded.

6.4.2 Starting the Test

Before starting the test, the weight and the dimensions of the specimen were measured and recorded. White silica flour particles were randomly spread out on one surface of the specimen to help capturing the displacement by the digital imaging. Then, the test was started (Figure 6.11). The test was conducted following ASTM D3967-16. This standard suggests that the sample fails between 1 to 10 minutes to obtain reliable results. The 0.5 % strain per minute was found to meet that duration for all the tested soils.

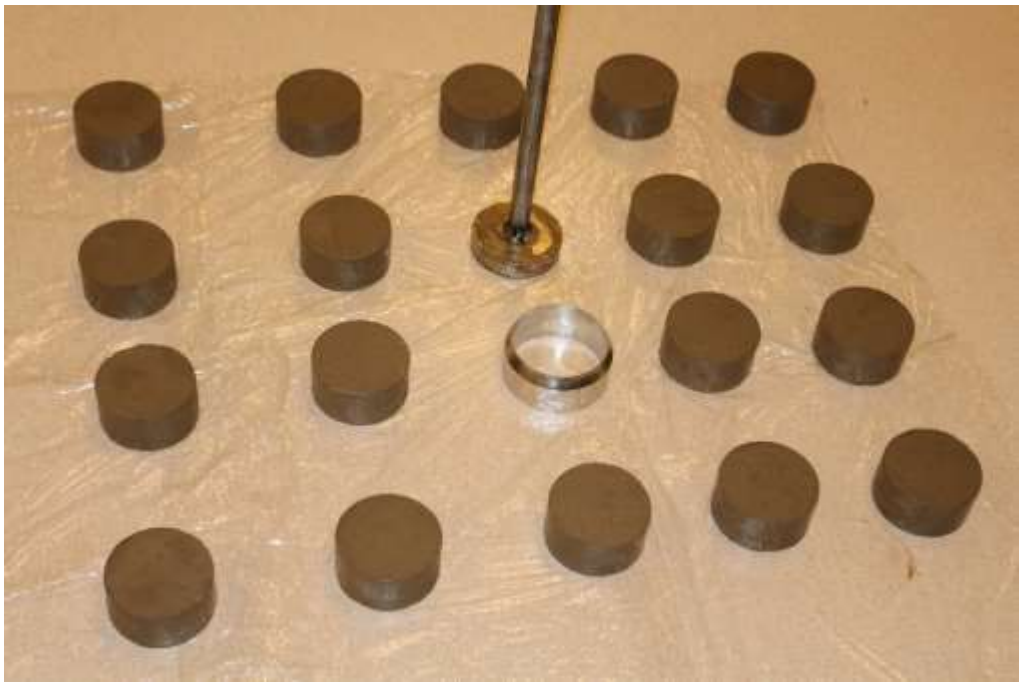

Figure 6.9 The Prepared Specimens for the Brazilian Test (Ardmore Soil)

Figure 6.10 Air Drying of the Specimens for the Brazilian Test (Ardmore Soil)

Figure 6.11 The Brazilian Test for Ardmore Soil

CHAPTER VII

TEST RESULTS AND DISCUSSIONS

Extensive numbers of tests were conducted by restrained ring testing method to investigate and analyze the soil volumetric strain and cracking behavior based on the stress developed, water content, soil suction, and degree of saturation. To fulfill that, the soil water characteristic curve and shrinkage characteristic curve were predicted.

7.1 Soil Water Characteristic Curve and Soil Shrinkage Characteristic Curve

For all the soils, the experimental results from the WP4 device and tensiometer sensor are fitted to find the soil water characteristic curve (SWCC) by Fredlund and Xing (1994) model:

$$w(\psi) = \left[1 - \frac{\ln(1 + \psi/\psi_r)}{\ln(1 + 10^6/\psi_{r)}}\right] \frac{w_s}{\{\ln[\mathrm{e} + (\psi/a)^n]\}^m} \qquad (7.1)$$

Where $w(\psi)$ is the gravimetric water content at given suction ψ, w_s is the saturated water content, ψ is the total suction, ψ_r is the residual suction, and a, n, m are the curve fitting parameters. Note that tensiometer sensor measures only the matric suction, while WP4 measures the total suction. However, for the tested reconstituted soil samples, it is assumed that the osmotic suction component is negligible, and therefore, total suction is approximately equal to matric suction.

The soil shrinkage characteristic curve is predicted using digital image processing technique for specimens with 1.9 cm in height and 6.4 cm in diameter undergoing a free shrinkage. Two kinds of specimens were tested: i) compacted specimens at optimum water content and ii) non compacted specimens at high water content (slightly below the liquid limit). The preparation details are presented in Section 6.3.

The digital image analysis is undertaken using *GeoPIV-RG* subroutines employed in MATLAB software. More details regarding *GeoPIV-RG* subroutines and how it analyzes the image series is given in Appendix 1. The results provided by *GeoPIV-RG* subroutines can only represent the strain taking place for the sample surface. Therefore, the images were captured from the top and the sides of the specimen using two cameras.

The results from both cameras are incorporated to find the strain in three dimensions. After estimating the shrinkage strain, a new volume for the desiccated specimen can be computed at every shrinkage stage. The obtained volume with the weights from the balance can be used to estimate the density. Thus, the void ratio can be determined from the following equation:

$$e(w) = (1 + w)\frac{Gs\ \gamma_w}{\gamma(w)} - 1 \qquad (7.2)$$

Where $e(w)$ is the void ratio for water content, w is the water content, Gs is the specific gravity, γ_w is the unit weight of water, and $\gamma(w)$ is the total unit weight of soil

The void ratio results from Equation (7.2) with the corresponding water content were fitted to predict the soil shrinkage characteristic curve (SHCC) using Fredlund et al. (2002) model:

$$e(w) = a\left[\frac{w^c}{b^c} + 1\right]^{(\frac{1}{c})} \qquad (7.3)$$

Where $e(w)$ is the void ratio for a given water content (w), a, b, and c are curve fitting parameters.

Finally the relationship between the void ratio and the suction (e log s curve) was derived by incorporating the results from the SHCC and SWCC. The e log s curve was developed to study the following:

1- The relation between the e log s curve and SWCC and the effect of volume change on the SWCC.
2- The difference between the volume change and SWCC derived for initially slurry samples and those for initially compacted samples. That can help analyze the cracking characteristics in slurry and compacted soils.

7.1.1 The Relation between the e log s Curve and SWCC

The SWCC, SHCC, e log s curve are illustrated in Figure (7.1), (7.2), (7.3) for Ardmore soil, and Figure (7.4), (7.5), (7.6) for Lake Hefner soil. The e log s curve in Figure 7.3 and 7.6 is generated by incorporating the two fitting curves (i.e. SWCC and SHCC) of high-water content specimens. The suction vs. the gravimetric water content (SWCC) was fitted using Fredlund and Xing (1994) model. The gravimetric water content vs. the void ratio (SHCC) was fitted using Fredlund et al. (2002) model. Furthermore, by taking the volume change into account, the SWCC in terms of the degree of saturation (i.e. suction vs. degree of saturation) was constructed. The curves of the other soils are given in Appendix 2. The results show how the volume change affects the shape of the SWCC particularly the air entry value when drawn in terms of the degree of saturation.

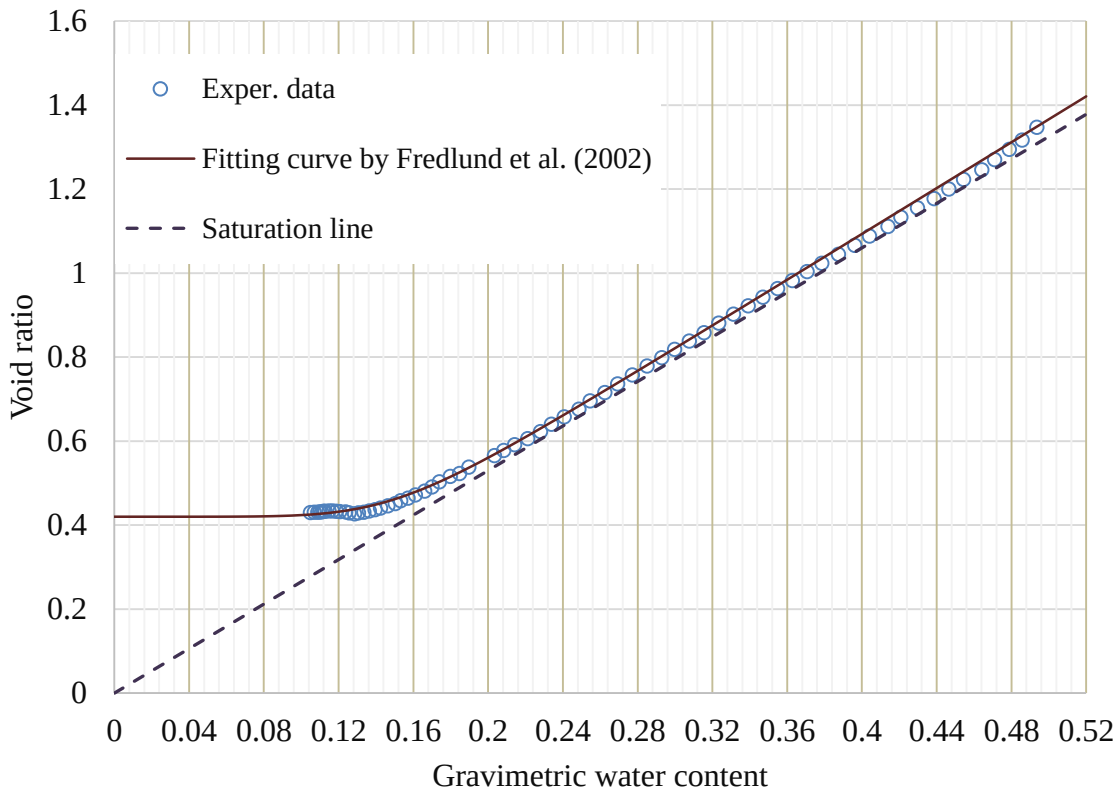

Figure 7.1. The Soil Shrinkage Characteristic Curve for High-Water Content Specimen of Ardmore Soil

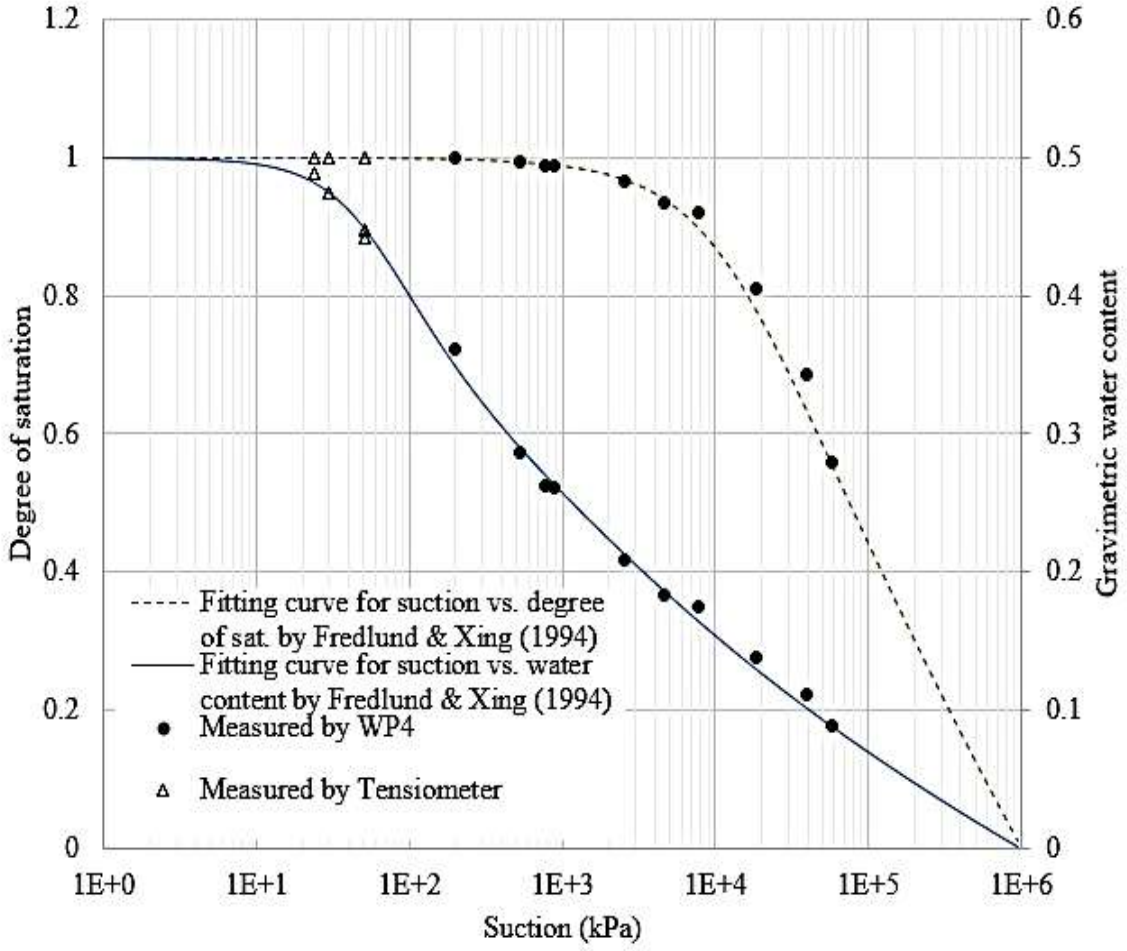

Figure 7.2. The Soil Water Characteristic Curve for High-Water Content Specimen of Ardmore Soil

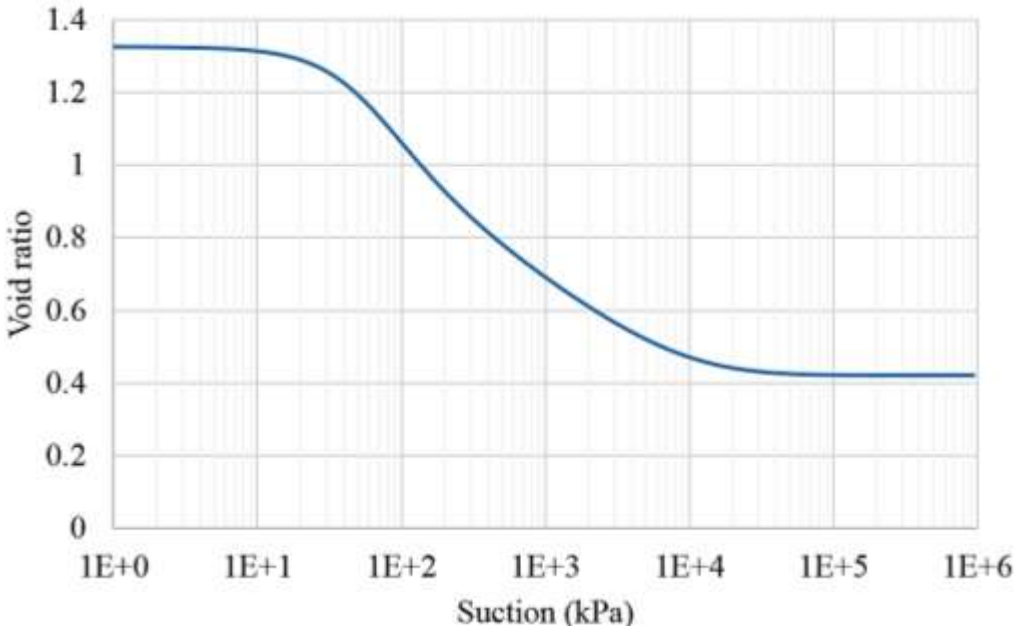

Figure 7.3. The e log s Curve for High-Water Content Specimen of Ardmore Soil

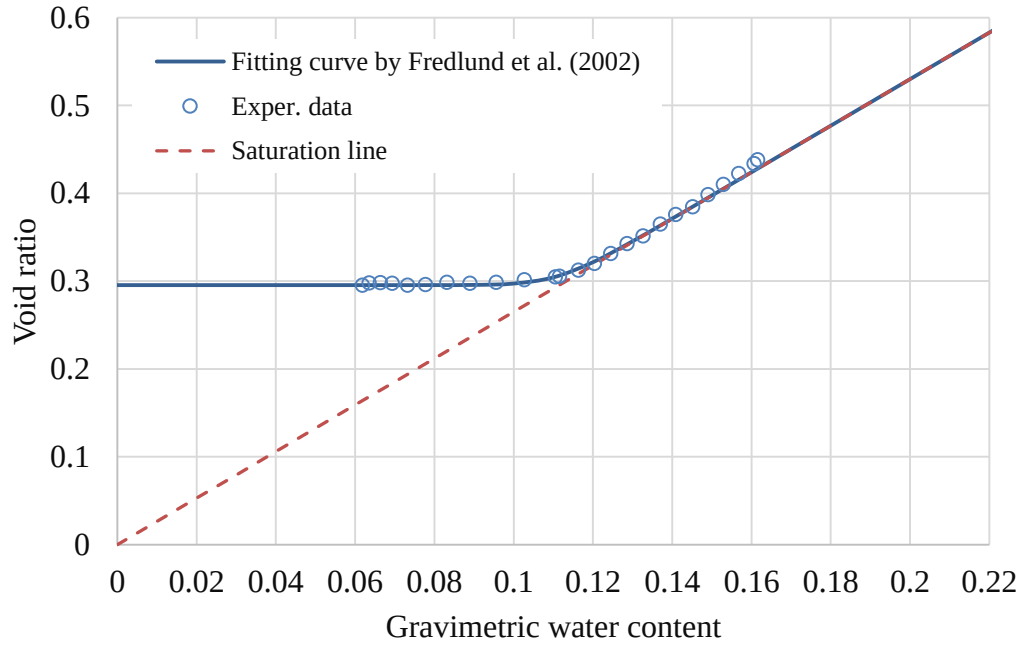

Figure 7.4. The Soil Shrinkage Characteristic Curve for High-Water Content Specimen of Lake Hefner Soil

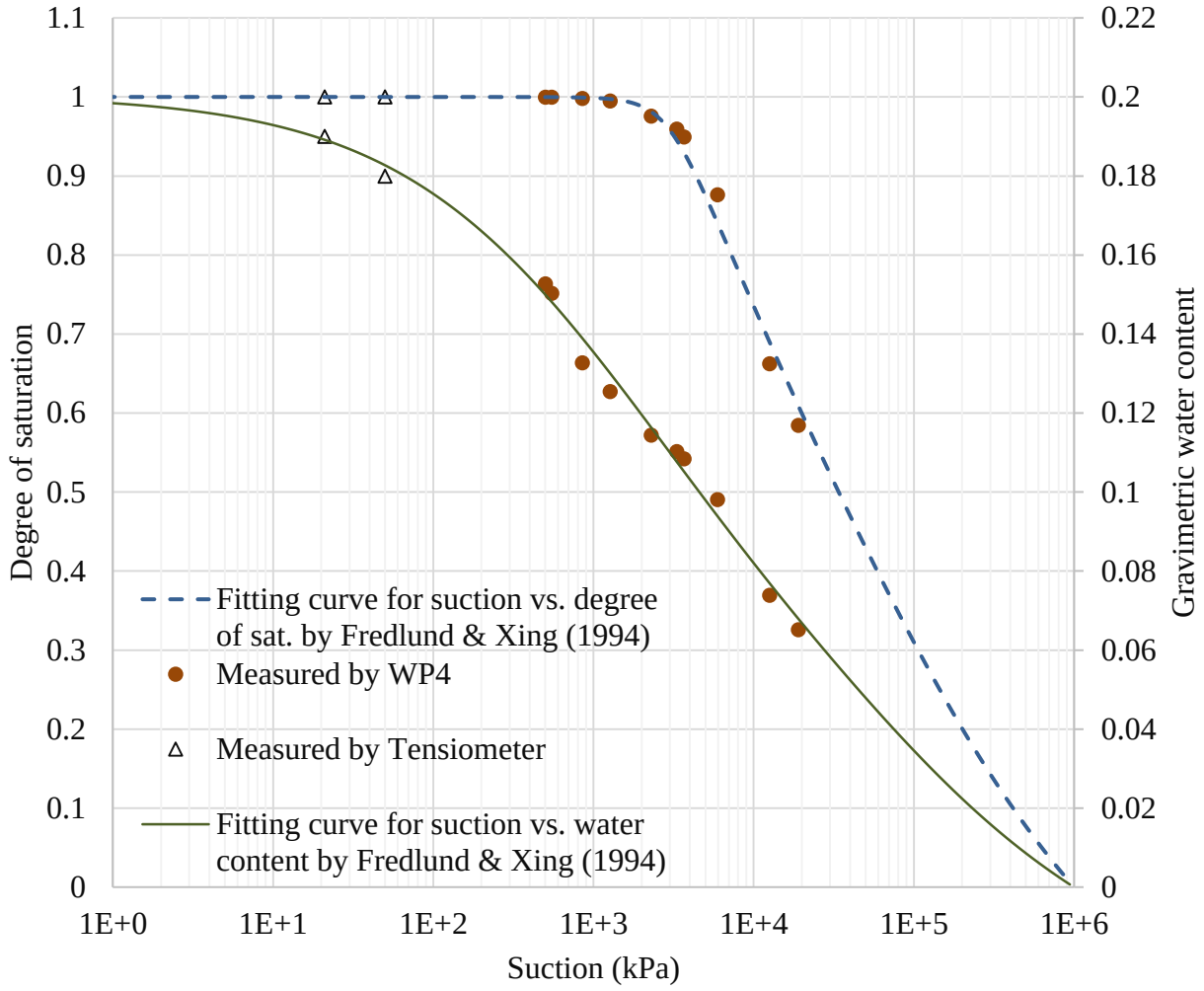

Figure 7.5. The Soil Water Characteristic Curve for High-Water Content Specimen of Lake Hefner Soil

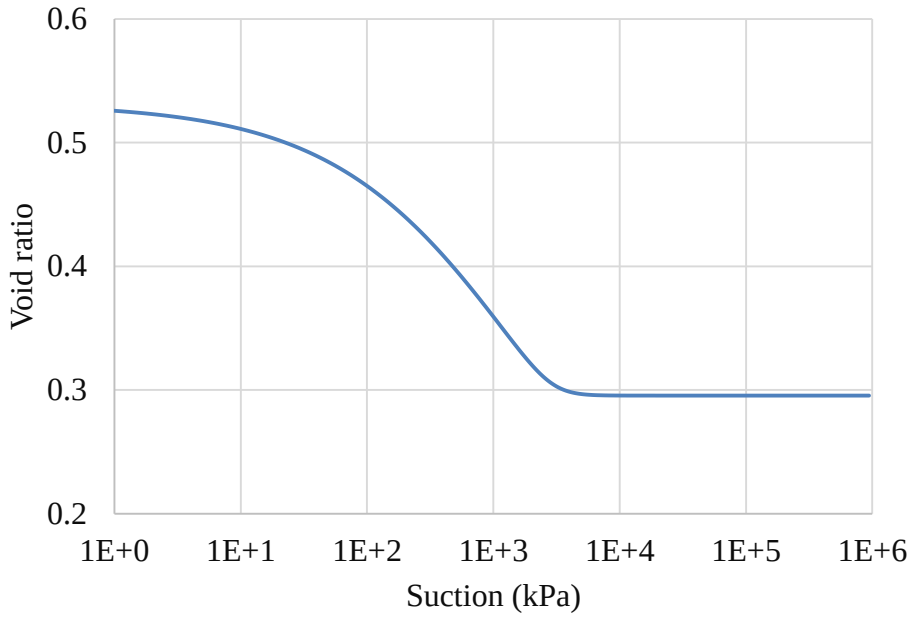

Figure 7.6. The e log s Curve for High-Water Content Specimen of Lake Hefner Soil

7.1.2 Comparison between SWCC and Volume Change Derived from Compacted and High-Water Content Specimens

Drying SWCC and shrinkage characteristic curve (SHCC) for high-water content and compacted specimens for Ardmore soil were predicted. The initial water content of the high-water content specimen and compacted specimen is 49% and 30% (which is close to the optimum water content), respectively. Two identical cylindrical specimens with 1.9 cm in height and 6.4 cm in diameter were prepared for compacted and high-water content condition, one for SWCC prediction and the other for SHCC prediction. The SWCC of high-water content specimen was predicted by WP4 and tensiometer since the initial water content is high. The SWCC of compacted specimen was predicted by WP4 only since its initial suction is out of tensiometer measurement range. The SHCC was predicted using the free shrinkage test by air drying and digital image analysis. The results of SWCC and SHCC are compared for both specimen conditions and plotted in Figures 7.7 and 7.8.

By taking the volume change into account, the predicted SWCC in terms of the degree of saturation was predicted for both high-water content and compacted samples and compared as in Figure (7.9).

Figure (7.7) shows that even though the soil starts drying from different water content and compaction condition, the SWCC (i.e. suction vs. gravimetric water content) of both high-water content and compacted specimen combines in one curve at high suction values (i.e. greater than 2 MPa). The latter confirms the uniqueness of the slope of the SWCC in terms of the gravimetric water content that was explained in chapter four, which is that the SWCC has a single virgin slope that does not change as long as the pore size distribution is not altered.

However, due to the existence of clods which make the degree of saturation less than 100%, the compacted soil reveals different SHCC from that of high-water content specimen (Figure 7.8). Therefore, the obtained SWCC in terms of the degree of saturation for compacted soil is significantly different from that of high-water content specimen (Figure 7.9). The existence of clods also increases the minimum void ratio the soil reaches at the shrinkage limit. That can change the slope of the e log s curve. Note that the slope of the e log s curve is changed only because of the variation of the minimum void ratio between the compacted and high-water content soil, not the variation of the degree of saturation (Figure 7.10).

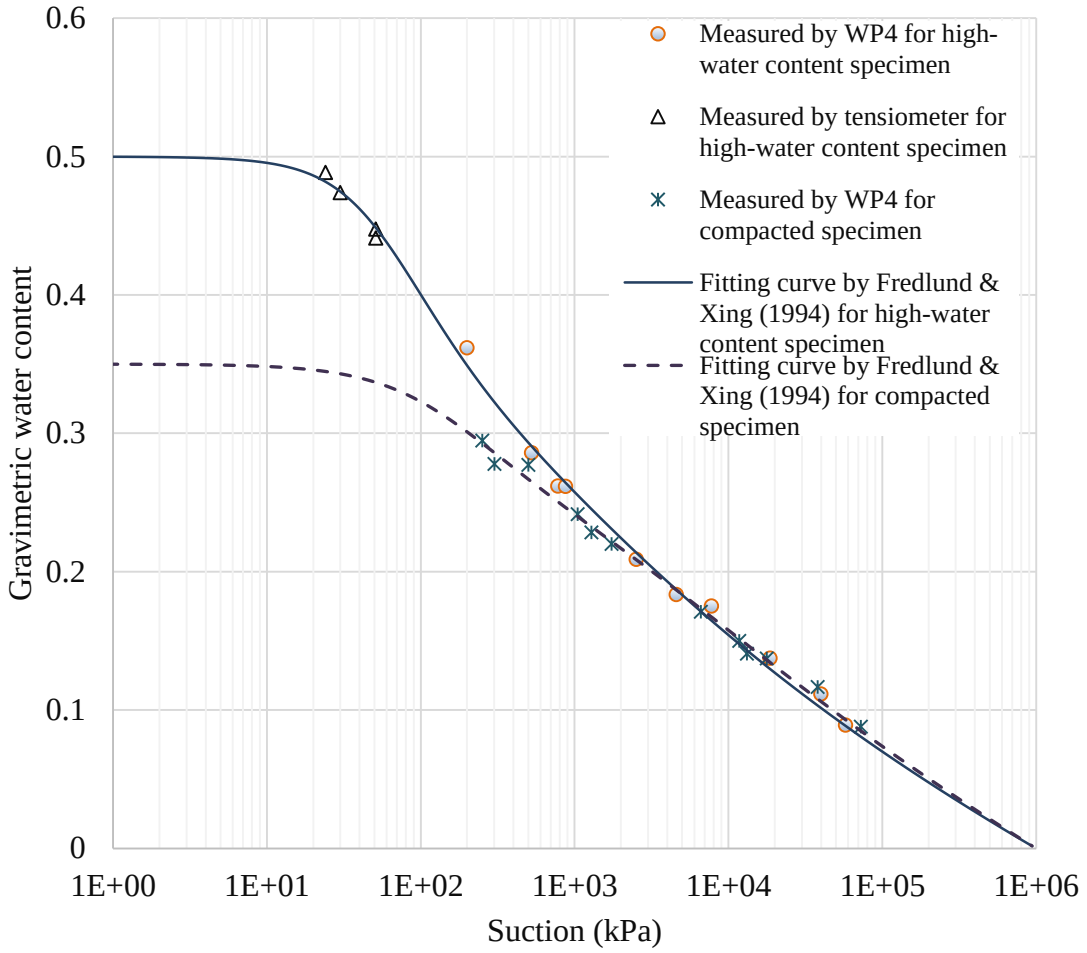

Figure 7.7 Comparison between the Soil Water Characteristic Curve Derived for high-Water Content Specimen and That Derived for Compacted Specimen of Ardmore Soil

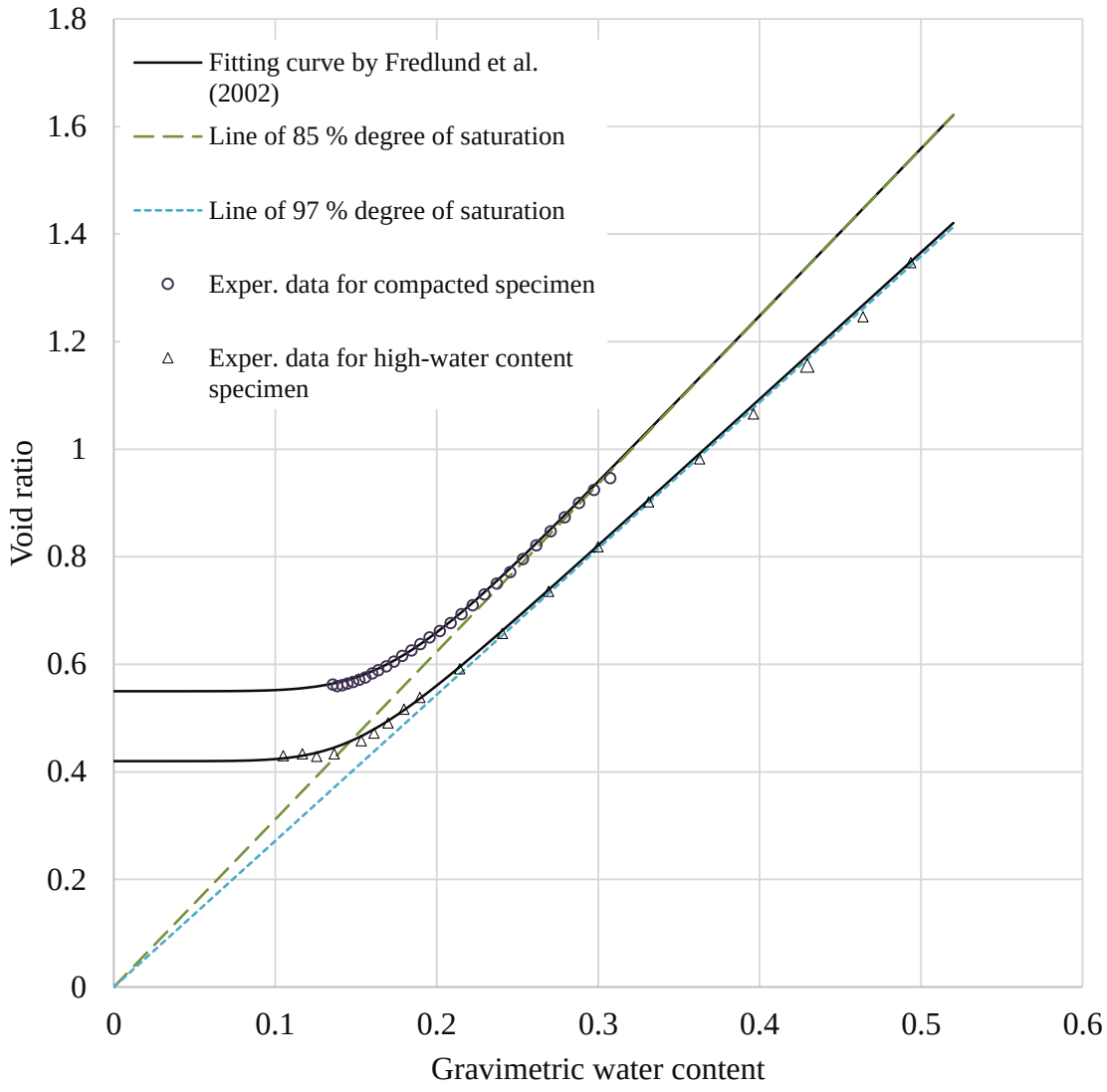

Figure 7.8 Comparison between the Soil Shrinkage Characteristic Curve Derived for High-Water Content Specimen and That Derived for Compacted Specimen of Ardmore Soil

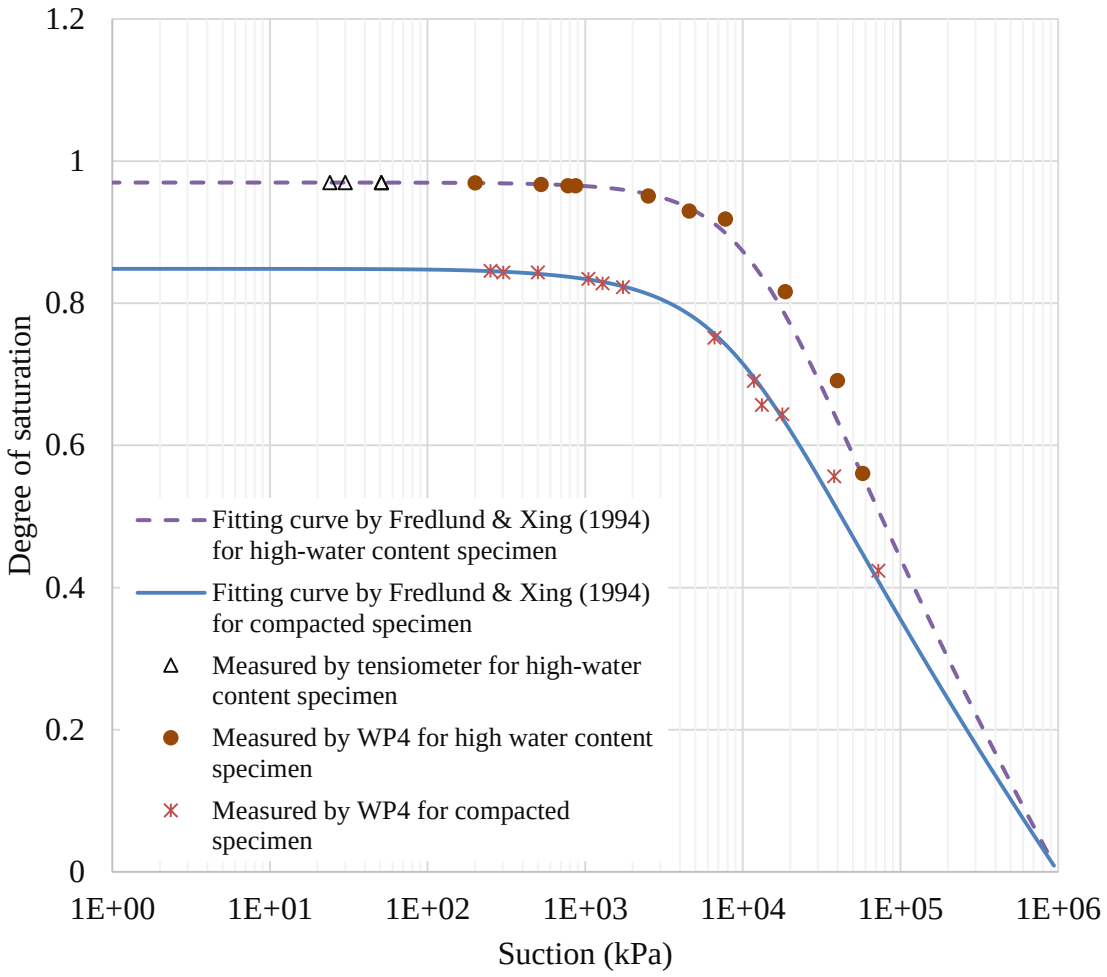

Figure 7.9 Comparison between the Soil Shrinkage Characteristic Curve Derived for High-Water Content Specimen and That Derived for Compacted Specimen of Ardmore Soil

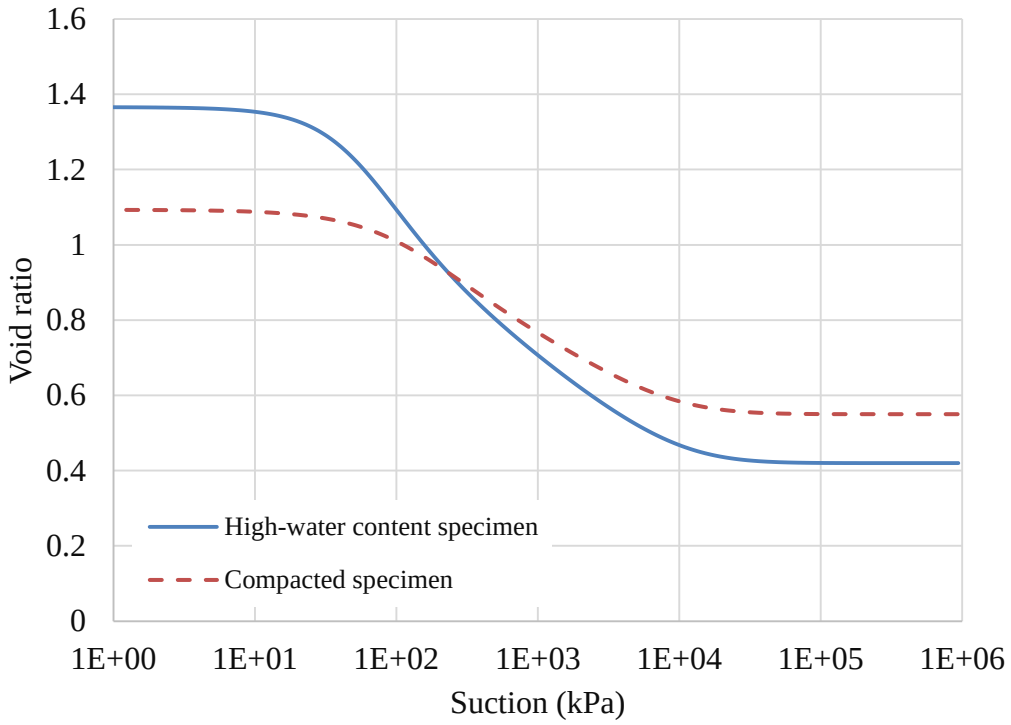

Figure 7.10 Comparison between the e log s Curve Derived for High-Water Content Specimen and That Derived for Compacted Specimen of Ardmore Soil

7.2 Restrained Ring Test

The restrained ring test is conducted on samples with different initial water contents and compaction conditions to achieve different varieties of soil conditions.

7.2.1 Cracking Characteristics

As the soil starts drying, it shrinks radially. The PVC ring restricts the shrinkage which induces tensile stress in the tangential direction. While shrinking, a single crack initiates as shown in Figure (7.11). After the crack initiation, the shrinkage will be totally led by the crack tip. The volume

change analysis using the digital image series was undertaken by *GeoPIV-RG* subroutines in MATLAB. The results are shown in Figure (7.12) for different shrinkage and drying stages.

Figure 7.11. The Cracking Mode of the Samples in the Restrained Ring Test

The formation of crack initiation in high plasticity soil (Ardmore soil) is different from low plasticity soil (Lake Hefner soil). Lake Hefner soil cracks suddenly over the whole radius. However, the crack initiates in the internal face for Ardmore soil sample and gradually grows toward the exterior edge. After the crack initiation the crack width keeps increasing until it reaches a stable stage. That is the shrinkage limit of the soil at which the water loss does not accompany with crack growth or shrinkage. That stage occurs earlier for Lake Hefner soil than for Ardmore soil.

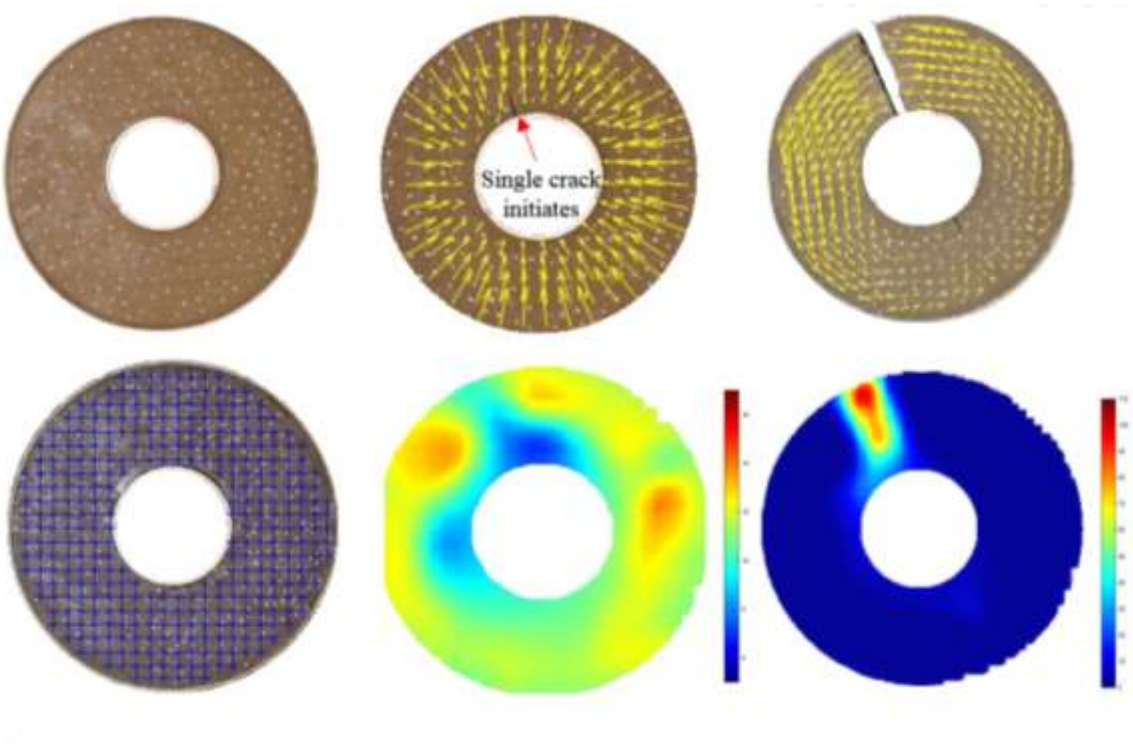

(A) w = 30.7 % (B) w = 19.8 % (C) w = 13.9 %

Figure 7.12 Drying Stages and the Strain of the Sample in the Restrained Ring Test (A) Initial Water Content before Starting the Test and Subsets Meshing (B) Crack Initiation Stage (C) Crack Growth. *w* is the gravimetric water content.

7.2.1.1 High-Water Content Specimens

High-water content specimens with different water contents were prepared and tested. The mixing water content is high yet still less than the liquid limit. The details of specimen preparation are presented in Section 7.1.1. During drying, the water content, volume change, and soil suction were determined with time. The results are depicted in Figures 7.13 and 7.14.

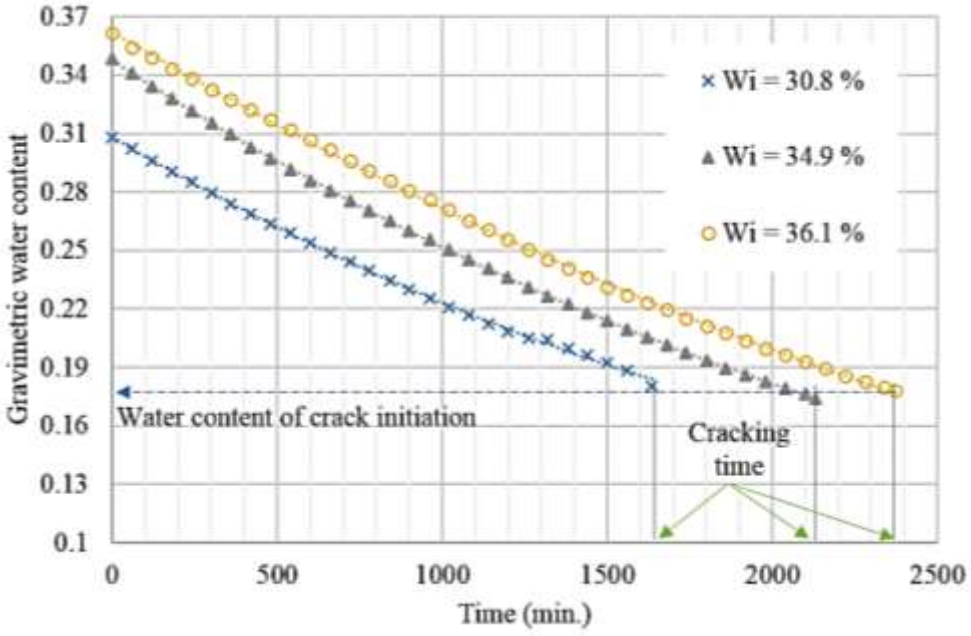

Figure 7.13. The Gravimetric Water Content vs. Time in the Restrained Ring Test before the Crack Initiation (High-Water Content Ardmore Soil)

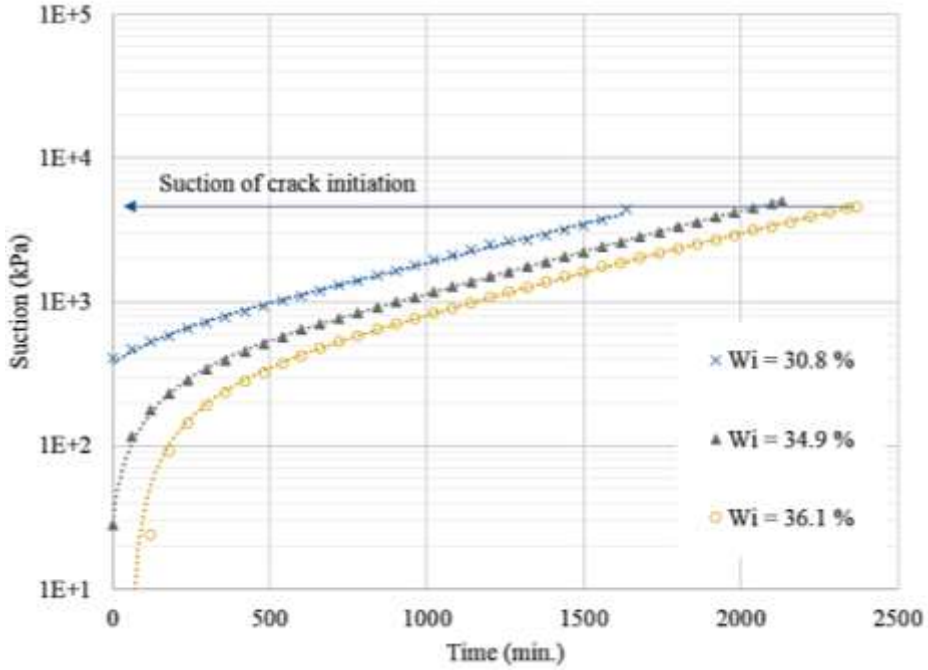

Figure 7.14. The Suction vs. Time in the Restrained Ring Test before the Crack Initiation (High-Water content Ardmore Soil)

Even though the high-water content specimens of Ardmore soil commence drying from different initial water contents, they crack at similar water content values. The water content of crack initiation is very close to 18% which is corresponding to a suction of 4.5 MPa. However, the drying time from the beginning of drying to the crack initiation is different. For example, the specimen of 27.5% initial water content cracks after 21 hours while the cracking time of the specimen of 36.1% is 39 hours.

The water content of crack initiation which is 18% is very close to the air entry point as shown in the SWCC in Figure 7.15 and SHCC in Figure 7.16. Therefore, the specimen with higher initial water content will experience greater shrinkage and cracking time.

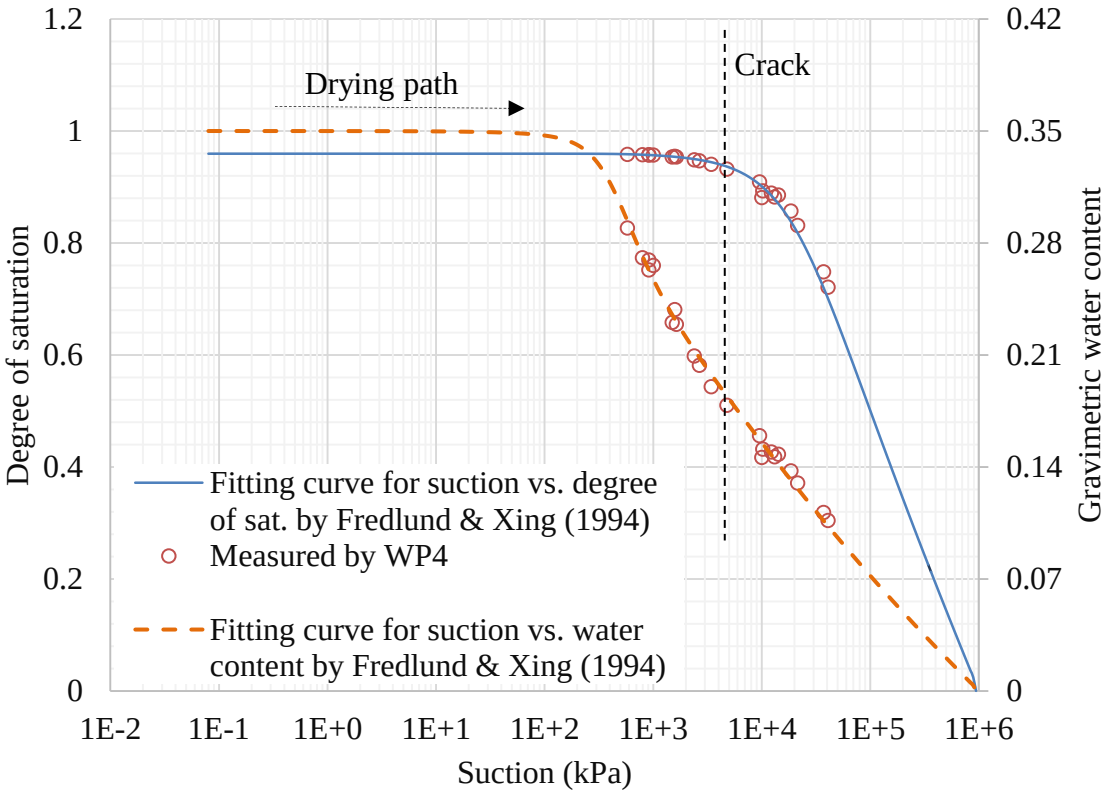

Figure 7.15. The Crack Initiation Taking Place at a Stage close to the Air Entry Value (SWCC of Ardmore Soil)

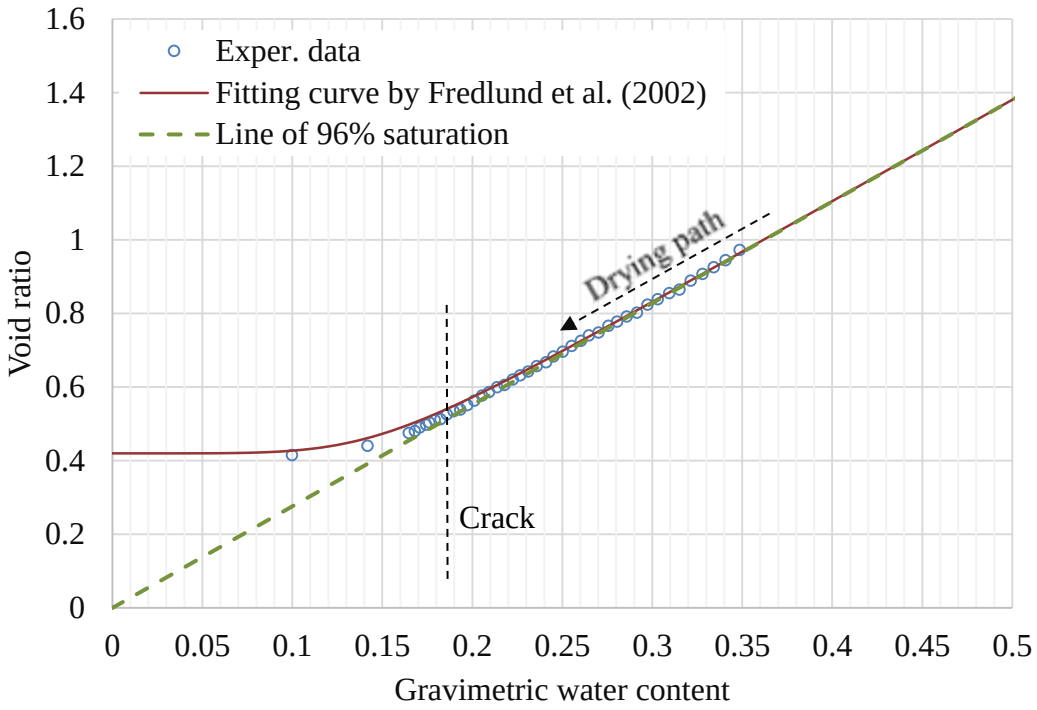

Figure 7.16. The Crack Initiation Taking Place at a Stage close to the Air Entry Value (SHCC of Ardmore Soil)

Since the crack initiates close to the air entry value which is the final stage of the normal shrinkage, all the specimens experience a linear shrinkage prior to cracking. That can be noticed from the surface strain of the specimen in the radial direction which is obtained by the digital image analysis. The surface strain versus the time curve from the beginning of the test until the cracking time is shown in Figure 7.17.

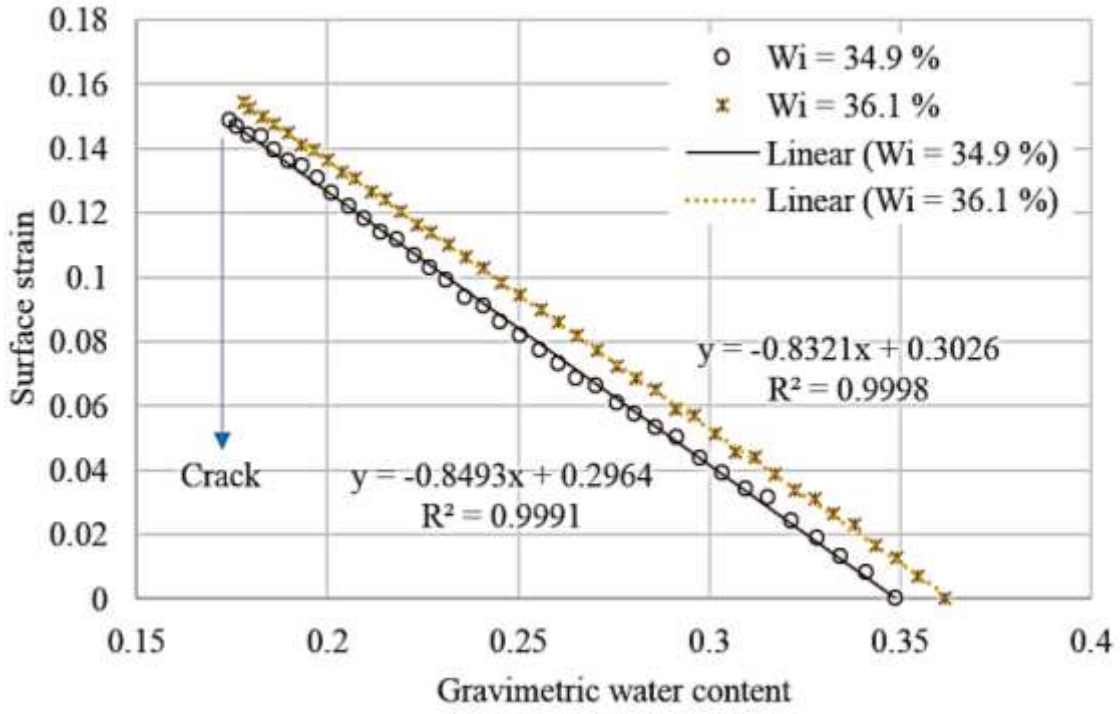

Figure 7.17. The Gravimetric Water Content vs. the Surface Strain of the Sample in the Restrained Ring Test before the Crack Initiation (High-Water Content Ardmore Soil)

The crack width is dependent on the residual shrinkage the soil undergoes. Since it has high plasticity and hence high residual shrinkage, Ardmore soil developed a wide crack before reaching the shrinkage limit while Lake Hefner soil showed a relatively narrow crack and reached the stable stage (i.e. the shrinkage limit) after a relatively short time.

Similar results have been found for the Osage and Lake Hefner 1 soils. The summary of the results for all the soil samples tested in a high water content condition without any compaction effort is listed in Table 7.1.

Table 7.1. Summary of the Results for the Soil Specimens of the High-Water Content in the Restrained Ring Test

Soil name	Test no.	Initial water content (%)	Initial suction (pF)	Final water content (%)	Final suction (pF)	Cracking time (hours)
Ardmore	1	30.9	3.6	18.3	4.63	27.6
	2	35	2.55	17.6	4.69	35.75
	3	36.1	2.4	17.8	4.67	38.5
Lake Hefner	1	20.2	2.4	13.2	4.06	22.5
	2	17.7	2.93	12.7	4.16	15.8
Osage	1	30.4	3.6	17.3	4.7	36
	2	32.7	3.3	17	4.75	41.7
	3	37.2	2	17	4.74	40
Lake Hefner 1	1	25.4	2.2	17.2	4.15	24

7.2.1.2 Compacted Specimens

The results of the compacted specimens at optimum water content come slightly different from those of high-water content specimens. The specimens were mixed with water content close to the optimum water content and compacted using the standard Proctor testing method. The water content and suction versus the time are illustrated in Figure (7.18) and (7.19) respectively.

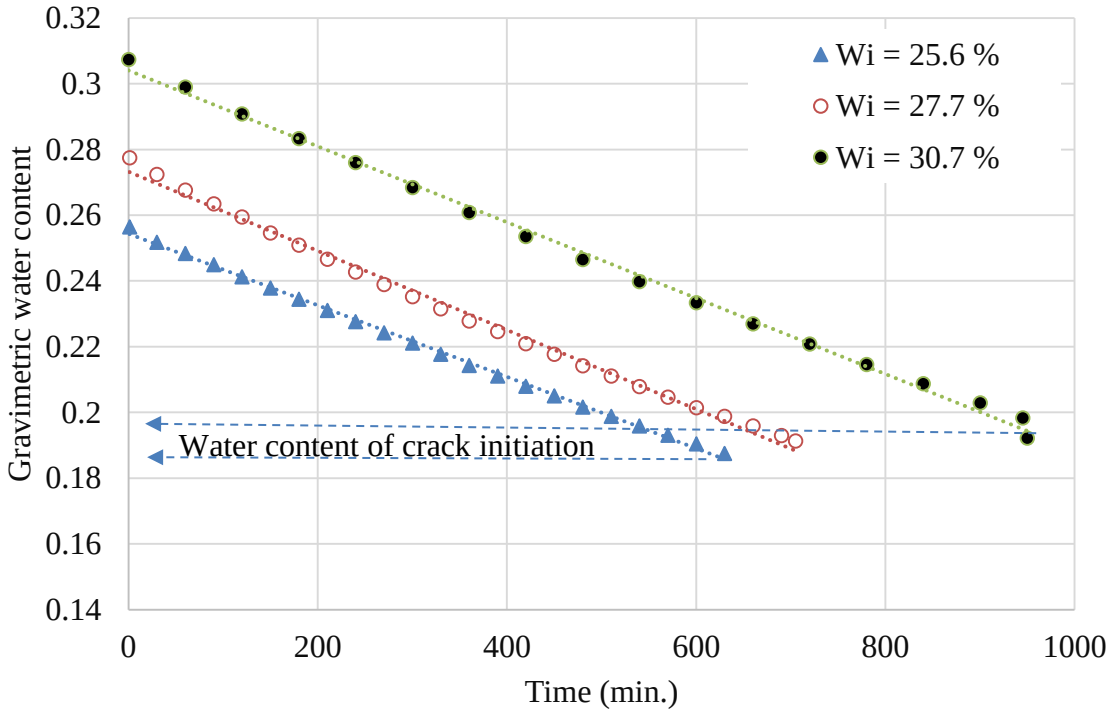

Figure 7.18. The Gravimetric Water Content vs. Time in the Restrained Ring Test before the Crack Initiation (Compacted Ardmore Soil)

The compacted specimens were also cracked at a stage close to the end of the normal shrinkage. However, they show a slight difference. The specimen mixed with 30.7% water content cracked at 19.8% water content, while the one mixed with 25.6% cracked at 18.6%. This difference arises from the variation of the compaction effort absorbed by the specimen which is reflected in the

volume change characteristics. The radial surface shrinkage strain versus the water content before and after the cracking is shown in Figure 7.20. Figure 7.20 shows that the normal shrinkage of the specimen with 30.7% initial water content ends at a slightly higher water content than the specimen with 25.6% initial water content.

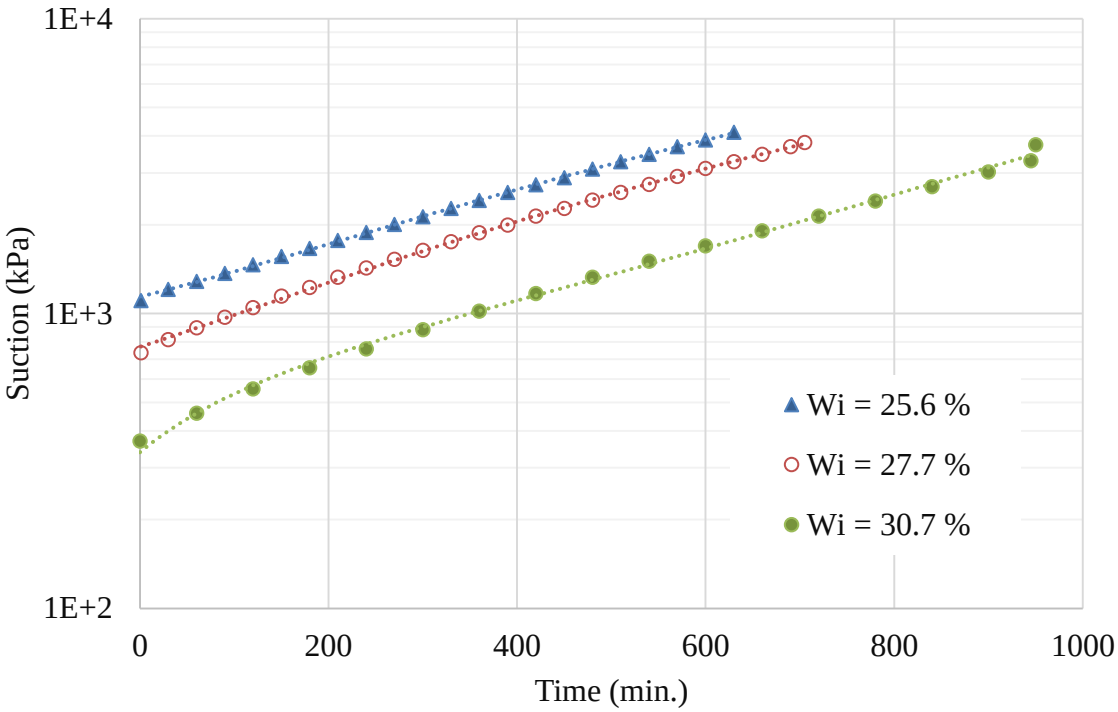

Figure 7.19. The Suction vs. Time in the Restrained Ring Test before the Crack Initiation (Compacted Ardmore Soil)

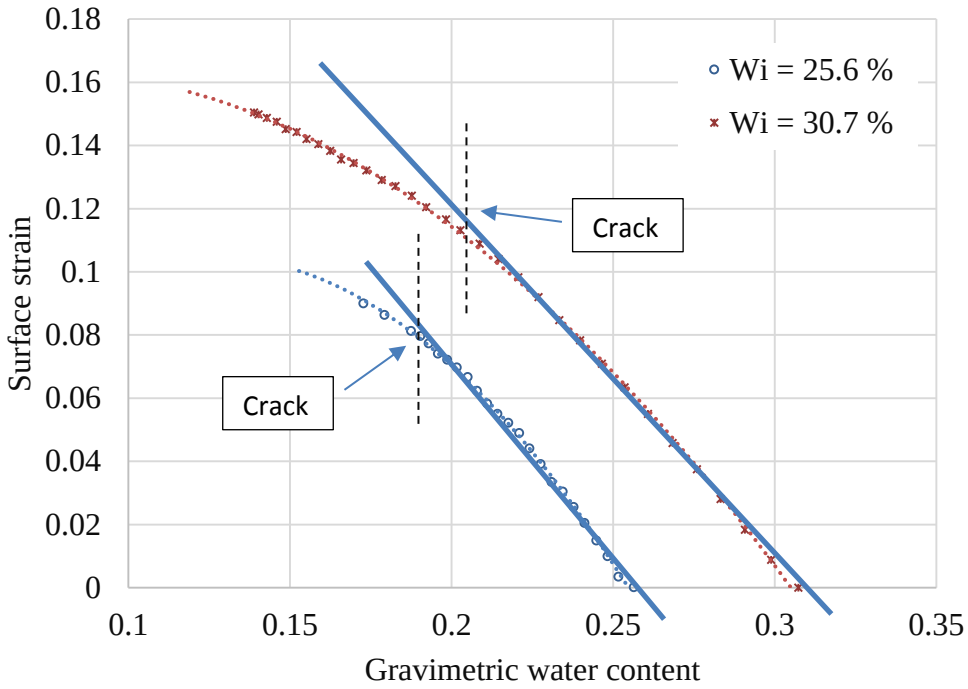

Figure 7.20. The Gravimetric Water Content vs. the Surface Strain of the Sample in the Restrained Ring Test before and after the Crack Initiation (Compacted Ardmore Soil)

In general, the compacted samples cracked at water content slightly higher than that of high-water content specimens. The difference is less than 2% for Ardmore soil. The cracking time of the compacted soil samples is significantly less than that of the high-water content specimens for the same range of water content. That can perhaps be attributed to the existence of clods in the compacted samples which increase the soil permeability and therefore the desiccation rate.

The results of all the compacted soil specimens are summarized in Table 7.2.

Table 7.2. Summary of the Results for the Compacted Soil Specimens in the Restrained Ring Test

Soil name	Test no.	Initial water content (%)	Initial suction (pF)	Final water content (%)	Final suction (pF)	Cracking time (hours)
Ardmore	1	25.6	4.04	18.6	4.63	10.5
	2	27.75	3.87	19.1	4.58	11.75
	3	30.7	3.57	19.8	4.52	16.08
Lake Hefner	1	16	2.9	11.2	3.88	12.6
	2	19.4	2.46	14	3.28	12.2
	3	20	2.4	14.6	3.16	10.4
	4	20.1	2.38	13.6	3.36	13.9
Lake Hefner 1	1	22.4	2.43	15.4	3.53	14.6
	2	24	2.23	18	3.02	13

7.2.1.3 Effect of Sample Size on Cracking

To study the effect of the sample size on the crack initiation stage and the cracking time, a specimen with a smaller diameter (10.16 cm) and a height of (1.55 cm) was prepared. A high-water content specimen was prepared. It was molded inside a PVC ring without compaction. This soil will be referred to as high-water content specimen.

The results also show that the crack first initiates at a stage close to the air entry value after the soil completes the normal linear shrinkage and reaches the residual non-linear shrinkage. That can be observed from the relationship between the water content and the sample surface strain as shown in Figure 7.21. Figure 7.21 confirms that the crack occurs at a stage close to the air entry value and the final point of the normal shrinkage is independent from the specimen geometry. The results are summarized in the Table 7.3.

Table 7.3. Summary of the Results for the Small Size Soil Specimen in the Restrained Ring Test (High-Water content Ardmore Soil)

Soil name	Initial water content (%)	Initial suction (pF)	Final water content (%)	Final suction (pF)	Cracking time (hours)
High-water content Ardmore specimen	49.4	2.1	19.8	4.55	38

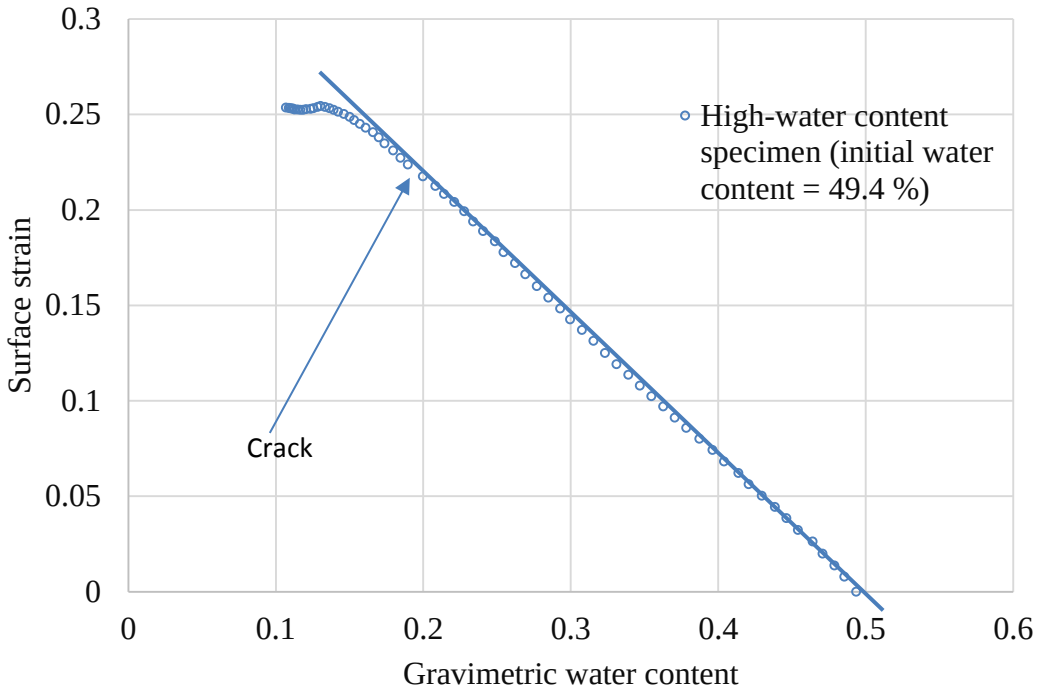

Figure 7.21. The Gravimetric Water Content vs. the Surface Strain of the Small Size specimen in the Restrained Ring Test before and after the Crack Initiation (Ardmore Soil)

7.2.1.4 Unexpected Crack Initiation

Cracks of some samples initiate at unexpected stages. Two high-water content specimens one of Osage soil and the other of Ardmore soil cracked at lower water content values than the others. The high-water content Ardmore specimen, which supposes to crack at a water content between 18 % and 20 %, cracked at water content of 15.8 %. The high-water content Osage specimen, which supposes to crack at a water content between 17 % and 18 %, cracked at water content of 15.2 %. That occurs because these samples could delay the air entry value probably due to the lake of the flaws or the large macropores. The flaws and macropores play a role in the air bubbles penetration through the water-soil particles system and hence the development of the visual crack from the existent micro cracks.

Another case happened that the crack did not initiate at all. That occurred for two compacted specimens from Lake Hefner 2 soil, which is a low plastic soil. The water content of these specimens exceeded the shrinkage limit and they did not develop cracks. The water content versus the radial surface shrinkage is graphed in Figure (7.22). That is probably because the shrinkage developed was not sufficient to initiate cracks. That occurred for two samples with initial water content being 11.8 % and 15.1 %. However, a third compacted sample also tested with 16 % initial water content of the same soil cracked at 11.4 % water content with a cracking time equal to 11.75 hours.

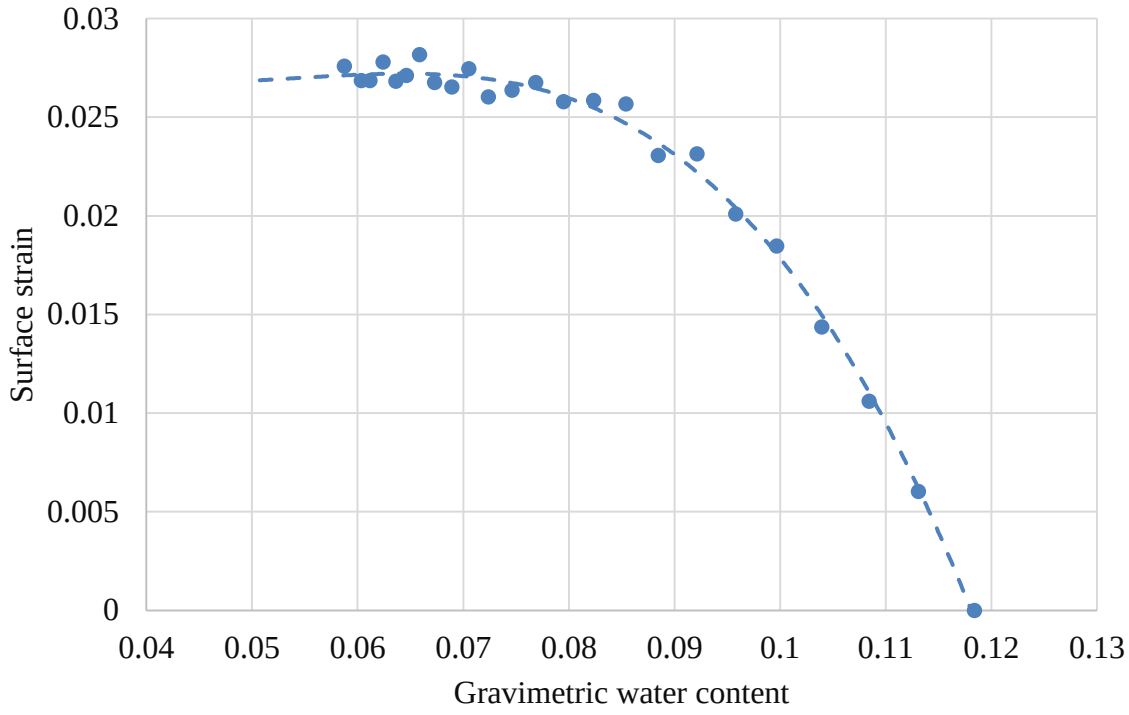

Figure 7.22. The Gravimetric Water Content vs the Surface Strain for Compacted Specimen of Lake Hefner 2 Soil in the Restrained Ring Test

7.2.1.5 Crack Initiation in Cracked Specimen

To investigate the possibility of extending the crack initiation observation to include the crack growth as well. That is the air entry value (AEV) is not only the event of crack initiation but also crack propagation, at which the tensile stress exceeds the soil tensile strength. A compacted cracked specimen of Ardmore soil was prepared at water content equal to 30.3 %. The specimen was compacted by mixing at the optimum moisture content and compacted in three layers inside a standard mold with a standard compaction following ASTM D698. A PVC ring with the same diameter as the standard mold 10.16 cm and 1.55 cm in height was gently pushed around the soil specimen. The soil was cut and trimmed in both PVC surfaces. Then a single artificial crack was made in the internal side of the specimen (Figure 7.23).

Figure 7.23 Specimen with Artificial crack in the Internal Side (Compacted Ardmore Soil)

The results of the surface strain vs. the gravimetric water content are shown in Figure 7.24. The results also showed that the new crack did not initiate until the shrinkage of the soil reached the

end of the normal shrinkage zone. That probably indicates that the air entry value is point at which new crack or the existent crack grows or propagates. The results are summarized in Table 7.4.

Table 7.4 Summary for the Restrained Ring Test of Initially Cracked Specimen (Compacted Ardmore soil)

Soil name	Initial water content (%)	Initial suction (pF)	Final water content (%)	Final suction (pF)	Cracking time (hours)
Compacted Ardmore specimen	30.3	3.3	24	4	10

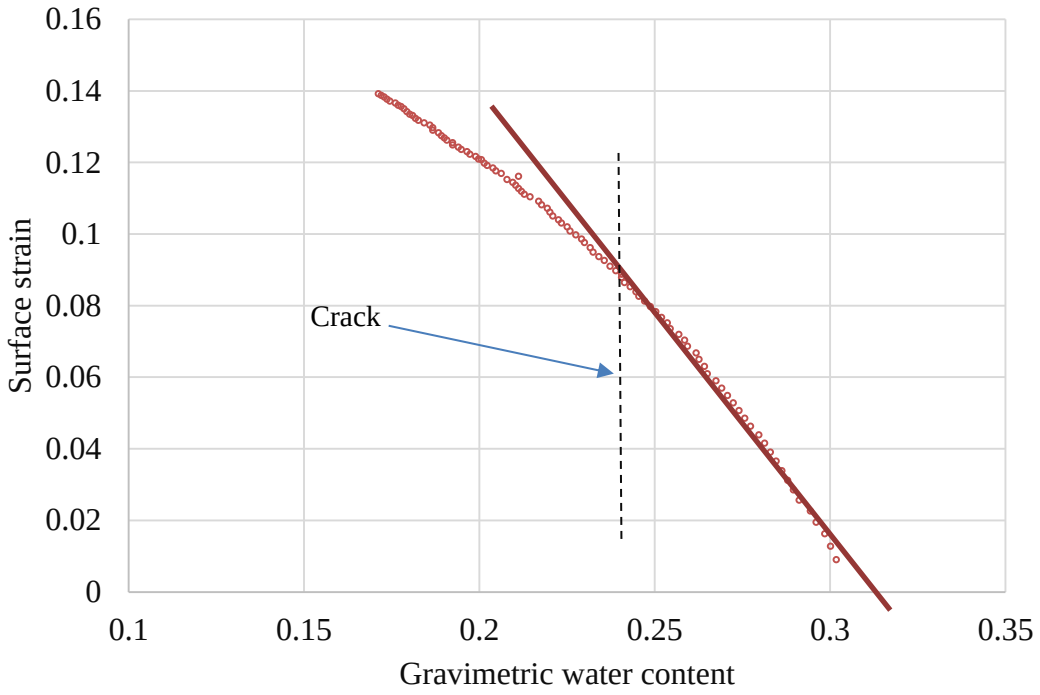

Figure 7.24. The Gravimetric Water Content vs. the Surface Strain of Initially Cracked Specimen (Compacted Ardmore Soil)

7.2.2 Results of Micro Strain Gauges

Three micro strain gauges were installed on the inner face of the restraining PVC ring (Figure 7.25). The angle between them is approximately 120°. As the soil sample shrinks radially and applies a pressure on the PVC ring, the produced micro strain will be sensed by the strain gauges.

The working principle of the strain gauge is that the resistance of strain gauge varies with its length when subjected to any stress. As a result, the strain is determined from the calibration equation between the resistance and the strain gauge length (Mayergoyz and Lawson 1996). To measure the change in resistance, a very low electric current is issued through the data acquisition device (Chen 2015).

The results of the strain gauges will be read by a data acquisition system collecting the strain gauge recordings from every channel connected to a strain gauge. The data acquisition is also accessed to a computer to control the system and output the results.

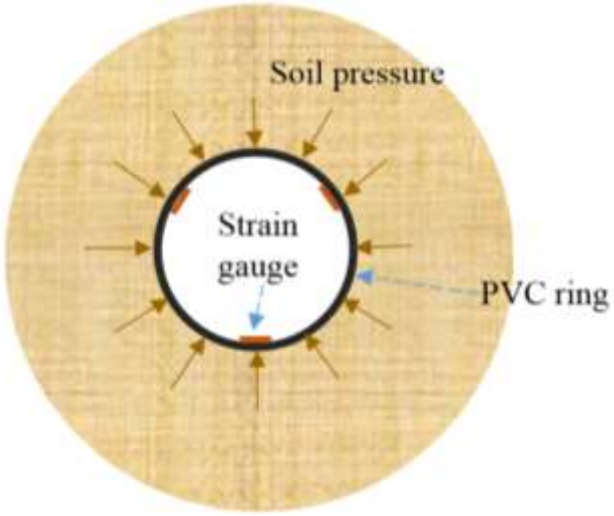

Figure 7.25. Schematic Drawing for the Soil Pressure on the PVC Ring and the Strain Gauges in the Restrained Ring Test

As the soil sample shrinks toward the core (the PVC ring), two kinds of stresses are induced. One is a tensile stress the soil experiences. This stress arises from the restrained shrinkage resulted from the restraining ring. The other stress is a compressive stress applied by the soil on the ring. The illustration of the stresses regime in the restrained ring test is given in Figure 7.26 (Abou Najm et al. 2009).

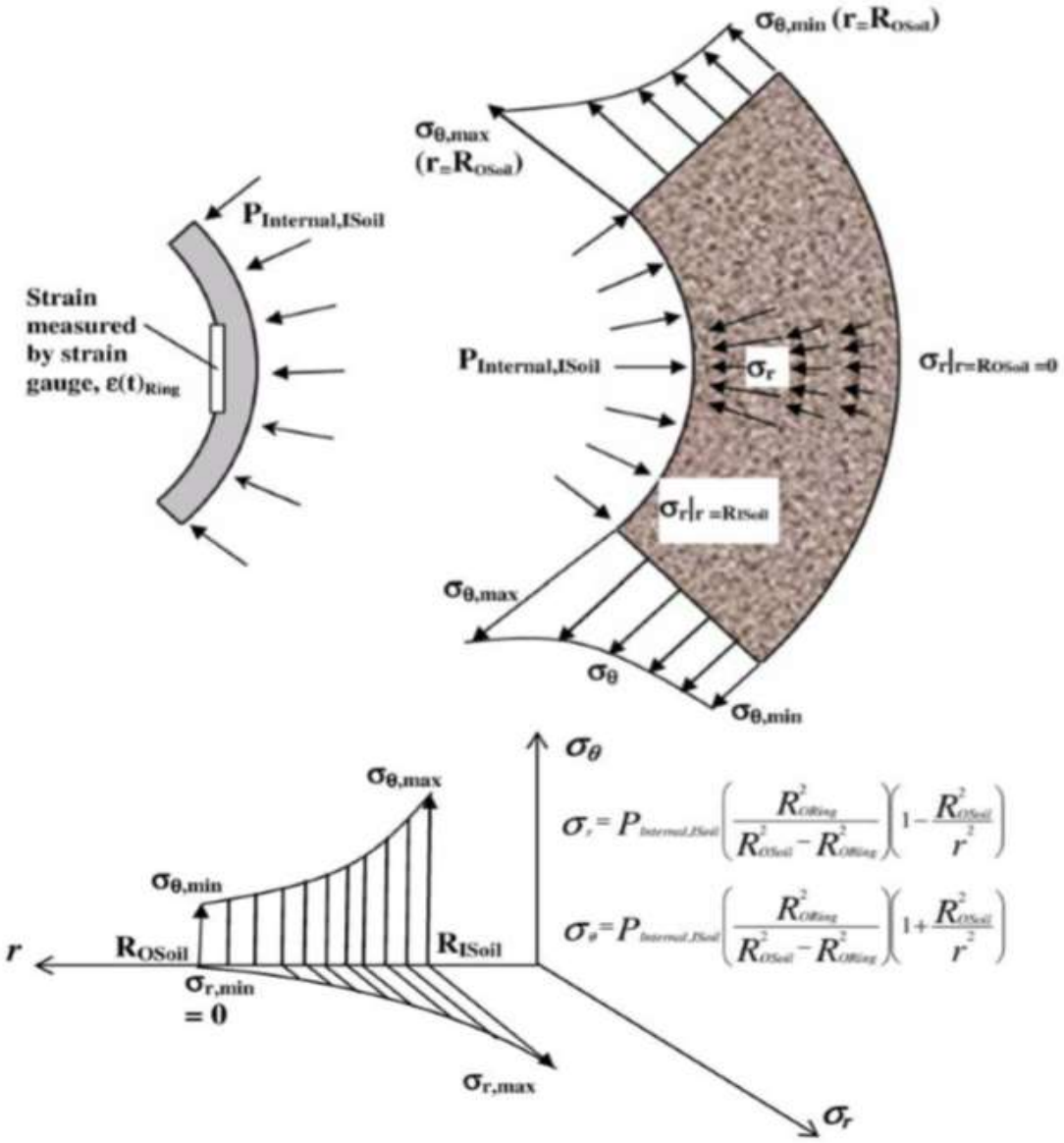

Figure 7.26. The Tensile and Compressive Stress Distribution in the Restrained Ring Test (Abou Najm et al. 2009)

The determination of the tensile and compressive stress from the strain gauges using this method is proposed by Weiss and Ferguson (2001) for concrete, and Abou Najem et al. (2009) for soil. They use the solution for an elastic stress in pressurized cylinders by considering the sample as an elastic and isotropic material before cracking. Therefore, the maximum tensile stress is given as follows:

$$\sigma_{t\,max} = -\epsilon(t)E\left(\frac{R_{Osoil}^2 + R_{Oring}^2}{R_{Osoil}^2 - R_{Oring}^2}\right)\left(\frac{R_{Oring}^2 - R_{Iring}^2}{2R_{Oring}^2}\right) \quad (7.4)$$

Where $\epsilon(t)$ is the micro-strain captured by the strain gauges for time *t*, E is the modulus of elasticity for the PVC ring (2.9 GPa), R_{Osoil} is the radius of the soil, R_{Oring} is the radius of the ring to the out face, R_{Iring} is the internal radius of the ring.

7.2.2.1 Correction for the Strain Gauges Readings

When the core PVC ring is fitted in the center of the soil specimen, a small gab can exist between the soil surface and the exterior ring face. As a result, the soil will not apply a pressure on the ring until it shrinks radially and comes in touch with the ring. For that reason, a correction should be carried out. That is achieved by neglecting any results the strain gauge senses before the soil comes in touch with the ring surface. For example, Figure (7.27) shows typical results from the three strain gauges. The point where the strain gauges reading path deviates indicates the time that the soil just touches the ring and starts applying a pressure on it. The results are corrected by setting this point to zero for each strain gauge.

.

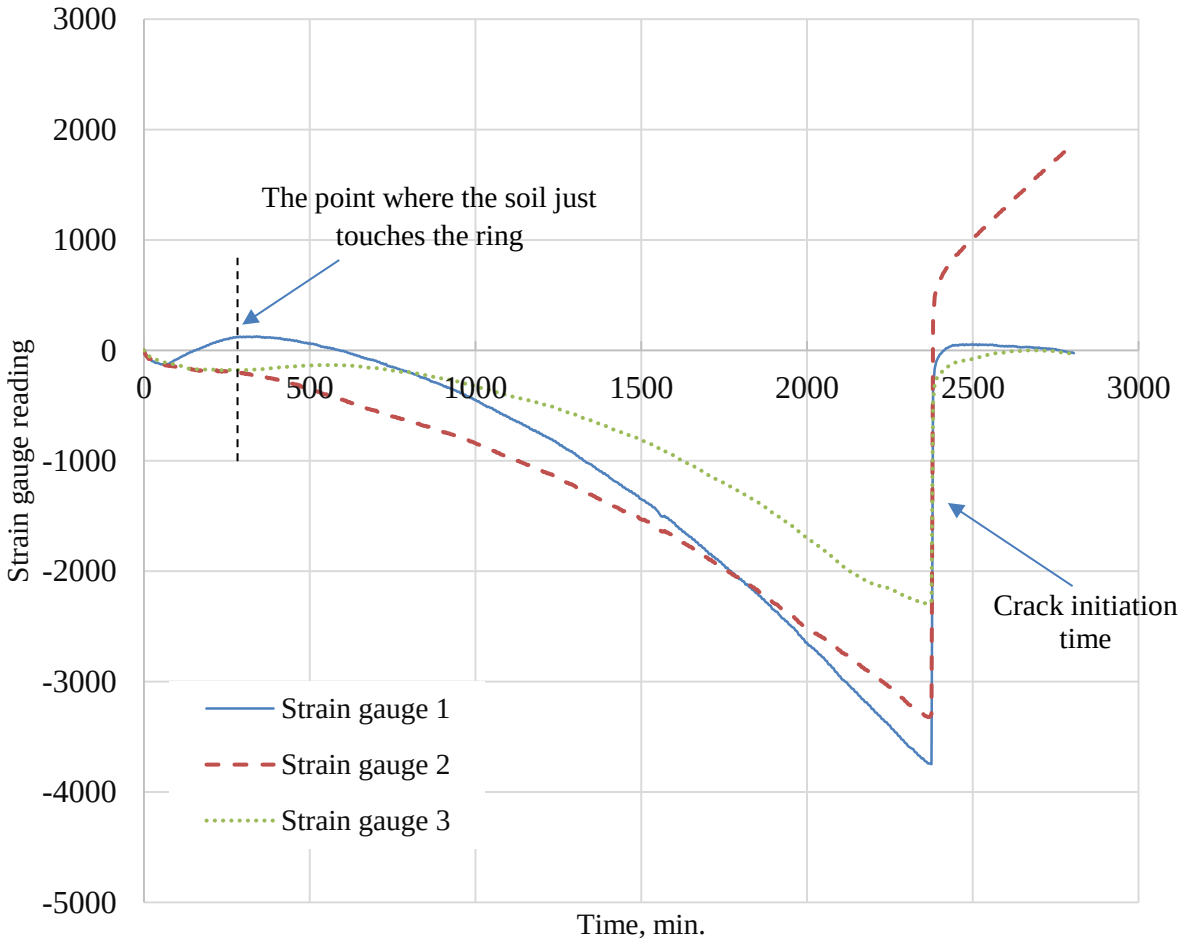

Figure 7.27. Typical Results from Strain Gauges in the Restrained Ring Test

7.2.2.2 Tensile Stress

The results of the tensile stress for high-water content specimens of Ardmore soil are illustrated in Figure 7.28 and 7.29.

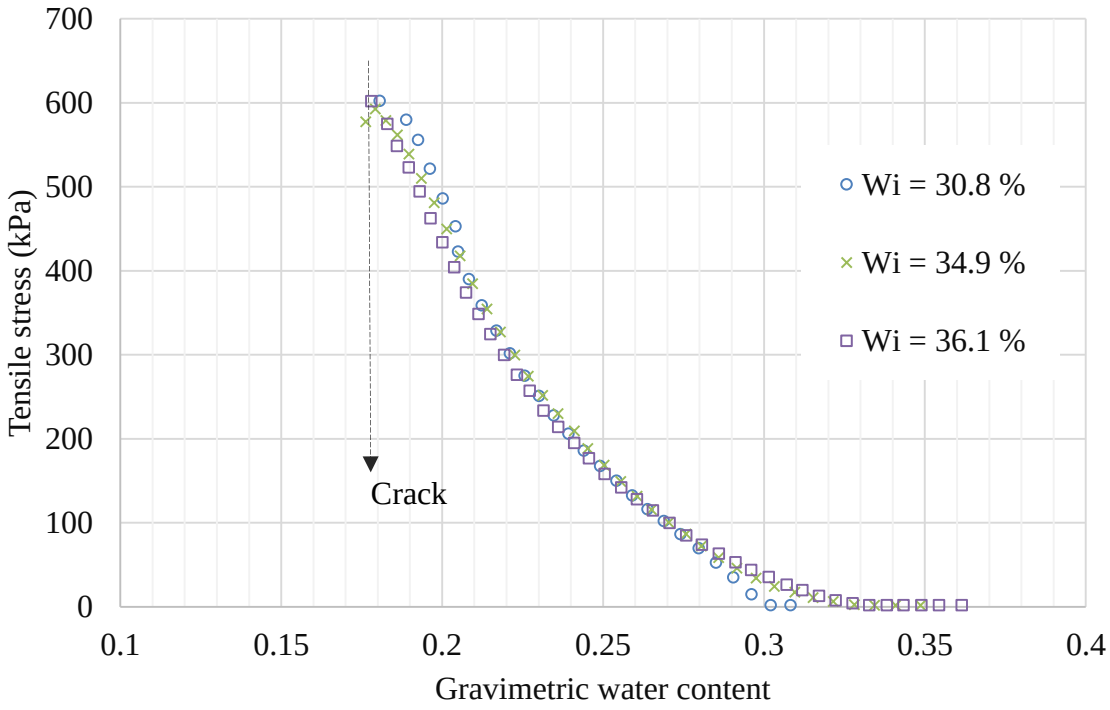

Figure 7.28. The Gravimetric Water Content vs. the Tensile Stress in the Restrained Ring Test before the Crack Initiation (High-Water Content Ardmore Soil)

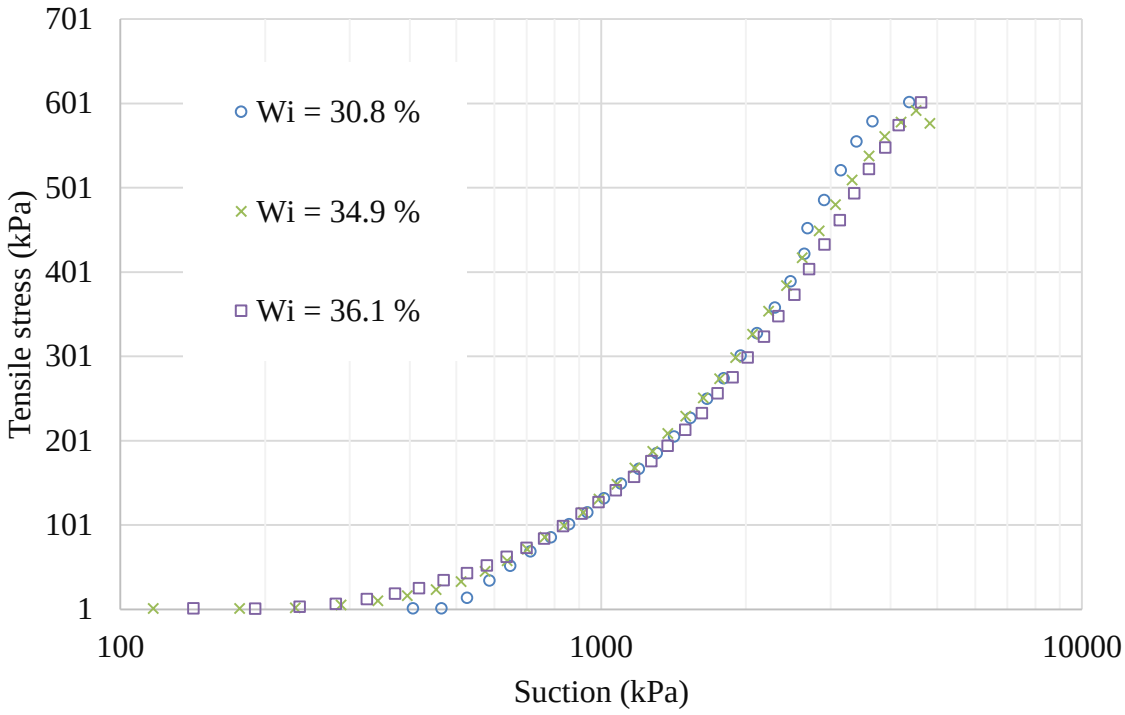

Figure 7.29. The Suction vs. the Tensile Stress in the Restrained Ring Test before the Crack Initiation (High-Water Content Ardmore Soil)

The results from Figures 7.28 and 7.29 suggest that the three specimens with initial water content 30.8%, 34.9%, and 36.1%, developed similar tensile stresses before cracking. Since the crack initiated at a stage close to the air entry value, the air entry value can be considered as the most suspect point where the tensile stress exceeds the soil tensile strength.

Similar tendency is also found for the tensile stress results from the compacted specimens with a slight difference. That is maybe because the compaction varies the shrinkage characteristics and most likely makes it non-uniform. That is probably because the existence of clods in the compacted specimens or any non-uniformity of the specimen density that can be induced in the specimen

preparation stage. The tensile stress results of the compacted specimens of Ardmore soil are shown in Figure 7.30.

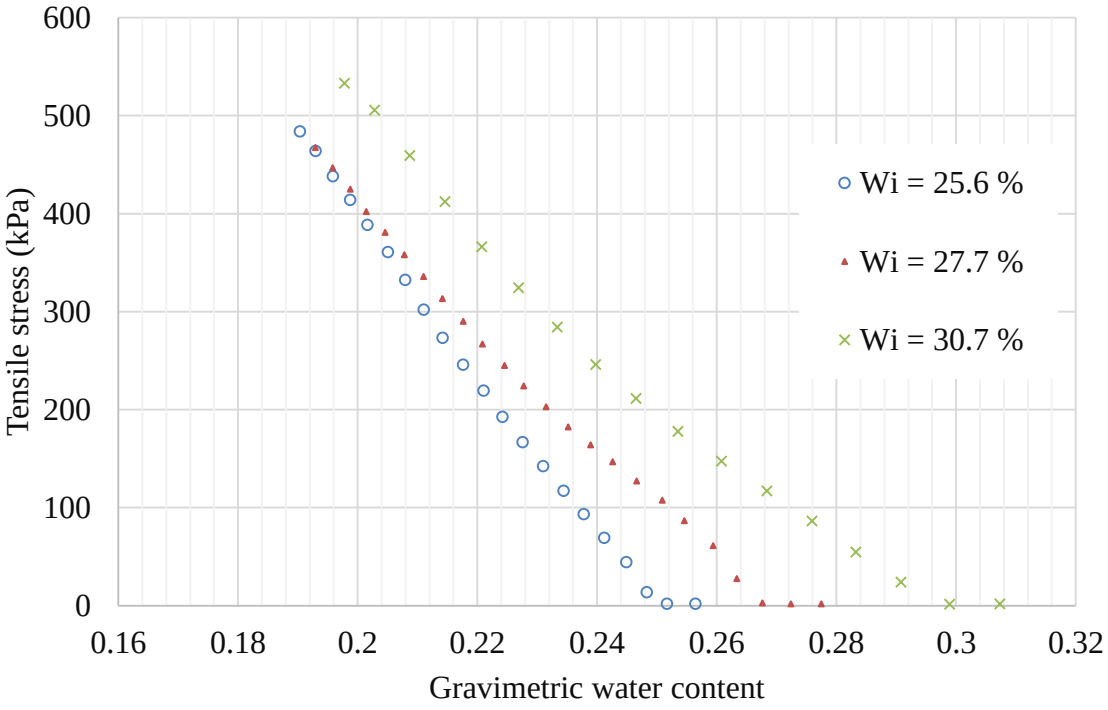

Figure 7.30. The Gravimetric Water Content vs. the Tensile Stress in the Restrained Ring Test before the Crack Initiation (Compacted Ardmore Soil)

7.1 Tensile Strength Measurements

The results obtained from the Brazilian test were used to estimate the tensile strength using the following equation (ASTM D3967 2016):

$$\sigma_t = \frac{2\,P}{\pi\,t\,D} \qquad (7.5)$$

Where σ_t is the soil tensile strength, P is the maximum load (the failure load applied), t is the tested specimen thickness, and D is the tested specimen diameter. One soil was tested (i.e. Ardmore soil). The results of the tensile strength together with the results of shrinkage (soil shrinkage characteristic curve) are illustrated in Figure 7.31. The results of the tensile strength agree with previous studies (e.g. Vesga 2009; Villar et al. 2009). Figure 7.31 shows that the soil shows a peak tensile strength during desiccation at a stage close to the air entry point. That can probably justify the common observation of crack initiation at stage near to the air entry point.

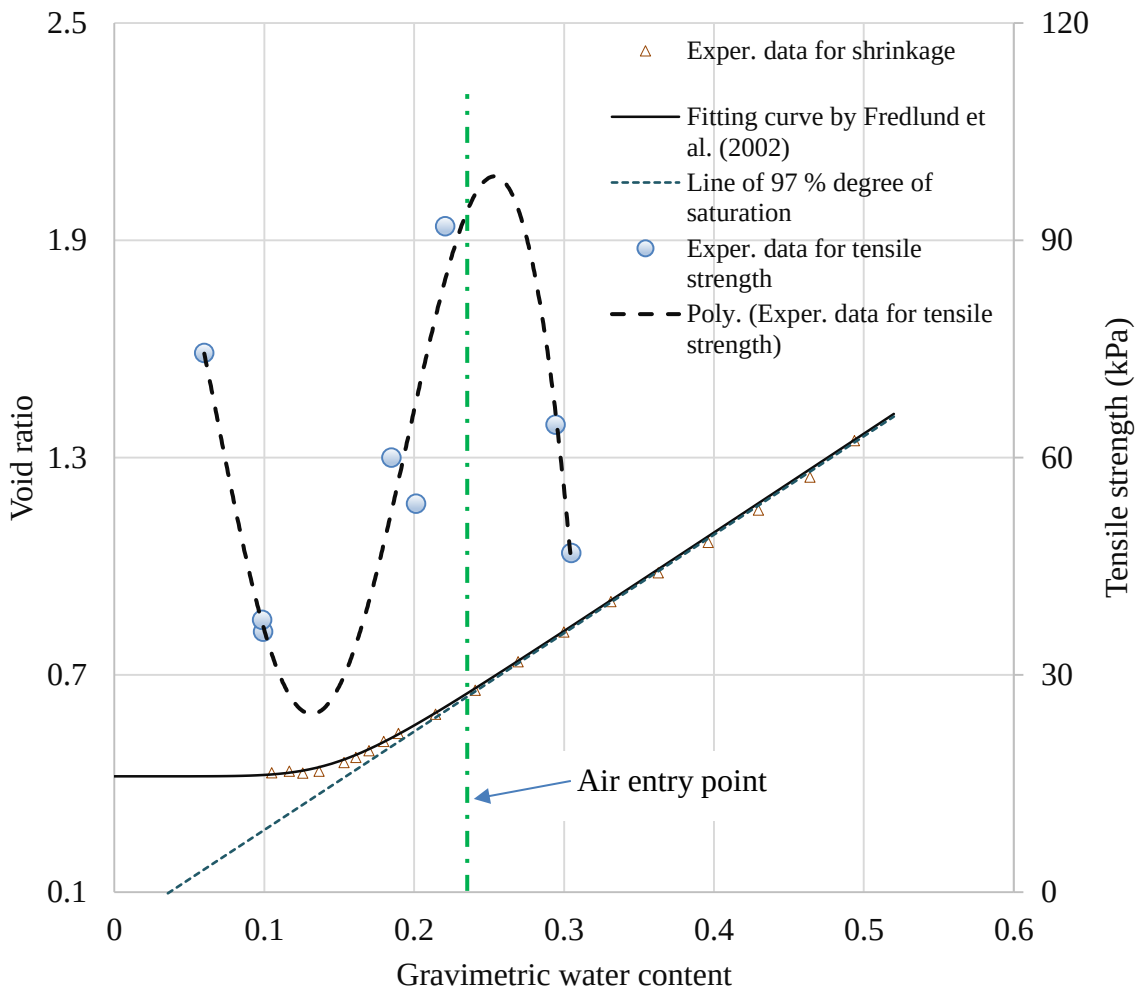

Figure 7.31 The Tensile Strength Characteristic Curve and the Shrinkage Characteristic Curve of Ardmore Soil

CHAPTER VIII

CONCLUSIONS AND RECOMMENDATIONS

8.1 Conclusions

Soil samples with different properties and preparation conditions collected across Oklahoma are tested. Four kinds of tests are conducted: suction measurement tests, free shrinkage tests, splitting tensile tests, and restrained shrinkage tests. Suction is measured for each soil specimen using a tensiometer sensor for low suction values and a WP4 device for high suction values. Free shrinkage test is conducted on small samples set on a balance and let them dry until the water content exceeds the shrinkage limit. The shrinkage process is captured using two high resolution cameras, one for the top view and one for the side view. The digital image processing is run to find the shrinkage magnitude in three dimensions by combining the results from both cameras. The obtained volumetric shrinkage with the water content are used to estimate the void ratio. The void ratio with the water content results are fitted using the Fredlund et al. (2002) model to predict the soil shrinkage characteristic curve. The suction measurements from the WP4 device and tensiometer sensor with the water content are fitted to predict the soil water characteristic curve using the Fredlund and Xing (1994) model. As a result, the obtained soil water characteristic curve and the soil shrinkage characteristic curve are incorporated to generate the void ratio-suction curve.

For the restrained ring test, samples with various preparation conditions in terms of compaction and initial water content are tested. Soils are compacted by mixing with water content close to the optimum moisture content (OMC) inside a PVC ring with 1.65 cm height and 15.24 cm diameter. Other samples are mixed at high water contents, higher than the OMC and the plastic limit but less than the liquid limit inside the same ring dimensions. These high-water content samples are molded easily inside the ring without any compaction effort. These samples are referred to as high water-content samples. The goal from the high-water content samples is to obtain uniform specimens that have minimum number of clods and high degree of saturation. Both kinds of samples are subject to drying using the restrained ring testing method. In this test, as the soil shrinks radially, a PVC ring in the center of the sample restrain the shrinkage. Consequently, a single crack initiates from the interior face of the sample and grows toward the outer edge. The surface strain of the sample is predicted and analyzed using the digital image technique. Further, the tensile stress developed in the soil prior to cracking is measured using strain gauges. These gauges are attached to the inner face of the core PVC ring. The results from the strain gauges are used to find the tensile stress using the method outlined by Weiss and Ferguson (2001) and Abou Najem et al. (2009).

The following points are concluded from the free shrinkage and suction measurement tests:

1- The results show that the slope of SWCC (water content vs. suction) combines at high suction values even though the initial water content and the dry density are different. However, the variation of the initial water content and density leads to differences in the initial degree of saturation and the final void ratio beyond the shrinkage limit (i.e. the minimum void radio. Because of the different initial degree of saturations, the SWCC (degree of saturation vs. suction) reveals significant difference. Similarly, because of the different minimum void ratio the slope of the void ratio-suction curve shows considerable difference.

2- The shrinkage has a substantial effect on the soil water characteristic curve (degree of saturation vs. suction), particularly on the air entry value. Such results also are reported by Fredlund and Houston (2013).

From the restrained ring test, the following points are concluded:

1- The crack initiation occurs at a stage very close to the air entry value for all the tested soils. These results have been found to be independent from the sample size and sample preparation conditions.

2- Since the determination of the air entry value is affected by the volume change, it should be estimated either from the SWCC in terms of the degree of saturation or the soil shrinkage characteristic curve. The air entry value is the point between the normal shrinkage zone and the residual shrinkage zone of the soil shrinkage characteristic curve

3- The factors that affect the crack initiation also influence the air entry value which is the end point of the normal shrinkage compacted soils. For example, for compacted specimen with less initial degree of saturation than 100%, the air entry value is higher than that of the high-water content specimens with degree of saturation close to 100%. As a result, the crack initiation comes at high water content for compacted samples than at that for reconstituted samples. The water content at crack initiation is predicted from the gravimetric water content vs. surface strain curve of samples in the restrained ring test. In all cases of crack initiation this water content falls on close region to the point between the normal shrinkage zone and the residual shrinkage zone.

4- The above results are interpreted using the ductility level of the soil. At the air entry value stage, the soil starts to transit in behavior from a plastic material to brittle material. The results of soil tensile strength from the previous studies also indicate that. Most of these results show that the soil appears a peak value in stage close to the air entry value. Similar results of the tensile strength have also been obtained in this study for Ardmore soil. In

other words, the soil at high water content is plastic and fracture failure is most likely far to occur. At stage of air entry value and due to the existence of cavitation in the soil, the soil starts to show brittle behavior and meanwhile the tensile strength starts decreasing. Consequently, any extra residual shrinkage of the soil beyond the normal shrinkage will add a tensile stress on the soil and initiate the cracks. That is supported by the results from Lake Hefner 2 soil. This soil has low plasticity index so that it did not show a residual shrinkage. Thereafter, the crack of this soil did not initiate during the drying process in the restrained ring test ever after the soil reaches high suction value and very low water content.

5- The crack width highly depends on the residual shrinkage the soil can show
6- The results of the tensile stress predicted from the micro strain gauges of Ardmore soils show that the soil can develop similar tensile stress and reaches close tensile strength value at the stage of crack initiation. That occurs for samples have different initial water content (up to 6% difference).

From the overall results, some similarities have been observed between the shrinkage and the consolidation of clay soils. They are listed as follows:

1- In the consolidation, the soil keeps saturated for the whole process. The normal shrinkage, which is the major part of the shrinkage, occurs almost for a single degree of saturation, being 100% for initially saturated soil.
2- The consolidation has a virgin slope or virgin line referred to as virgin compression line. Such a line has been found in the results of this thesis for the soil water characteristic curve in terms of the gravimetric water content and the void ration-suction curve.
3- The consolidation process has a pre-consolidation pressure which is close to the breaking point in the void ratio-effective pressure curve (e log p curve). The shrinkage has a similar breaking point. If the suction is considered as a stress state variable, this breaking point can be referred to as the pre-shrinkage suction. This point appears in the soil water

characteristic curve (gravimetric water content vs. suction) and void ratio-suction curve. This point has been referred to as the air entry value in most previous studies.

4- The rate of the consolidation is predicted by the coefficient of consolidation. The rate of shrinkage can be predicted by the coefficient of diffusivity.

8.2 Recommendations

The following points are recommended for future research studies:

1- Using the analysis conducted in this study to evaluate any solution proposed for the problem of soil cracking. The soil shrinkage characteristic curve can be used as a key tool to meet the purpose.

2- Using fracture mechanics principles to model the soil cracking. Soil suction should be employed in any proposed framework. The fracture factors (e.g. fracture toughness) should not be constant. It is recommended to relate the stress intensity factor to the suction.

3- This study investigates only the soil shrinkage mechanism using the shrinkage characteristic curve. It is recommended for future research to pursue the swelling characteristic curve for complete representation of soil volume change.

REFERENCES

ASTM Standard D3967, 2016. "Standard Test Method for Splitting Tensile Strength of Intact Rock Core Specimens". ASTM International, West Conshohocken, PA, www.astm.org

ASTM D698, 2012. "Standard Test Methods for Laboratory Compaction Characteristics of Soil Using Standard Effort". ASTM International, West Conshohocken, PA, www.astm.org

Abou Najm, M., Mohtar, R. H., Weiss, J., & Braudeau, E. (2009). Assessing internal stress evolution in unsaturated soils. *Water Resources Research*, *45*(5).

Abu-Hejleh, A. N., & Znidarcic, D. (1995). Desiccation theory for soft cohesive soils. *Journal of Geotechnical Engineering*, *121*(6), 493-502.

Amarasiri, A. L., Costa, S., & Kodikara, J. K. (2011). Determination of cohesive properties for mode I fracture from compacted clay beams. *Canadian Geotechnical Journal*, *48*(8), 1163-1173.

Amarasiri, A. L., & Kodikara, J. K. (2011). Numerical modeling of desiccation cracking using the cohesive crack method. *International Journal of Geomechanics*, *13*(3), 213-221.

Atique, A., & Sanchez, M. (2011). Analysis of cracking behavior of drying soil. In *2nd International Conference on Environmental Science and Technology IPCBEE, Singapore* (Vol. 6).

Aubeny, C., & Lytton, R. (2003). *Long-term strength of compacted high-PI clays* (No. FHWA/TX-03/2100-1,).

Bani Hashem, E. (2013). *Volume change consideration in determining appropriate unsaturated soil properties for geotechnical applications* (Doctoral dissertation, Arizona State University).

Bani Hashem, E., & Houston, S. L. (2015). Volume Change Consideration in Determining Unsaturated Soil Properties for Geotechnical Applications. *International Journal of Geomechanics*, D4015003.

Brinker, C. J., & Scherer, G. W. (1990). Sol-gel science, 1990. *The physics and chemistry of sol–gel processing*.

Braudeau, E., Mohtar, R. H., & Chahinian, N. (2004). Estimating soil shrinkage parameters. *Developments in Soil Science*, *30*, 225-240.

Brooks, R. H., & Corey, A. T. (1964). Hydraulic properties of porous media and their relation to drainage design. *Transactions of the ASAE, 7*(1), 26-0028.

Bulut, R., Chen, L.Z., Mantri, S., Amer, O., Tian, Y. and Zaman, M. (2014). "Drying shrinkage problems in high PI subgrade soils". *ODOT SP&R Item Number 2236*. Oklahoma

Bulut R, Hineidi SM, Bailey B (2002) Suction measurements—filter paper and chilled mirror psychrometer. In: Proceedings of the Texas Section American Society of Civil Engineers, Fall Meeting, Waco, 2–5 October

Bulut, R., & Leong, E. C. (2008). Indirect measurement of suction. *Geotechnical and Geological Engineering*, *26*(6), 633-644.

Bulut, R., Lytton, R. L., & Wray, W. K. (2001). Soil suction measurements by filter paper. In *Expansive clay soils and vegetative influence on shallow foundations* (pp. 243-261). ASCE.

Chen, L. (2007). Development of a new tensile stress model for expansive soils. Ph.D. Dissertation. Oklahoma State University, Oklahoma.

Chertkov, V. Y. (2007). The reference shrinkage curve at higher than critical soil clay content. *Soil Science Society of America Journal*, *71*(3), 641-655.

Childs, E. C., & Collis-George, N. (1950). The permeability of porous materials. In *Proceedings of the Royal Society of London: Mathematical, Physical and Engineering Sciences* (Vol. 201, No. 1066, pp. 392-405). The Royal Society.

Cornelis, W. M., Corluy, J., Medina, H., Diaz, J., Hartmann, R., Van Meirvenne, M., & Ruiz, M. E. (2006). Measuring and modelling the soil shrinkage characteristic curve. *Geoderma*, *137*(1), 179-191.

Dhowian, A., Erol, A.O., and Youssef, A. (1987). "Assessment of oedometer methods for heave prediction," Proceedings, 6th International Conference of Expansive Soils, New Delhi, India. P 99-103.

Favaretti, M. (1995). Tensile strength of compacted clays. In *proceedings of the first international conference on unsaturated soils. Paris, France, September, 1995. Volume 1*.

Fredlund, D. G., & Houston, S. L. (2013). Interpretation of soil-water characteristic curves when volume change occurs as soil suction is changed. *Advances in unsaturated soils. CRC Press, Boca Raton, FL*, 15-31.

Fredlund, D. G., & Morgenstern, N. R. (1977). Stress state variables for unsaturated soils. *Journal of Geotechnical and Geoenvironmental Engineering*, *103*(ASCE 12919).

Fredlund, D. G., Rahardjo, H., & Fredlund, M. D. (2012). *Unsaturated soil mechanics in engineering practice*. John Wiley & Sons.

Fredlund, D. G., & Sedgwick, A. (2011). "Determination of water storage and permeability functions of oil sands tailings." Proc., Int. Conf. on Tailings and Mine Waste, Norman B. Keevil Institute of Mining Engineering, Univ. of British Columbia, Vancouver, BC, Canada.

Fredlund, M. D., Wilson, G. W., & Fredlund, D. G. (2002, March). Representation and estimation of the shrinkage curve. In *Proc., 3rd Int. Conf. on Unsaturated Soils, UNSAT 2002* (pp. 145-149).

Fredlund, D. G., Xing, A., & Huang, S. (1994). Predicting the permeability function for unsaturated soils using the soil-water characteristic curve. *Canadian Geotechnical Journal*, *31*(4), 533-546.

Fredlund, D. G., & Xing, A. (1994). Equations for the soil-water characteristic curve. *Canadian geotechnical journal*, *31*(4), 521-532.

Gardner, W. R. (1958). Some steady-state solutions of the unsaturated moisture flow equation with application to evaporation from a water table. *Soil science*, *85*(4), 228-232.

Hamilton, J. M., Daniel, D. E., & Olson, R. E. (1981). Measurement of hydraulic conductivity of partially saturated soils. In A. S. 746, & T.F. Zimmie and C.O. Riggs (Ed.), *Permeability and Groundwater Contaminant Transport* (pp. 182-196). Philadelphia: ASTM.

Harison, J. A., Hardin, B. O., & Mahboub, K. (1994). Fracture toughness of compacted cohesive soils using ring test. *Journal of geotechnical engineering*, *120*(5), 872-891.

Jones, D. E. J., and Holtz, WG (1973) "Expansive Soils–The hidden Disaster," *Civil Engineering*, *43*.

Kodikara, J., & Costa, S. (2012). Evaluation of J integral for clay soils using a new ring test. *Geotechnical Testing Journal.*1-9.

Kodikara, J., & Costa, S. (2013). Desiccation cracking in clayey soils: Mechanisms and Modelling. In *Multiphysical Testing of Soils and Shales* (pp. 21-32). Springer Berlin Heidelberg.

Konrad, J. M., & Ayad, R. (1997). A idealized framework for the analysis of cohesive soils undergoing desiccation. *Canadian Geotechnical Journal*, *34*(4), 477-488.

Lakshmikantha, M. R., Prat, P. C., & Ledesma, A. (2012). Experimental evidence of size effect in soil cracking. *Canadian Geotechnical Journal*, *49*(3), 264-284.

Leong, E. C., & Rahardjo, H. (1997). Permeability functions for unsaturated soils. *Journal of Geotechnical and Geoenvironmental Engineering*, *123*(12), 1118-1126.

Leong, E. C., & Wijaya, M. (2015). Universal soil shrinkage curve equation. *Geoderma*, *237*, 78-87.

Li, X., Zhang, L. M., & Wu, L. Z. (2014). A framework for unifying soil fabric, suction, void ratio, and water content during the dehydration process. *Soil Science Society of America Journal*, *78*(2), 387-399.

Lloret A, Ledesma A, Rodriguez R, Sanchez MJ, Olivella S, Suriol J (1998) Crack initiation in drying soils. Unsaturated Soils, P´ekin, International Academic Publishers, pp 497–502.

Likos, W.J. (2004). Measurement of crystalline swelling in expansive clay. *Geotechnical Testing Journal, 27,* 540-546.

Lu, N., & Likos, W. J. (2004). *Unsaturated soil mechanics*. Wiley.

Lu, N., & Kaya, M. (2013). A drying cake method for measuring suction-stress characteristic curve, soil–water-retention curve, and hydraulic conductivity function. *Geotechnical Testing Journal*.

Lu, N., Kim, T. H., Sture, S., & Likos, W. J. (2009). Tensile strength of unsaturated sand. *Journal of engineering mechanics*, *135*(12), 1410-1419.

Luo, R., & Prozzi, J. (2009). Combining Geogrid Reinforcement and Lime Treatment to Control Dry Land Longitudinal Cracking. *Transportation Research Record: Journal of the Transportation Research Board*, (2104), 88-96.

Lytton, R. L. (1994). "Prediction of movement in expansive clays." Proc., Vertical and Horizontal Deformations of Foundations and Embankments, Geotechnical Special Publication No. 40, A. T. Yeung and G.Y. Felio, eds., Vol. 2, ASCE, New York, 1827–1845.

Lytton, R., Aubeny, C., & Bulut, R. (2004). *Design procedure for pavements on expansive soils* (Vol. 1). Texas Transportation Institute, Texas A & M University System.

Mantri, S. (2014). *Determination of moisture diffusion coefficient at low suctions using thermal conductivity sensors*. Master Thesis, Oklahoma State University, Oklahoma.

Mabirizi, D., & Bulut, R. (2010). Unified testing method for measuring diffusion coefficients for unsaturated soil drying and wetting in laboratory. *Transportation Research Record: Journal of the Transportation Research Board*, (2170), 109-118.

Mayergoyz, I.D. & Lawson, W. (1996). "Basic Electric Circuit Theory: A One-Semester Text". Academic Press. ISBN-13: 978-0124808652.

McCartney, J., Villar, L., & Zornberg, J. (2007). Estimation of the hydraulic conductivity function of unsaturated clays using an infiltration column test. *University of Texas-Austin*, 1-8.

McKeen, R.G. (1992). "A Model for Predicting Expansive Soil Behavior", Proceedings of the 7th International Conference on Expansive Soils, pp. 1-6

Mitchell, P.W. (1979), "The Structural Analysis of Footings on Expansive Soil" Kenneth W. G. Smith and Associates Research Report No. 1, (1st Edition), Newton, South Australia.

Mitchell, J. K., & Soga, K. (2005). Fundamentals of soil behavior. *John Wiley& Sons, Hoboken, New Jersey, USA.*

Morris, P. H., Graham, J., & Williams, D. J. (1992). Cracking in drying soils. *Canadian Geotechnical Journal*, *29*(2), 263-277.

Mualem, Y. (1976). A new model for predicting the hydraulic conductivity of unsaturated porous media. *Water resources research*, *12*(3), 513-522.

Mualem, Y. (1986). "Hydraulic conductivity of unsaturated soils: prediction and formulas." Methods of soil analysis. Part 1. Physical and minteralogical methods. 2nd Ed., Agronomy A. Klute. ed., Am. Soc. of Agronomy, Inc. and *Soil Sci. SOC. of Am.* Inc. Madison. Wis. 799-823.

Nahlawi, H., Chakrabarti, S., & Kodikara, J. (2004). A direct tensile strength testing method for unsaturated geomaterials. *Geotechnical Testing Journal*. 1-6.

Nahlawi, H., Kodikara, J.K., 2006. Laboratory experiments on desiccation cracking of thin soil layers. *Geotechnical and Geological Engineering* 24, 1641–1664.

Narain J., & Rawat P.C. (1970). Tensile strength of compacted soils. J SMFD, ASCE 96, SM6, pp. 2185-2190.

Narvaez, B., Aubertin, M., & Saleh-Mbemba, F. (2015). Determination of the tensile strength of unsaturated tailings using bending tests. *Canadian Geotechnical Journal*, *52*(11), 1874-1885.

Peng, X., J. Dorner, Y. Zhao, and R. Horn. 2009. Shrinkage behavior of transiently- and constantly-loaded soils and its consequences for soil moisture release. *Eur. J. Soil Sci*. 60:681–694.

Péron, H., Hueckel, T., Laloui, L., & Hu, L. (2009). Fundamentals of desiccation cracking of fine-grained soils: experimental characterization and mechanisms identification. *Canadian Geotechnical Journal*, *46*(10), 1177-1201.

Peron, H., Laloui, L., Hu, L. B., & Hueckel, T. (2013). Formation of drying crack patterns in soils: a deterministic approach. *Acta Geotechnica*, *8*(2), 215-221.

Prat, P. C., Ledesma, A., Lakshmikantha, M. R., Levatti, H., & Tapia, J. (2008, October). Fracture mechanics for crack propagation in drying soils. In *Proceedings of the 12th International Conference of the International Association for Computer Methods and Advances in Geomechanics (IACMAG), Goa, India* (pp. 1-6).

Rao, S.M. (2012). Volume change of tropical residual soil. In Huat, B. B., Toll, D. G., & Prasad, A. (Eds.). (2012). *Handbook of tropical residual soils engineering*. CRC Press, p. 147-182.

Richards, L. A., & Weeks, L. (1953). Capillary conductivity values from moisture yield and tension measurements on soil columns. *Soil Science Society of America J.* (55), 206–209

Rodríguez, R., Sanchez, M., Ledesma, A., & Lloret, A. (2007). Experimental and numerical analysis of desiccation of a mining waste. *Canadian Geotechnical Journal*, *44*(6), 644-658.

Safari, E., Ghazizade, M. J., Abduli, M. A., & Gatmiri, B. (2014). Variation of crack intensity factor in three compacted clay liners exposed to annual cycle of atmospheric conditions with and without geotextile cover. *Waste management*, *34*(8), 1408-1415.

Saleh-Mbemba, F., Aubertin, M., Mbonimpa, M., & Li, L. (2016). Experimental Characterization of the Shrinkage and Water Retention Behaviour of Tailings from Hard Rock Mines. *Geotechnical and Geological Engineering*, *34*(1), 251-266.

Shannon, B., Kodikara, J., & Pathmanathan, R. (2015). The use of restrained ring test method for soil desiccation studies. *Geotechnical Testing Journal [P]*, *38*(1), 98-112.

Slowik, V., Hübner, T., Schmidt, M. & Villmann, B. 2009. Simulation of capillary shrinkage cracking in cement-like materials. Cement & Concrete Composites 31(7): 461-469.

Slowik, V., & Ju, J. W. (2010). Discrete modeling of plastic cement paste subjected to drying. Fracture Mechanics of Concrete and Concrete Structures, Recent Advances in Fracture Mechanics of Concrete - B. H. Oh, et al.(eds), p. 516-521.

Shin, H., & Santamarina, J. C. (2011). Desiccation cracks in saturated fine-grained soils: particle-level phenomena and effective-stress analysis. *Géotechnique*, *61*(11), 961.

Standards Australia (1988). Residential slabs and footings, Standard 2807.1. Standards Association of Australia, North Sydney, N.S.W

Standards Australia (1996). Residential slabs and footings, Standard 2870. Standards Association of Australia, North Sydney, N.S.W

Stanier, S. A., Blaber, J., Take, W. A., & White, D. J. (2016). Improved image-based deformation measurement for geotechnical applications. *Can. Geotech. J*, *53*.

Tang, C. S., Cui, Y. J., Shi, B., Tang, A. M., & Liu, C. (2011). Desiccation and cracking behaviour of clay layer from slurry state under wetting–drying cycles. *Geoderma*, *166*(1), 111-118.

Tang, C. S., Pei, X. J., Wang, D. Y., Shi, B., & Li, J. (2014). Tensile strength of compacted clayey soil. *Journal of Geotechnical and Geoenvironmental Engineering*, *141*(4).

Terzaghi, K. (1925). Principles of soil mechanics. *Engineering News-Record*, *95*.

Terzaghi, K. (1943). Theoretical Soil Mechanics. *New York, Wiley*.

Thakur, A. (2005). Determination of Diffusion Coefficient through Laboratory Tests and Analytically Validating It Using Empirical Relations for Unsaturated Soils. College Station, Texas: MS Thesis, Department of Civil Engineering, Texas A&M University.

Thusyanthan, N. I., Take, W. A., Madabhushi, S. P. G., & Bolton, M. D. (2007). Crack initiation in clay observed in beam bending. *Geotechnique*, *57*(7), 581-594.

Thyagaraj, T., & Rao, S. M. (2010). Influence of osmotic suction on the soil-water characteristic curves of compacted expansive clay. *Journal of geotechnical and geoenvironmental engineering*, *136*(12), 1695-1702.

Trabelsi, H., Jamei, M., Guiras, H., Hatem, Z., Romero, E., & Sebastia, O. (2010). Some investigations about the tensile strength and the desiccation process of unsaturated clay. In *EPJ Web of Conferences* (Vol. 6, p. 12005). EDP Sciences

U.S. Department of the Army (1983). Foundations in expansive soils. Washington, Dc, TM 5-818-7.

Uday, K. V., Jayanthi, P. N., & Singh, D. N. (2014). A generalized relationship for determination of tensile strength of fine-grained soils from shrinkage characteristics. *Drying Technology*, *32*(7), 869-876.

UMS (2009). "T5/T5x Pressure Transducer Tensiometer User Manual". Version 12/2009.

Van Genuchten, M. T. (1980). A closed-form equation for predicting the hydraulic conductivity of unsaturated soils. *Soil science society of America journal*, *44*(5), 892-898.

Vanapalli, S., & Lu, L. (2012). A state-of-the art review of 1-D heave prediction methods for expansive soils. *International Journal of Geotechnical Engineering*, *6*(1), 15-41.

Vesga, L. F. (2009). Direct tensile-shear test (DTS) on unsaturated kaolinite clay. *Geotechnical Testing Journal.* 1-13.

Vesga, L. F., & Vallejo, L. E. (2006). Direct and indirect tensile tests for measuring the equivalent effective stress in a kaolinite clay. In *Unsaturated Soils 2006* (pp. 1290-1301). ASCE.

Villar, L. D. S., de Campos, T. M. P., Azevedo, R. F., Zornberg, J. G., Hamza, M., Shahien, M., & El-Mossallamy, Y. (2009). Tensile strength changes under drying and its correlations with total and matric suctions. In *Proceedings of the 17th International Conference on Soil Mechanics and Geotechnical Engineering: The academia and practice of geotechnical engineering, Alexandria, Egypt, 5-9 October 2009.* (pp. 793-796). IOS Press.

Wang, J. J., Zhu, J. G., Chiu, C. F., & Zhang, H. (2007). Experimental study on fracture toughness and tensile strength of a clay. *Engineering Geology*, *94*(1), 65-75.

Wanyan, Y., Abdallah, I., Nazarian, S., & Puppala, A. J. (2014). Moisture content-based longitudinal cracking prediction and evaluation model for low-volume roads over expansive soils. *Journal of Materials in Civil Engineering*, *27*(10), 04014263.

Weiss, W., and Furgeson, S. (2001). "Restrained shrinkage testing: The impact of specimen geometry on quality control testing for material performance assessment". Concreep 6: Creep, Shrinkage, and Curability Mechanic of Concrete and Other Quasi-Brittle Materials, Elsevier, New York, pp. 645–651.

Wijaya, M., Leong, E. C., & Rahardjo, H. (2015). Effect of shrinkage on air-entry value of soils. *Soils and Foundations*, *55*(1), 166-180.

White, D. J., & Take, W. A. (2002). GeoPIV: Particle Image Velocimetry (PIV) software for use in geotechnical testing.

White, D. J., Take, W. A., & Bolton, M. D. (2003). Soil deformation measurement using particle image velocimetry (PIV) and photogrammetry. *Geotechnique*, *53*(7), 619-632.

Yesiller, N., Miller, C. J., Inci, G., & Yaldo, K. (2000). Desiccation and cracking behavior of three compacted landfill liner soils. *Engineering Geology*, *57*(1), 105-121.

Zapata, C. E., Houston, W. N., Houston, S. L., & Walsh, K. D. (2000). Soil-water characteristic curve variability. *Geotech Spec Publ*, (99), 84-124.

Zeh, R. M., & Witt, K. J. (2007). The tensile strength of compacted clays as affected by suction and soil structure. In *Experimental unsaturated soil mechanics* (pp. 219-226). Springer Berlin Heidelberg.

APPENDIX A

DEFORMATION USING *GEOPIV-RG* SOFTWARE

GeoPIV-RG subroutines are image analysis modules capturing the deformations and displacements for any series of images. Recently, *GeoPIV-RG* has widely been used in geotechnical research studies (White and Take 2002; Lu and Kaya 2013; Shannon et al. 2015). *GeoPIV-RG* is MATLAB based subroutines employing the particle image velocimetry (PIV) or also called digital image processing (DIP) to evaluate the displacement and strain. It divides the interested area into mesh of subsets or patches (Figure A.1). Then, the strain is computed for each patch by capturing the displacement in the horizontal direction and vertical direction, as well as the rotation of the patch (Figure A.2 and A.3). More information about the background and the theory involved in these software subroutines can be found in White et al. (2003) and Stanier et al. (2016).

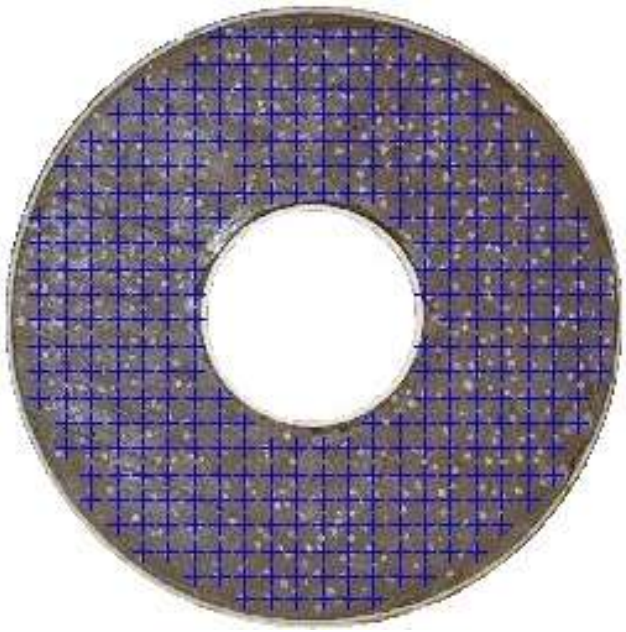

Figure A.1 Meshing of Specimen in the Restrained Ring Test into Patches

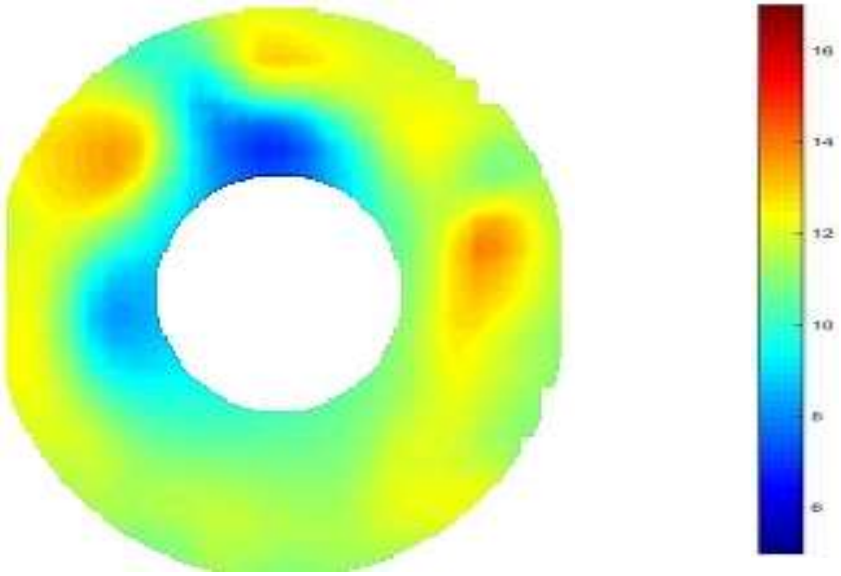

Figure A.2 The Resultant Strain Computed by *GeoPIV-RG* for a Specimen in the Restrained Ring Test from the Beginning of the Test until just before the Crack Initiation

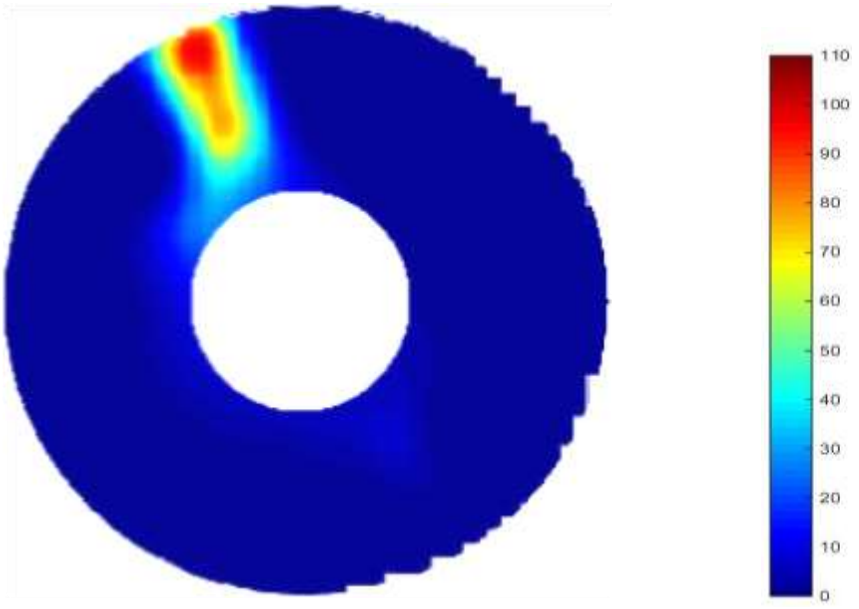

Figure A.3 The Resultant Strain Computed by *GeoPIV-RG* for a Specimen in the Restrained Ring Test from the Crack Initiation Stage until the Stage of Shrinkage Limit

APPENDIX B

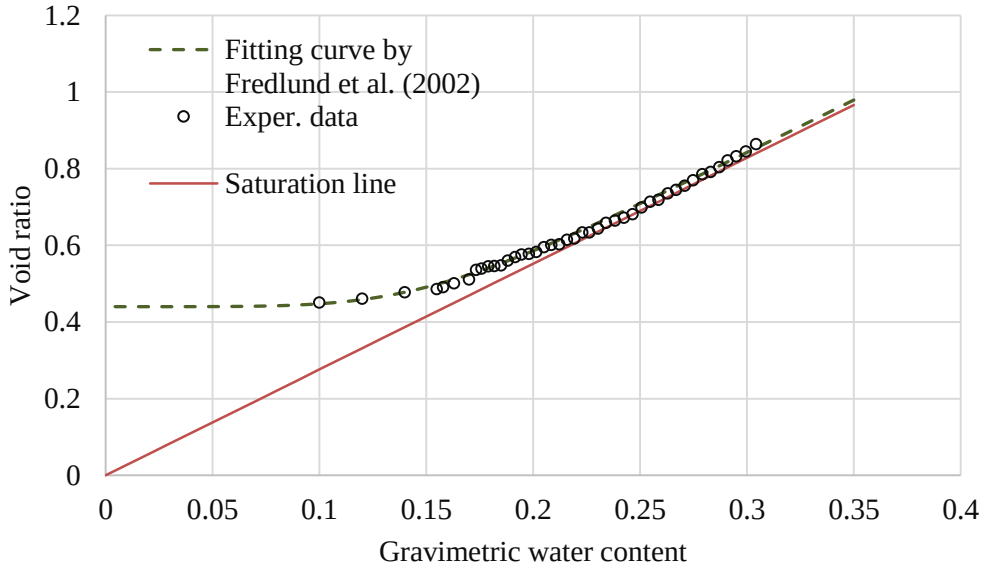

Figure B.1 Soil Shrinkage Characteristic Curve of Osage Soil

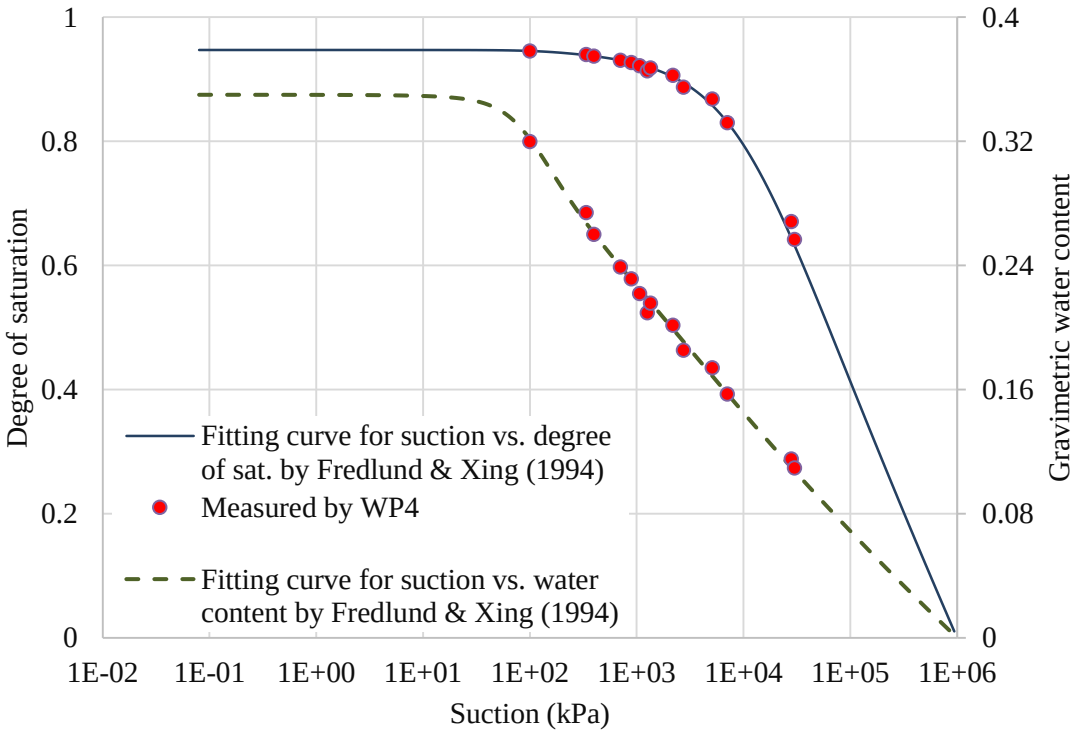

Figure B.2 Soil Water Characteristic Curve of Osage Soil

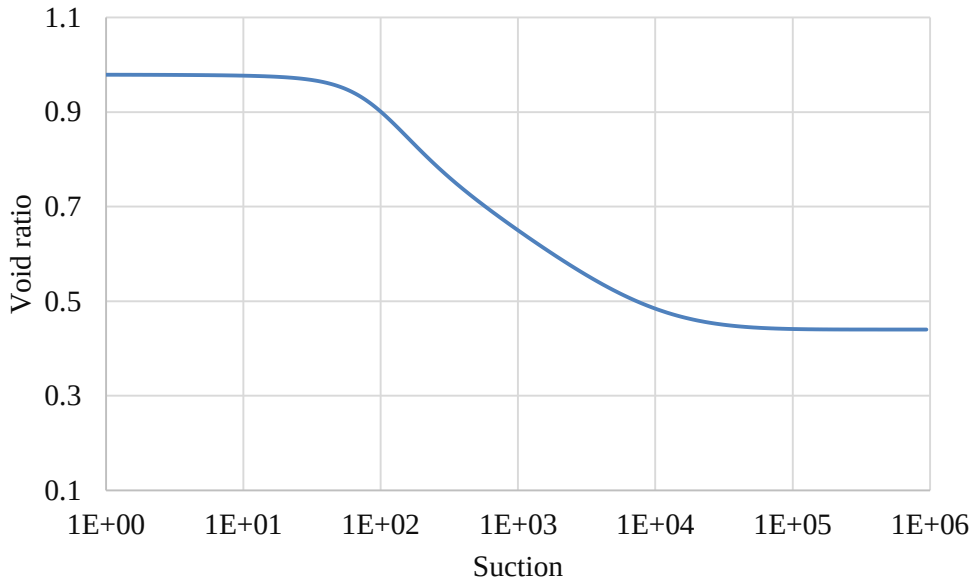

Figure B.3 Void Ratio-Suction Curve (e-log s curve) of Osage Soil

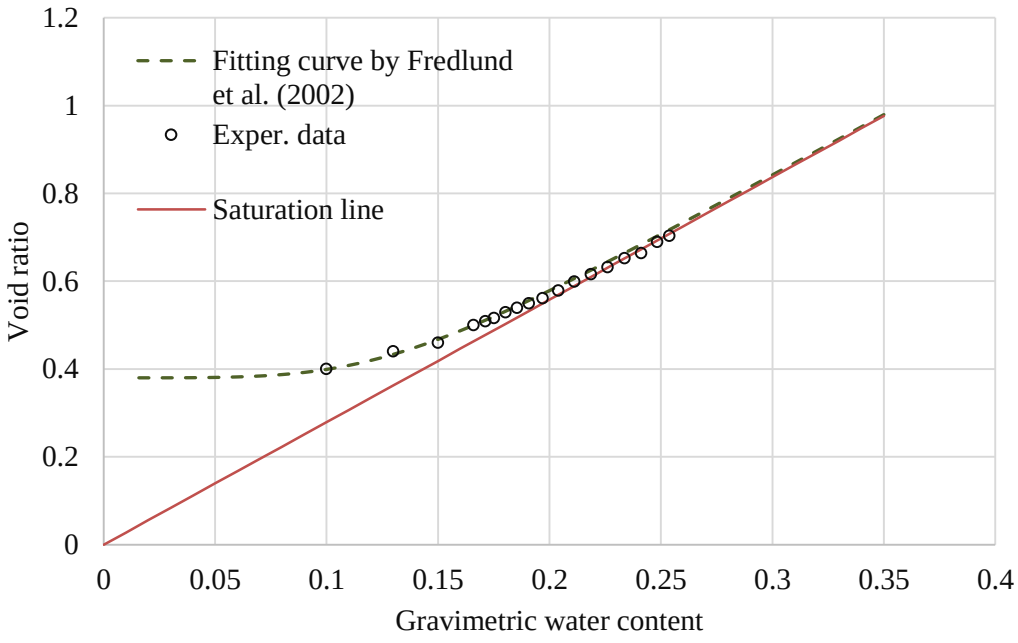

Figure B.4 Soil Shrinkage Characteristic Curve of Lake Hefner 1 Soil

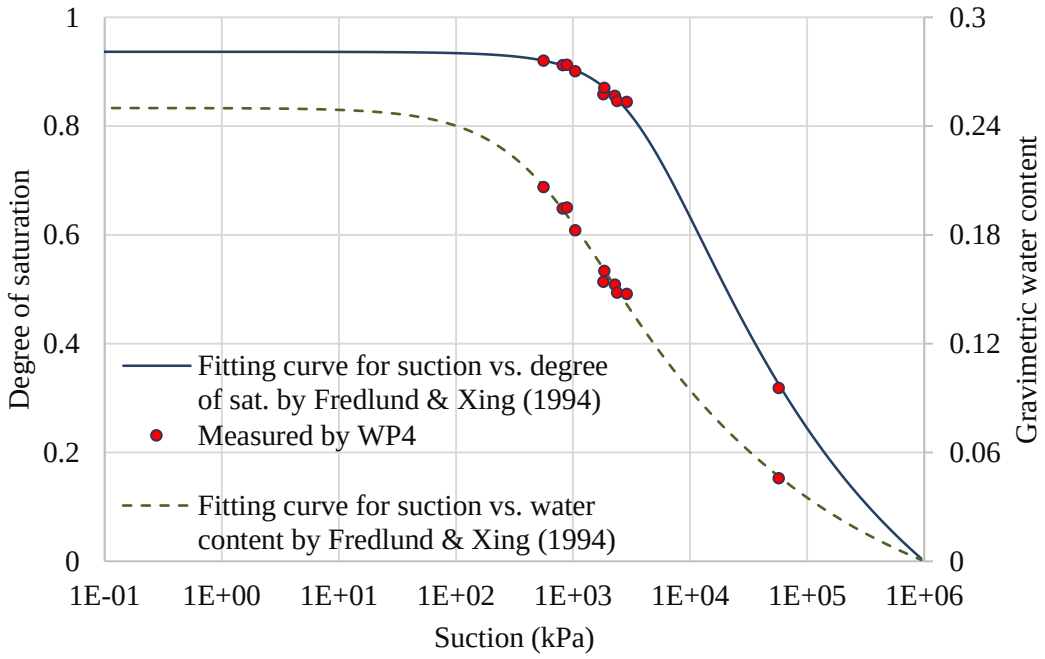

Figure B.5 Soil Water Characteristic Curve of Lake Hefner 1 Soil

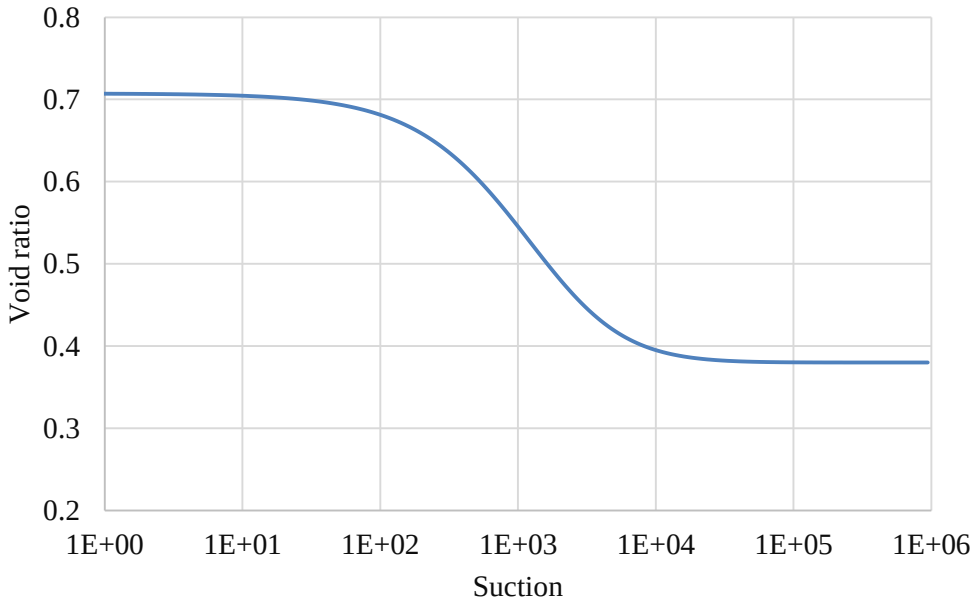

Figure B.6 Void Ratio-Suction Curve (e-log s curve) of Lake Hefner 1 Soil

APPENDIX C

Table C.1 The Restrained Ring Test Results for High-Water Content Ardmore Soil (Test 1)

Time (min.)	Surface Strain	Strain gauge reading (-)	Water content	Suction (kPa)	Suction (pF)	Tensile stress (kPa)
1	0.0%	0	36.1%	1	1.00	0.0
60	0.7%	0	35.4%	3	1.50	0.0
120	1.3%	0	34.9%	24	2.38	0.0
180	1.7%	0	34.3%	92	2.96	0.0
240	2.3%	5	33.8%	142	3.15	1.0
300	2.7%	10	33.3%	191	3.28	2.0
360	3.1%	20	32.8%	236	3.37	4.0
420	3.4%	37	32.2%	281	3.45	7.5
480	3.9%	65	31.7%	326	3.51	13.1
540	4.4%	98	31.2%	373	3.57	19.7
600	4.6%	131	30.7%	418	3.62	26.1
660	5.2%	177	30.2%	471	3.67	35.3
720	5.7%	220	29.6%	526	3.72	43.9
780	5.9%	265	29.1%	579	3.76	53.1

840	6.5%	317	28.6%	637	3.80	63.3
900	6.9%	370	28.1%	700	3.85	73.9
960	7.2%	425	27.6%	762	3.88	85.0
1020	7.7%	498	27.1%	834	3.92	99.7
1080	8.2%	573	26.5%	911	3.96	114.6
1140	8.6%	640	26.1%	989	4.00	127.9
1200	9.0%	710	25.6%	1074	4.03	142.1
1260	9.5%	789	25.1%	1172	4.07	157.9
1320	9.8%	884	24.6%	1273	4.10	176.8
1380	10.3%	975	24.1%	1376	4.14	195.0
1440	10.6%	1069	23.6%	1497	4.18	213.9
1500	11.0%	1167	23.2%	1621	4.21	233.5
1560	11.4%	1285	22.7%	1748	4.24	257.0
1620	11.6%	1380	22.3%	1877	4.27	276.1
1680	12.1%	1499	21.9%	2018	4.30	299.7
1740	12.4%	1622	21.5%	2184	4.34	324.4
1800	12.6%	1743	21.1%	2340	4.37	348.7
1860	13.1%	1871	20.7%	2525	4.40	374.1

1920	13.3%	2021	20.4%	2711	4.43	404.2
1980	13.7%	2168	20.0%	2916	4.46	433.7
2040	14.0%	2311	19.6%	3139	4.50	462.3
2100	14.1%	2471	19.3%	3363	4.53	494.3
2160	14.5%	2616	19.0%	3607	4.56	523.1
2220	14.7%	2743	18.6%	3899	4.59	548.6
2280	15.0%	2875	18.3%	4164	4.62	574.9
2340	15.3%	2972	18.0%	4481	4.65	594.4
2370	15.4%	3009	17.8%	4635	4.67	601.8
Crack	Crack	Crack	Crack	Crack	Crack	Crack

Table C.2 The Restrained Ring Test Results for High-Water Content Ardmore Soil (Test 2)

Time (min.)	Surface Strain	Strain gauge reading (-)	Water content	Suction (kPa)	Suction (pF)	Tensile stress (kPa)
0	0.0%	0	34.9%	28	2.45	0.0
60	0.8%	0	34.1%	117	3.07	0.0
120	1.4%	1	33.4%	177	3.25	0.2
180	1.9%	14	32.8%	231	3.36	2.8
240	2.4%	32	32.1%	288	3.46	6.5
300	3.1%	56	31.5%	343	3.54	11.2
360	3.4%	87	31.0%	395	3.60	17.5
420	3.9%	122	30.3%	454	3.66	24.3
480	4.4%	171	29.8%	511	3.71	34.1
540	5.0%	230	29.2%	574	3.76	46.1
600	5.3%	293	28.6%	638	3.80	58.7
660	5.7%	362	28.1%	702	3.85	72.5
720	6.1%	434	27.6%	764	3.88	86.8
780	6.6%	503	27.0%	838	3.92	100.5
840	6.9%	579	26.5%	918	3.96	115.8

900	7.3%	659	26.1%	990	4.00	131.8
960	7.7%	746	25.5%	1078	4.03	149.2
1020	8.2%	843	25.0%	1175	4.07	168.5
1080	8.6%	943	24.5%	1280	4.11	188.5
1140	9.1%	1048	24.1%	1375	4.14	209.6
1200	9.4%	1150	23.6%	1500	4.18	230.1
1260	9.9%	1258	23.1%	1631	4.21	251.6
1320	10.3%	1373	22.7%	1765	4.25	274.7
1380	10.7%	1498	22.3%	1903	4.28	299.7
1440	11.2%	1636	21.8%	2065	4.31	327.3
1500	11.4%	1773	21.4%	2231	4.35	354.7
1560	11.8%	1924	20.9%	2429	4.39	384.9
1620	12.2%	2089	20.6%	2618	4.42	417.8
1680	12.6%	2249	20.1%	2842	4.45	449.8
1740	13.1%	2405	19.7%	3072	4.49	481.1
1800	13.4%	2550	19.4%	3326	4.52	510.1
1860	13.6%	2694	19.0%	3606	4.56	538.8
1920	14.0%	2809	18.6%	3891	4.59	561.8

1980	14.4%	2895	18.3%	4203	4.62	578.9
2040	14.4%	2962	17.9%	4517	4.65	592.5
Crack	Crack	Crack	Crack	Crack	Crack	Crack

Table C.3 The Restrained Ring Test Results for High-Water Content Ardmore Soil (Test 3)

Time (min.)	Strain gauge reading (-)	Water content	Suction (kPa)	Suction (pF)	Tensile stress (kPa)
0	0	30.8%	406	3.61	0.0
60	0	30.2%	466	3.67	0.0
120	73	29.6%	526	3.72	14.7
180	175	29.0%	586	3.77	35.0
240	263	28.5%	647	3.81	52.7
300	349	28.0%	713	3.85	69.7
360	432	27.4%	787	3.90	86.3
420	510	26.9%	858	3.93	101.9
480	580	26.4%	936	3.97	116.0
540	663	25.9%	1015	4.01	132.6
600	750	25.4%	1101	4.04	150.1
660	838	24.9%	1199	4.08	167.5
720	930	24.4%	1307	4.12	186.0
780	1030	23.9%	1419	4.15	205.9
840	1139	23.5%	1535	4.19	227.8

900	1254	23.0%	1661	4.22	250.8
960	1375	22.6%	1800	4.26	274.9
1020	1508	22.1%	1953	4.29	301.7
1080	1643	21.7%	2111	4.32	328.5
1140	1793	21.2%	2298	4.36	358.6
1200	1950	20.8%	2478	4.39	390.0
1260	2113	20.5%	2646	4.42	422.6
1320	2265	20.4%	2690	4.43	453.0
1380	2431	20.0%	2910	4.46	486.1
1440	2607	19.6%	3152	4.50	521.5
1500	2778	19.3%	3399	4.53	555.6
1560	2898	18.9%	3671	4.56	579.6
1635	3011	18.1%	4379	4.64	602.2
Crack	Crack	Crack	Crack	Crack	Crack

Table C.4 The Restrained Ring Test Results for High-Water Content Osage Soil (Test 1)

Time (min.)	Surface Strain	Strain gauge reading (-)	Water content	Suction (kPa)	Suction (pF)	Tensile stress (kPa)
1	0.0%	5	30.4%	443	3.65	0.9
60	0.7%	88	30.0%	491	3.69	17.5
120	1.2%	118	29.5%	537	3.73	23.6
180	1.7%	173	29.1%	580	3.76	34.5
240	2.4%	236	28.7%	624	3.80	47.2
300	2.9%	297	28.3%	671	3.83	59.4
360	3.1%	361	27.9%	720	3.86	72.1
420	3.7%	429	27.5%	775	3.89	85.7
480	4.3%	496	27.1%	830	3.92	99.3
540	4.7%	569	26.7%	888	3.95	113.9
600	5.1%	644	26.3%	950	3.98	128.9
660	5.8%	723	25.9%	1020	4.01	144.6
720	6.0%	805	25.5%	1091	4.04	161.0
780	6.6%	885	25.1%	1166	4.07	176.9
840	7.3%	965	24.7%	1253	4.10	193.1
900	7.7%	1045	24.3%	1341	4.13	209.0
960	8.0%	1130	23.8%	1442	4.16	226.0
1020	8.2%	1215	23.4%	1552	4.19	243.1
1080	8.8%	1304	23.0%	1655	4.22	260.8
1140	9.2%	1380	22.6%	1776	4.25	276.1
1200	9.3%	1471	22.3%	1888	4.28	294.3

1260	9.9%	1565	21.9%	2018	4.30	313.0
1320	10.0%	1680	21.6%	2149	4.33	336.0
1380	10.5%	1782	21.2%	2303	4.36	356.3
1440	10.6%	1904	20.9%	2470	4.39	380.8
1500	10.8%	2022	20.5%	2638	4.42	404.3
1560	11.3%	2135	20.1%	2836	4.45	427.0
1620	11.6%	2273	19.8%	3036	4.48	454.6
1680	11.6%	2403	19.5%	3253	4.51	480.7
1740	11.9%	2541	19.2%	3470	4.54	508.1
1800	12.3%	2694	18.8%	3726	4.57	538.9
1860	12.8%	2858	18.5%	3983	4.60	571.7
1920	12.9%	3017	18.2%	4260	4.63	603.5
1980	12.9%	3172	17.9%	4534	4.66	634.4
2040	13.1%	3338	17.6%	4859	4.69	667.6
Crack	Crack	Crack	Crack	Crack	Crack	Crack

Table C.5 The Restrained Ring Test Results for High-Water Content Lake Hefner 1 Soil (Test 1)

Time (min.)	Surface Strain	Strain gauge reading (-)	Water content	Suction (kPa)	Suction (pF)	Tensile stress (kPa)
0	0.0%	0	25.4%	1	1.00	0.0
15	0.1%	0	25.3%	5	1.70	0.0
75	0.5%	0	24.8%	15	2.18	0.0
135	1.0%	0	24.5%	51	2.71	0.0
195	1.5%	5	24.1%	89	2.95	1.0
255	1.6%	10	23.8%	128	3.11	2.0
315	1.9%	20	23.4%	172	3.24	4.0
375	2.3%	61	23.0%	219	3.34	12.2
435	2.6%	100	22.6%	269	3.43	20.0
495	2.9%	157	22.2%	321	3.51	31.3
555	3.2%	224	21.9%	372	3.57	44.7
615	3.5%	304	21.5%	431	3.63	60.8
675	3.9%	395	21.1%	488	3.69	79.0
735	4.4%	477	20.8%	549	3.74	95.4
795	4.6%	566	20.4%	614	3.79	113.3
855	5.0%	653	20.0%	683	3.83	130.5
915	5.3%	721	19.7%	751	3.88	144.3
975	5.5%	802	19.4%	817	3.91	160.3
1035	5.7%	862	19.1%	887	3.95	172.3
1095	5.9%	933	18.8%	955	3.98	186.5

1155	6.1%	1014	18.5%	1019	4.01	202.7
1215	6.4%	1078	18.2%	1101	4.04	215.5
1275	6.5%	1174	18.0%	1159	4.06	234.9
1335	6.7%	1250	17.8%	1234	4.09	250.0
1395	7.0%	1338	17.5%	1312	4.12	267.6
Crack	Crack	Crack	Crack	Crack	Crack	Crack

Table C.6 The Restrained Ring Test Results for Compacted Ardmore Soil (Test 1)

Time (min.)	Surface Strain	Strain gauge reading (-)	Water content	Suction (kPa)	Suction (pF)	Tensile stress (kPa)
1	0.0%	10	25.6%	1106	4.04	2.0
30	0.3%	40	25.2%	1207	4.08	8.0
60	1.0%	69	24.8%	1285	4.11	13.8
90	1.5%	221	24.5%	1369	4.14	44.2
120	2.0%	346	24.1%	1464	4.17	69.1
150	2.6%	466	23.8%	1559	4.19	93.2
180	3.0%	585	23.4%	1660	4.22	117.1
210	3.3%	711	23.1%	1768	4.25	142.2
240	3.9%	834	22.8%	1883	4.27	166.7
270	4.4%	962	22.4%	2006	4.30	192.4
300	4.9%	1097	22.1%	2127	4.33	219.4
330	5.2%	1228	21.8%	2268	4.36	245.7
360	5.5%	1367	21.4%	2420	4.38	273.3
390	5.8%	1510	21.1%	2570	4.41	302.1
420	6.2%	1661	20.8%	2731	4.44	332.2
450	6.7%	1803	20.5%	2888	4.46	360.5
480	7.0%	1942	20.2%	3089	4.49	388.3
510	7.2%	2070	19.9%	3271	4.51	414.1
540	7.4%	2191	19.6%	3465	4.54	438.2
570	7.7%	2319	19.3%	3674	4.57	463.7
600	8.0%	2419	19.0%	3876	4.59	483.7
Crack	Crack	Crack	Crack	Crack	Crack	Crack

Table C.7 The Restrained Ring Test Results for Compacted Ardmore Soil (Test 2)

Time (min.)	Surface Strain	Strain gauge reading (-)	Water content	Suction (kPa)	Suction (pF)	Tensile stress (kPa)
1	0.0%	5	27.7%	736	3.87	1.0
30	0.7%	10	27.2%	815	3.91	2.0
60	1.5%	15	26.8%	894	3.95	3.0
90	2.0%	139	26.3%	970	3.99	27.7
120	2.8%	307	25.9%	1046	4.02	61.4
150	3.2%	434	25.5%	1144	4.06	86.9
180	3.8%	539	25.1%	1226	4.09	107.7
210	4.3%	637	24.7%	1326	4.12	127.4
240	4.9%	734	24.3%	1427	4.15	146.9
270	5.5%	821	23.9%	1528	4.18	164.2
300	5.9%	912	23.5%	1636	4.21	182.4
330	6.4%	1014	23.1%	1753	4.24	202.9
360	6.9%	1121	22.8%	1878	4.27	224.1
390	7.2%	1226	22.5%	1992	4.30	245.2
420	7.8%	1335	22.1%	2136	4.33	267.1
450	7.9%	1451	21.8%	2268	4.36	290.1
480	8.2%	1566	21.4%	2422	4.38	313.3
510	8.5%	1680	21.1%	2574	4.41	335.9
540	8.7%	1791	20.8%	2738	4.44	358.1
570	9.0%	1905	20.5%	2913	4.46	381.0
600	9.2%	2011	20.1%	3102	4.49	402.3

630	9.7%	2125	19.9%	3270	4.51	425.0
660	9.6%	2234	19.6%	3468	4.54	446.8
690	9.9%	2338	19.3%	3680	4.57	467.6
Crack	Crack	Crack	Crack	Crack	Crack	Crack

Table C.8 The Restrained Ring Test Results for Compacted Ardmore Soil (Test 3)

Time (min.)	Surface Strain	Strain gauge reading (-)	Water content	Suction (kPa)	Suction (pF)	Tensile stress (kPa)
0	0.0%	0	30.7%	369	3.57	0.0
60	0.9%	8	29.9%	459	3.66	1.5
120	1.8%	120	29.1%	555	3.74	23.9
180	2.8%	274	28.3%	654	3.82	54.7
240	3.8%	433	27.6%	759	3.88	86.6
300	4.6%	586	26.8%	881	3.94	117.2
360	5.5%	737	26.1%	1018	4.01	147.5
420	6.3%	889	25.4%	1167	4.07	177.8
480	7.1%	1057	24.7%	1328	4.12	211.3
540	7.8%	1230	24.0%	1503	4.18	246.1
600	8.5%	1421	23.3%	1693	4.23	284.3
660	9.2%	1623	22.7%	1907	4.28	324.6
720	9.8%	1831	22.1%	2139	4.33	366.1
780	10.4%	2062	21.5%	2404	4.38	412.4
840	10.9%	2296	20.9%	2691	4.43	459.1
900	11.3%	2528	20.3%	3018	4.48	505.7
945	11.7%	2610	19.8%	3299	4.52	522.0
950	12.0%	2666	19.2%	3736	4.57	533.2
Crack	Crack	Crack	Crack	Crack	Crack	Crack
1010	12.4%		18.8%	4098	4.61	
1070	12.7%		18.3%	4555	4.66	

1130	12.9%		17.8%	4984	4.70	
1190	13.2%		17.4%	5529	4.74	
1250	13.4%		17.0%	6031	4.78	
1310	13.6%		16.6%	6588	4.82	
1370	13.8%		16.2%	7114	4.85	
1430	14.0%		15.9%	7740	4.89	
1490	14.2%		15.5%	8432	4.93	
1550	14.4%		15.2%	9074	4.96	
1610	14.5%		14.9%	9838	4.99	
1670	14.7%		14.6%	10532	5.02	
1730	14.9%		14.3%	11361	5.06	
1790	15.0%		14.0%	12094	5.08	
1850	15.0%		13.9%	12525	5.10	

Table C.9 The Restrained Ring Test Results for Compacted Lake Hefner Soil (Test 1)

Time (min.)	Surface Strain	Strain gauge reading (-)	Water content	Suction (kPa)	Suction (pF)	Tensile stress (kPa)
1	0.0%	0	16.2%	79	2.90	0.0
15	0.2%	8	16.1%	81	2.91	1.6
75	0.5%	18	15.7%	94	2.97	3.6
135	0.9%	25	15.3%	109	3.04	5.1
195	1.3%	183	14.9%	127	3.10	36.7
255	1.8%	324	14.5%	149	3.17	64.9
315	2.1%	584	14.1%	181	3.26	116.8
375	2.5%	941	13.7%	216	3.33	188.1
435	2.9%	1366	13.3%	264	3.42	273.2
495	3.2%	1818	12.9%	322	3.51	363.5
555	3.6%	2263	12.4%	393	3.59	452.6
615	4.0%	2635	12.0%	483	3.68	526.9
675	4.2%	2876	11.6%	594	3.77	575.1
750	4.5%	2891	11.2%	756	3.88	578.2
Crack	Crack	Crack	Crack	Crack	Crack	Crack
765	4.5%		11.0%	799	3.90	
885	4.6%		10.3%	1196	4.08	
1005	4.7%		9.6%	1743	4.24	
1125	4.7%		8.9%	2503	4.40	
1245	4.7%		8.3%	3453	4.54	
1365	4.8%		7.8%	4683	4.67	

1485	4.8%		7.3%	6082	4.78	
1605	4.7%		6.9%	7642	4.88	
1725	4.7%		6.6%	9152	4.96	
1845	4.7%		6.4%	10847	5.04	
1915	4.8%		6.2%	12055	5.08	

Table C.10 The Restrained Ring Test Results for Compacted Lake Hefner Soil (Test 4)

Time (min.)	Surface Strain	Strain gauge reading (-)	Water content	Suction (kPa)	Suction (pF)	Tensile stress (kPa)
1	0.0%	0	20.1%	24	2.38	0.0
15	0.2%	0	19.9%	25	2.40	0.0
75	0.6%	15	19.4%	29	2.46	3.0
135	1.2%	88	18.9%	34	2.53	17.7
195	1.9%	200	18.4%	39	2.59	40.0
255	2.3%	324	17.9%	45	2.65	64.9
315	2.9%	463	17.4%	52	2.72	92.7
375	3.3%	620	16.9%	61	2.79	124.1
435	3.8%	800	16.5%	70	2.85	159.9
495	4.1%	1018	16.0%	82	2.91	203.5
555	4.7%	1271	15.6%	97	2.99	254.3
615	5.1%	1555	15.1%	115	3.06	311.1
675	5.5%	1861	14.7%	137	3.14	372.1
735	5.9%	2151	14.2%	169	3.23	430.1
795	6.2%	2302	13.8%	205	3.31	460.5
Crack	Crack	Crack	Crack	Crack	Crack	Crack
825	6.4%		13.6%	228	3.36	
840	6.5%		13.5%	240	3.38	
900	7.0%		13.0%	295	3.47	
960	7.1%		12.6%	367	3.56	
1020	7.3%		12.2%	450	3.65	

1080	7.5%		11.8%	552	3.74	
1140	7.8%		11.4%	679	3.83	
1200	7.7%		11.0%	828	3.92	
1260	7.8%		10.6%	1022	4.01	
1320	7.9%		10.3%	1206	4.08	
1380	7.9%		9.9%	1478	4.17	
1440	7.9%		9.5%	1771	4.25	
1457	7.9%		9.4%	1859	4.27	

VITA

Hussein Al-Dakheeli

Candidate for the Degree of

Master of Science

Thesis: HYDRO-MECHANICAL ANALYSIS OF SHRINKAGE AND SHRINKAGE CRACKING DUE TO ENVIRONMENTAL LOADS ON SATURATED TO UNSATURATED EXPANSIVE SOILS

Major Field: Geotechnical Engineering

Biographical:

Education:

Completed the requirements for the Master of Science in geotechnical engineering at Oklahoma State University, Stillwater, Oklahoma in December, 2016.

Completed the requirements for the Bachelor of Science in civil engineering at University of Baghdad, Baghdad, Iraq in 2011.

Experience:

- 2011-2013 Iraqi Ministry of Construction and Housing
  Site engineer
- 2013-2014 French Company S.A.R.L UR
  Site engineer
- 2016 Oklahoma State University
  Graduate teaching assistant & graduate research assistant

Professional Memberships:

- ASTM, Member, American Society of Testing and Materials (ASTM)